Process Intensification: Mass Transfer and Pressure Drop for Countercurrent Rotating Packed Beds.

By

Haitem Mustafa Hassan-Beck, M.Sc.

A thesis submitted for the Degree of Doctor of Philosophy
Faculty of Engineering,
University of Newcastle-upon-Tyne.

July 1997

Department of Chemical and Process Engineering,
University of Newcastle-upon-Tyne.

Acknowledgements

I would like to take this opportunity to express my appreciation and thanks to my supervisor Professor Colin Ramshaw for his supervision and support throughout this project. Special thanks to Dr R.J.J.Jachuck for his support during the experimental work.

Thanks to Mr Eric Horsley for his help in the design and procurement of the experimental facility. Technicians Ian, Stuart, Chris, Jimmy, George, Brian, Rob and Vince for their help in constructing the experimental facility. In particular I would like to thank Ian and Stuart for their expert suggestions and contributions on any modification that was needed.

I would also like to thank my colleague Dr John Burns for his kind permission to allow me to show some of his photographs in this thesis.

Finally, the financial support from the Petroleum Research Centre (PRC) Tripoli-Libya, is greatly appreciated.

I dedicate this work to,

My mother, late father, wife, son, daughter,
brothers and sisters.

Abstract

The mass transfer and the pressure drop characteristics for countercurrent rotating packed bed (RPB) with a continuous gas phase for the removal of ethylene dichloride (EDC) from water using air stripping have been investigated. The aim of this research was to understand the behaviour of the mass transfer performance and the pressure drop behaviour in a centrifugal environment.

The mass transfer results showed that the height of a transfer unit (HTU) in a liquid film limited system can be in the range between 30 to 70mm at moderate centrifugal acceleration between 44 to 280g. Three packings of different packing densities ranging from 870 to 2300 m^2/m^3 were tested. The HTU values were found to vary with the centrifugal acceleration as $HTU \alpha g^{-0.11 \text{ to } -0.28}$. It has been shown that the packing density may not have a notable effect on the separation performance of the bed.

The pressure drop results indicated that in RPB the pressure drop is relatively higher than its equivalent packed beds operate at 1g. The usual flooding restrictions were relaxed thus high hydraulic capacities can be achieved per unit size of equipment. At the flooding point, experimental findings indicated that a part of the liquid is not accelerated by the bed. A model to predict the pressure drop was developed. The model was verified against experimental data and good agreement was obtained.

Key words: Process Intensification, Rotating Packed Bed (RPB), HiGee, Ethylene Dichloride (EDC), Height of Transfer Unit (HTU), Centrifugal Acceleration ($\omega^2 r_i$).

TABLE OF CONTENTS

List of Figures

List of Tables

List of Photographs

Chapter 1

Introduction

In recent years the need to improve mass and heat transfer equipment has had engineers and scientist searching for new methods and techniques to achieve this aim. The challenges were to design novel equipment and implement new ways of production. Motivation has not only come from economic pressures but also from the development of reliable, compact, safer and more efficient technologies using smaller components as a result of adopting new philosophies such as miniaturisation and decentralisation of a plant leading to distributed manufacturing facilities, instead of large plants.

Process Intensification (PI) was first highlighted by Ramshaw [R1,R2]. It is a novel design philosophy which aims to achieve significant reduction in the size of individual plant modules, by a factor of ten or more, resulting in cost reduction, efficiency enhancement and inherent safety. The concept of PI is to improve heat and mass transfer characteristics hence generating better contacts between fluids. The advantage of fast mixing properties can create improved heat and mass transfer rates. Thus systems with limitations in mixing, reaction times and heat and mass transfer could significantly benefit from PI.

In multiphase systems the fluid dynamic behaviour is dictated by the interphase buoyancy factors ($\Delta\rho g$). If $\Delta\rho g = 0$, (i.e. deep space) there will be no interphase slip velocity and the transfer process would be dictated by the dominating surface tension forces. However, if 'g' is increased (e.g. by generating centrifugal field by rotation) then a larger interphase slip velocity can be achieved and can produce stronger interphase transfer.

By reducing the equipment size, the main plant items cost will be reduced. The main plant items such as reactors, columns and heat exchangers contribute only partially to the fixed capital cost of a plant. Table 1.1 shows the breakdown of the cost for a typical plant. It can be seen from the table that a significant part of the capital cost is allocated to piping and other civil engineering works. Generally, the overall cost can fall in the region of 2 to 8 times the capital cost of the main plant items. Therefore, if this installation factor can be reduced, a significant saving in the capital cost can be made.

One possible way to implement PI philosophy is to apply the to all main plant items. In addition to cost reduction, PI can offer other benefits such as smaller items which would have lower residence time and thus easier controllability and intrinsically safer units in plants where flammable and toxic inventories of several tonnes are very common. Furthermore, PI can reduce the environmental impact of a plant because the unit hardware sizes are drastically reduced, the restrictions imposed by headroom limitations would be met and a complete plant can be built and put together on a small footprint area.

The use of rotating packed beds for countercurrent gas-liquid flow was highlighted by Ramshaw [R1]. The unit consists of a doughnut shape packed bed mounted in between two discs and rotates coaxially with the rotor's axis of rotation.

Table(1.1):Fixed Capital Cost Breakdown of a 90,000 TPA Ammonium Sulphate Plant [C1].

(Figures represent the percentage of the total fixed capital cost)

Item	Unit	Spares	Erection	Insulation	Design	Contingencies	Total
Mechanical	26.1	1.2	8.1	2.5	1.3	2.6	42.0
Civil	7.4	---	---	0.9	1.3	1.3	10.9
Structure	8.3	---	---	1.0	1.3	1.3	12.9
Pipework	13.8	---	4.3	1.5	0.2	2.0	21.8
Instrument	4.5	0.1	0.8	---	1.0	0.9	7.4
Electrical	1.6	---	0.1	---	0.3	0.2	2.3
Control	2.4	---	---	---	0.4	0.4	3.1
Total	64.1	1.3	13.3	5.8	5.8	8.6	100

The liquid is fed from the centre of the rotor onto the packing and flows outwardly under the action of high centrifugal acceleration. The gas is introduced from the periphery and flows inwardly to the centre of the rotor.

The high centrifugal acceleration environment generates high shear forces in the liquid, resulting in very thin liquid films. Accordingly these films can yield very large surface areas when fine packing is used, for a given value of throughput. In addition, centrifugal acceleration may cause rapid and continuous renewal of the interfacial surface. These factors coupled with the turbulence generated by the gas, e.g. in gas/liquid countercurrent flow, offer great mass transfer enhancement potential in the rotating packed beds (RPBs) and very low height of transfer units HTUs is achieved compared to those of conventional packed beds. This reduction in HTU was attributed to the higher values of volumetric mass transfer coefficients. Furthermore, when centrifugal accelerations of several 'g' are applied to countercurrent flow in packed beds, the usual flooding restrictions are relaxed. This allows the achievement of high mass fluxes for packing with large surface area per unit volume.

The lower HTUs obtained by using RPBs can be explained from figure 1.1. It can be seen that for fixed liquid and gas mass fluxes if ' g ' is increased the flooding value of the Y-axis must be constant and hence a higher surface area packing a_p can be used which in turn it helps to produce higher volumetric mass transfer coefficients $K_L a$.

The relaxation in the flooding limits can also be explained in terms of the Y-axis group from the Sherwood correlation in figure 1.1 for packed beds.

Fig.(1.1): The Sherwood Plot.

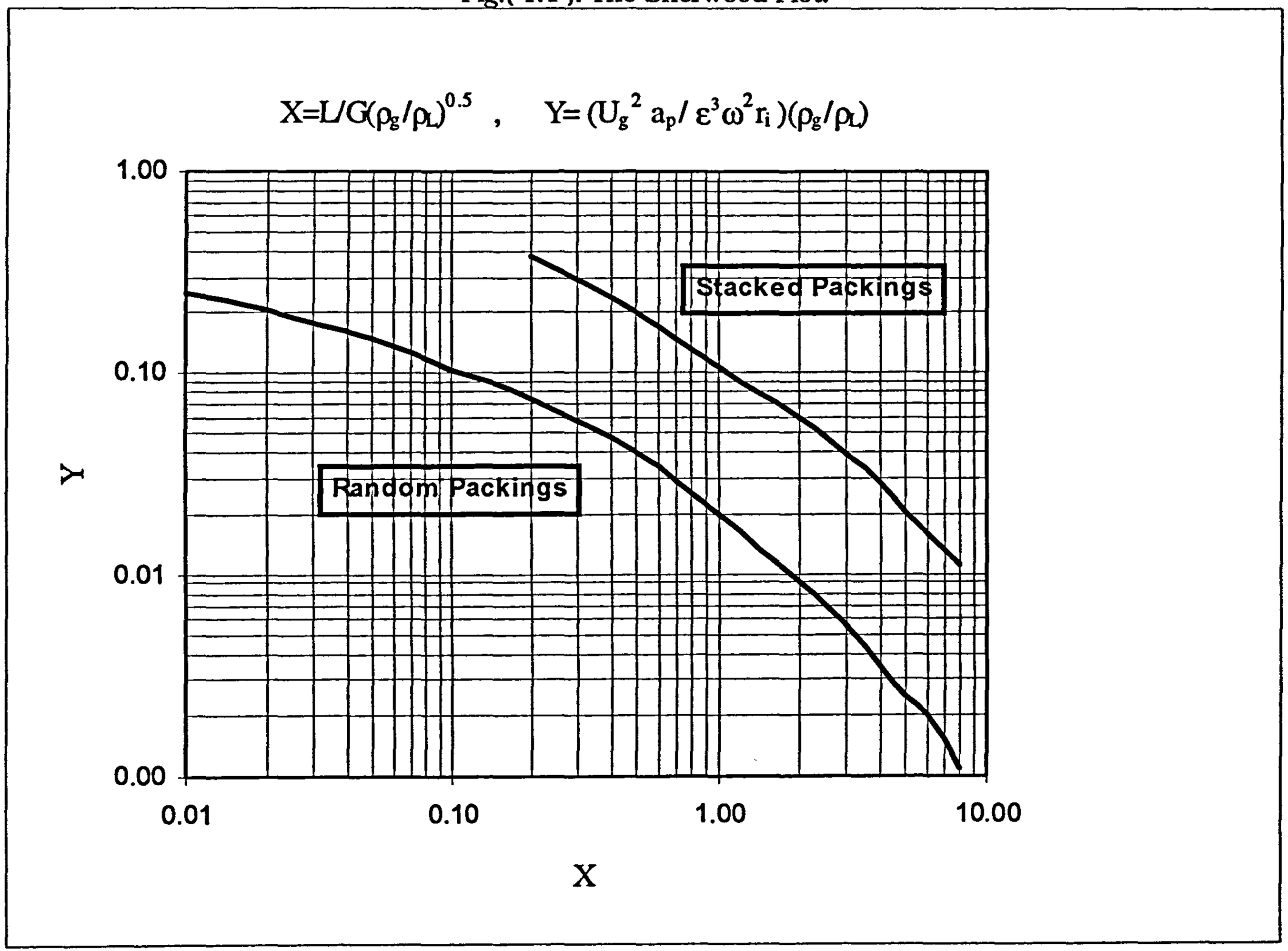

The Y-axis group suggests that if ' g ' is increased, for a given packing material with surface area a_p and porosity ε, a higher gas throughput (i.e. higher U_g) can be used per unit area of the packing at the inlet of the bed. Further details are discussed in section 1.9.3.

Higher values of U_g and lower values of HTU will produce a small size equipment. Ramshaw [R1] found that typical values for height of transfer units in liquid film limited system were between 30-50mm and for gas film limited system were between 10-30mm.

The background section 1.2 gives most of the research work available in the literature on rotating packed beds. Further information about conventional packed beds is also discussed. Chapter 2 describes the details of the experimental set up used for the mass transfer data together with the packings' specification and the influence of the end effect. In chapter 3 the mass transfer results are discussed in detail. The effect of rotational speed on the mass transfer performance using different packing material having different packing densities are also given. The experimental values of the height of transfer unit HTU were compared against values obtained from theoretical and empirical models. Chapter 4 discusses the effect of liquid distribution on the mass transfer performance in rotating packed beds. Results of the tests on effect of the initial liquid distribution on the mass transfer performance are also given.

Chapter 5 details a second smaller experimental set up used to study the behaviour of the flooding and pressure drop in rotating packed beds. Different flooding data at various liquid and gas loadings were given. The Sherwood approach were tested against the obtained experimental values for the gas flooding velocities. A mathematical model for the pressure drop across the packing section is given. The model is validated against experimental values. Chapter 6 outlined the conclusions of this thesis work and the recommendations for future investigations.

1.1 Scope of the Thesis.

Process Intensification is a new concept, and hence the literature about the rotating packed beds is very limited. A better understanding of the interaction between the phases involved (gas-liquid-packing) is therefore needed. Two rotating packed beds of 45mm and 20mm in diameter have been designed and commissioned to generate large centrifugal accelerations. The design details and specifications of both rotors are given in chapter 2 and 5.

The aim of this thesis is divided into two parts. In the mass transfer part, the aim was to investigate the effect of the liquid flow rate, gas flow rate, liquid to gas ratio for higher gas and liquid flow rates, rotor speed, liquid distribution and packing density and type on the mass transfer performance and to compare the experimental height of transfer units values with those estimated from theoretical models. Ethylene Dichloride -water-air system was used in the mass transfer experiments. In the flooding behaviour part, the air-water system was used and the aim was to investigate the flooding phenomenon, the liquid flow characteristics at the flooding conditions and the pressure drop behaviour across the radial depth of the bed.

1.2-Background.

One of the approaches used to implement PI philosophy is to exploit centrifugal acceleration. Ramshaw [R3,R4] highlighted different potential applications which can be intensified in a high acceleration environment by employing high centrifugal fields. In the last few years, attention has been focused on exploiting the centrifugal acceleration in rotating packed beds.

Cross and Ramshaw [C1] and more recently Caruana [C2] and Wegeng [W1] have highlighted a new approach in PI by using microchannels in the design of different unit

operations. The concept is, largely, based on: (1) engineered microchannels whereby better distribution within the channels can be achieved and (2) the generation of high surface area per unit size of the equipment thereby creating more interacting surface area between the fluids. Moreover, because of the laminar nature of the flow in these channels, the heat and/or mass transfer process takes place by the virtue of the diffusional mechanism. Another advantage of using microchannels is the relative simple controllability of different parameters such as temperature and residence time. Some tests in these studies were carried out on gas/liquid and liquid/liquid systems to prove the potential application of using the microtechnology.

Since the rotating packed beds RPBs can be regarded as an extension for conventional packed columns run at 1g, it could be useful to employ the different empirical and theoretical models developed in 1g to RPBs.

1.3- Liquid Distribution.

1.3.1- Liquid Maldistribution.

In packed beds the key assumption is that for any packing material the surface area is entirely active as a result of wetting the packing with sufficient liquid. However, because the inherent liquid maldistribution in packed beds results in the formation of relatively lower surface area flow patterns such as rivulets, it would be unreasonable to assume that the liquid progresses over the bed as a series of thin films wetting the whole surface area. Liquid maldistribution in packed beds leads to poor performance hence good liquid distribution is the key factor for achieving better performance with any type of packing material. In order to achieve good liquid distribution (i.e. maintaining the ratio between local liquid flow rate to the average liquid flow rate at unity) and optimum mass transfer performance, effective lateral spreading from the liquid source is desirable.

In every packed bed the liquid will flow in preferential paths instead of uniform thin films covering the whole packing. Accordingly the liquid maldistribution was classified into two broad categories; large and small scale maldistribution. The former is associated with the liquid flow and the structure of the bed near the wall of the column, and the latter is associated with the packing material itself over which the liquid or the created rivulets have poor capacity to spread all over the packing.

Albright [A1] simulated the liquid flow distribution through packed beds. For every packing material a small scale maldistribution or channelling known as natural flow will develop and it was found that, for good initial liquid distribution, the flow will disintegrate to natural flow quicker, after about a length equivalent to 8-10 times the packing size, than an inadequately distributed liquid which could take longer.

Hoek *et al* [H1] developed the concept of radial spreading coefficient (with linear dimension, m) for different packing sizes to measure the tendency of packing material to spread a liquid stream (e.g. rivulet) radially, as it trickles down the bed. They showed that the higher the radial spreading coefficient the faster the initial distribution becomes a natural flow. Further it was found that packing material with large radial spreading coefficient would improve the mass transfer performance for maldistributed liquid. They concluded that for packing with a higher radial spreading coefficient (i.e. large packing sizes) mass transfer performance is more efficient. It was shown that a typical value of the radial spreading coefficient could vary from 6% to 14% of the packing size.

Bremer and Zuiderwig [B1] studied the liquid maldistribution in packed beds using different sizes of Rasching rings packing. It was established in this work that both the maldistribution factor and the spreading coefficient are strongly dependent on the packing sizes rather than the wettability of the packing, and this has led to the conclusion that the bulk of the liquid progresses down the bed in stable channels.

Stanek [S1] has compiled and discussed in detail most of the research work in liquid distribution in packed beds. Liquid maldistribution in packed beds has been studied in great details [B1,A1,H1]. For a conventional packed column, the diffusion model has been widely used to predict the distribution of liquid in packed beds at various depths [H1,Z1,Z2]. The model is based on the superficial liquid velocity.

1.3.2- Initial Liquid Distribution

Normally, the quality of liquid distribution [P1] can be assessed on the basis of three factors; the distribution density or the number of distribution points, the geometric uniformity of the location of the distribution points (i.e. deployment of the distribution point uniformly above zones of equal surface area) and the uniformity or quality of liquid flow from the distribution points. These three factors collectively constitute the distribution quality; therefore a distributor with poor quality will have a detrimental effect that produces poor performance resulting in higher HTUs.

1.4- Wettability of Packing.

Wetting of packing material is an important factor to help to quantify the total wetted interfacial area of a packing in which mass transfer process normally occurs. Minimal disintegration of liquid films, however, will be desirable in order to prevent dry patches which can be ineffective. Hartley and Murgatroyd [H2] and Ponter *et al* [P2] have studied the criteria of liquid film break-up over vertical flat surfaces forming dry patches and liquid rivulets. Empirically, Onda [O1] studied the effect of the interactions among different forces such as the inertial, surface and gravitational forces and their effect in the prediction of the wetted area.

1.5- Gas-Liquid Interfacial Area.

In packed beds, not the whole surface area of the packing will be active during the mass transfer process, due to the inherent liquid maldistribution. Therefore the surface area can be classified as active, a_e (i.e. effective) and wet, a_w areas. The former represents the surface area whereby the liquid surfaces over the packing are continuously renewed. The latter represents the parts of the packing which are wet but have only a fraction of the area active because of the established channels and stagnant liquid pockets in which the bulk of the liquid will be inactive.

Shulman *et al* [S2] have studied the effect of liquid and gas flow rates on both wetted and interfacial areas in packed beds using two different packing materials, i.e. Rasching rings and Berl saddles for the sizes of 12, 25, 38 and 50mm. They showed that both the interfacial area, a_e, and the wetted area, a_w, change with liquid flow rate. They further showed that the increase in gas flow rate does not affect the interfacial area a_e below the loading point, after which the interfacial area starts to increase. On the other hand the wetted area a_w was found to decrease as the gas flow rate increases.

Davidson [D1] compiled data on both effective and wetted surface areas for different size Rasching rings packing of 12, 25 and 36mm. He showed that the effective area a_e, for each packing, are less than the wetted a_w area depending on the packing size; the smaller the packing the higher the difference between a_e and a_w.

Several correlations have been reported to estimate the wetted surface area, among which the Onda *et al* [O1] correlation can be used to calculate the wetted area. This correlation takes into account the effect of surface tension, the surface energy of the packing material and, the most importantly the gravitational force ' g ':

$$\frac{a_w}{a_p} = \frac{a_e}{a_p} = 1\text{-}\exp(-1.45(\sigma_c/\sigma)^{0.75}\, Re^{0.1}\, (L^2\, a_p/\rho^2\, g)^{-0.05}\, We^{0.2} \qquad (1.5.1)$$

The assumption of equality in the above equation between the a_w and a_e is that for packing material with small static hold up (i.e. large packing size) the wetted area may equal the interfacial area.

Puranik and Vogelpohl [P3] have analysed the effective interfacial area in terms of static and dynamic hold-up. Based on this approach, they have proposed a generalised correlation for 'effective' surface area using different mass transfer mechanisms, namely vaporisation and absorption with and without chemical reaction. The correlation was expressed in a non-dimensional form as follows:

$$\frac{a_e}{a_p} = 1.05\, Re^{0.047}\, We^{0.135}\, (\sigma/\sigma_c)^{-0.206} \qquad (1.5.2)$$

Munjal [M1] referred to equation 1.5.3 to calculate the interfacial area which is based on Fr and We numbers. It is worth pointing out that the We number in this equation depends not only on inertia but also on the characteristic length of the packing.

$$\frac{a_e}{a_p} = 0.34\, We^{2/3}\, Fr^{-1/2} \qquad (1.5.3)$$

1.6- Liquid Side Mass Transfer Coefficient.

1.6.1- Theoretical Models.

In liquid mass transfer problems, most of the limiting cases can, broadly, fall into two kinds of mass transfer mechanism. The diffusion process occurs across either a thin film at the interface or a semi-infinite slab (i.e. thick film). In the Penetration model in very short exposure time, the diffusion will take place as if the slab is infinitely thick, Higbie [H3], but in the Film model the diffusion will take place only in a thin film at the interface between the phases, Whitman [W2].

For Packed beds, the Penetration theory has been more widely used to describe the behaviour of diffusion in detail than the Film theory, and this is largely because at very short exposure time the diffusion process will take place across the film as though the film is infinite figure 1.2. Furthermore the mass transfer coefficient in the Penetration theory varies with the square root of the diffusivity ($K_L \alpha \sqrt{D}$) in comparison with the Film theory in which the mass transfer is directly proportional to the diffusivity ($K_L \alpha D$).

Figure 1.3 represents the solution for the unsteady state diffusion in a rectangular co-ordinates. The general form of the equation is given as:

$$\frac{\partial C}{\partial t} = D\frac{\partial^2 C}{\partial x^2} \qquad (1.6.1)$$

and boundary conditions to satisfy are:

$t = 0$	$0 < x < \infty$	$C = C_0$
$t \geq 0$	$x = 0$	$C = C_i$
	$x = \infty$	$C = C_0$

Figure 1.3 shows the concentration profile across the slab thickness (l) in rectangular co-ordinates. The numbers on the curves were the value of the dimensionless group (Dt/l^2). The profiles shown represent the concentration profile at any depth, into the slab, in a given time. After a very long exposure time, the whole slab becomes saturated.

Fig.(1.2): The Film and Penetration Theories.

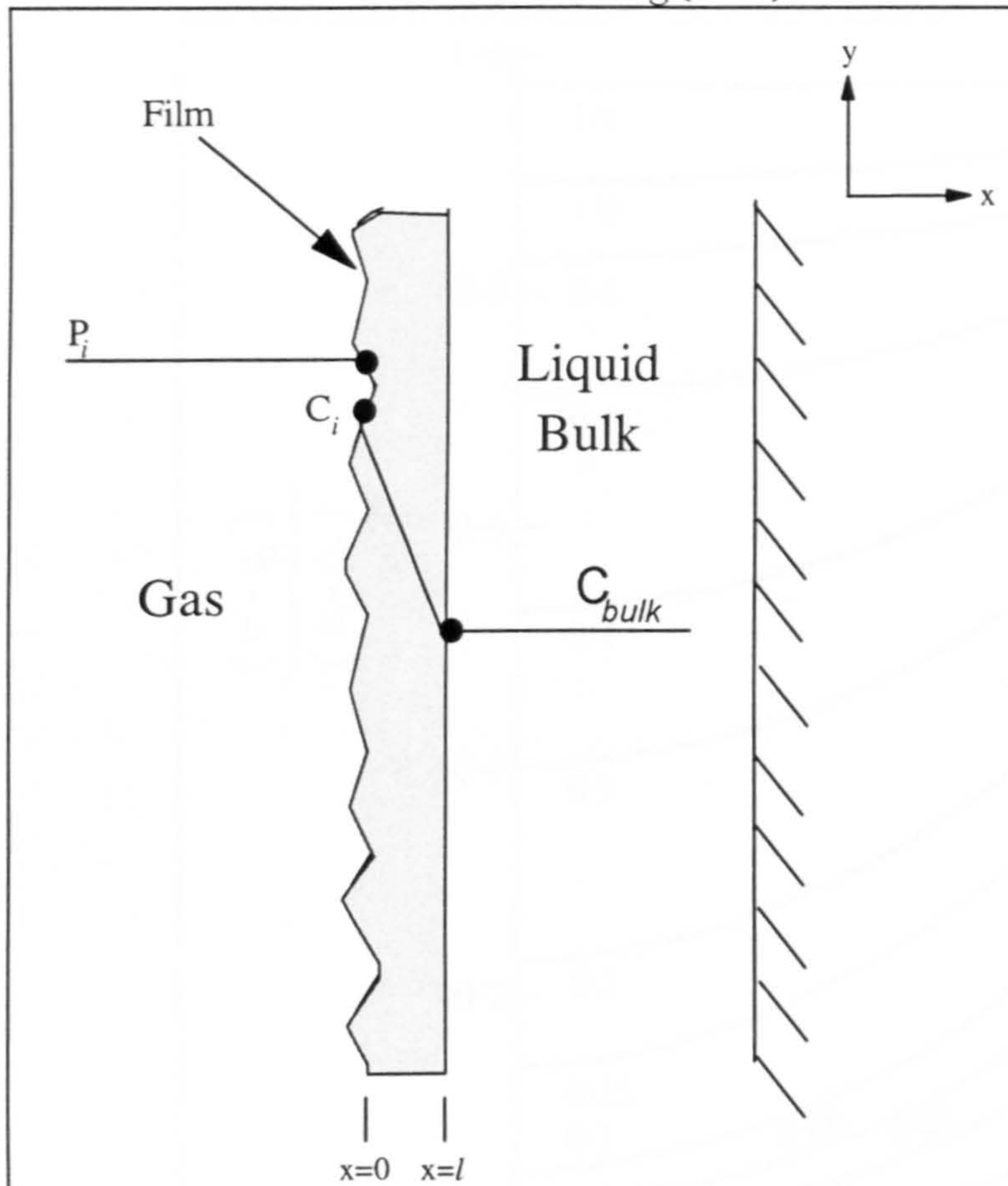

The Film Theory:
Hypothetical Film at the Interface

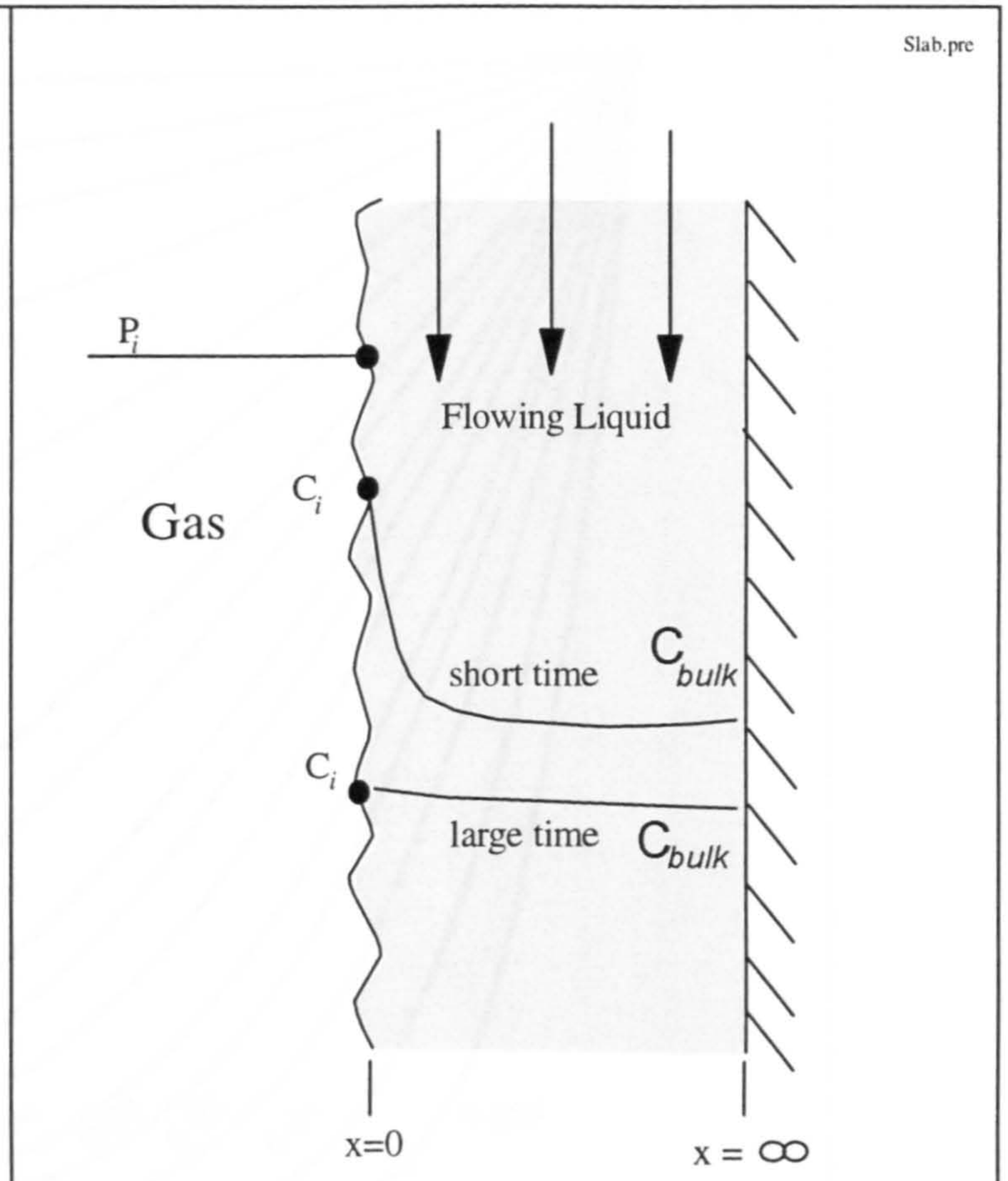

The Penetration Theory:
Film as a Semi-Infinite Slab

Fig.(1.3): Solution for equation 1.6.1, [C3].

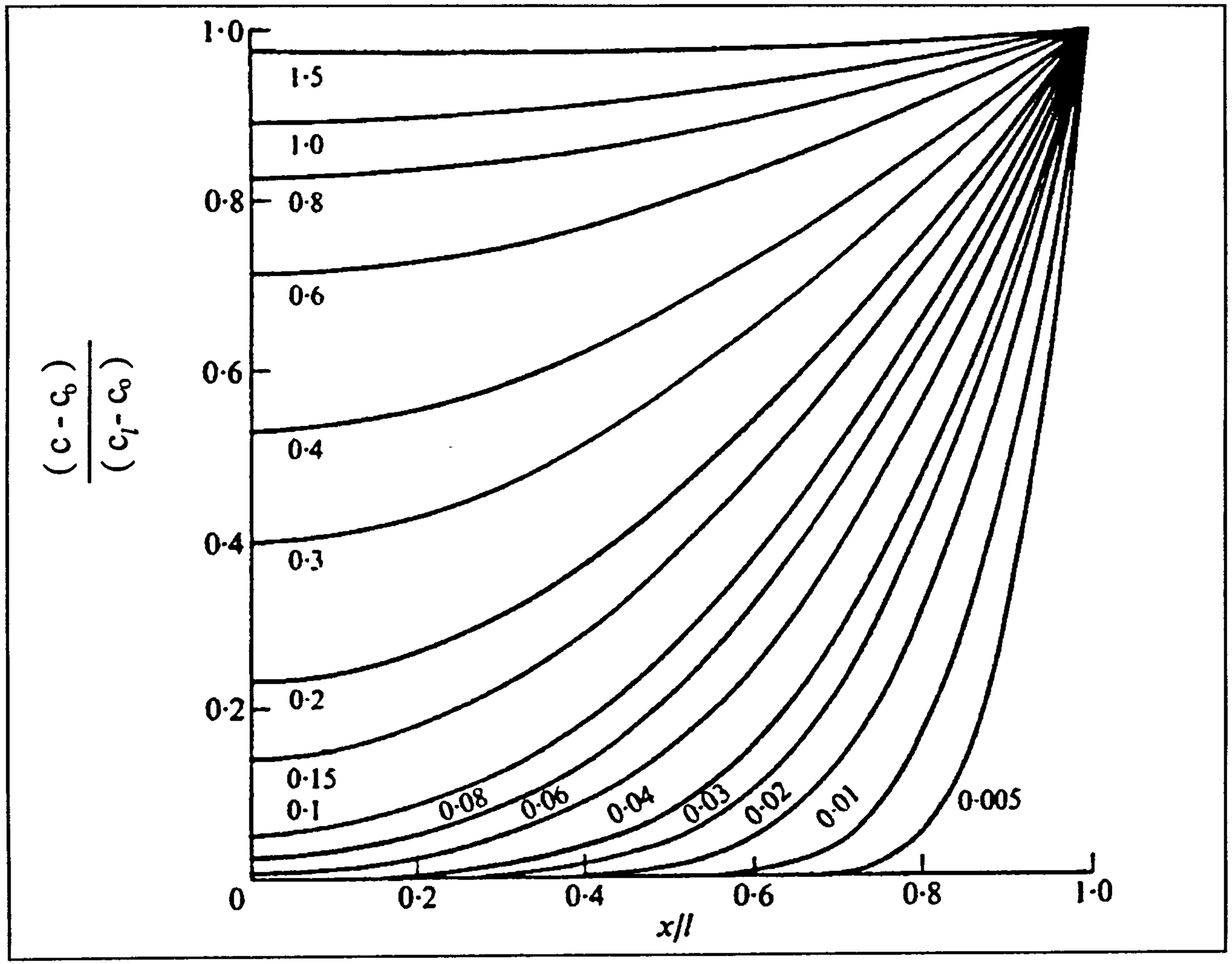

An example illustrating the relevance of the Penetration theory to RPBs will now be discussed. For O_2 in air to be absorbed using distilled water at 1 atmosphere and using an average centrifugal acceleration of 820 m/s^2 (~ 83g) in a rotor with 158 mm and 60 mm inside diameter and axial length, respectively. The diffusivity of O_2 in water is in the order of $1.8x10^{-9}$ m^2/s and the packing has a surface area per unit volume and packing filament thickness of 2500 m^2/m^3 and $1.1x10^{-4}$ m, respectively. For a liquid flow rate equal to 20 L/min. (11 Kg/m^2s), the calculated exposure time from equation 1.6.3 was 0.0015 second and the average liquid film velocity from equation 1.6.4 was 0.26 m/s. With such a very short exposure time, a value of 0.0042 for the parameter (Dt/l^2) is obtained, thus suggesting from figure 1.3 that the diffusion process at its early stages and the penetration theory should apply.

The Penetration model assumes that the flow of liquid over the packing elements is laminar and the liquid is completely remixed at the junctions of the packing material. The liquid mass transfer coefficient K_L, can be expressed as:

$$K_L=\sqrt{\frac{4D}{\pi t}} \qquad (1.6.2)$$

where t is the exposure time of the liquid to the gas and can be estimated by the following equation:

$$t=\frac{\pi\ d_p}{2\ v} \qquad (1.6.3)$$

where d_p is the characteristic dimension (e.g. filament thickness in reticulated packing) and v is the liquid film velocity which can be expressed as:

$$v=\left(\frac{\rho\ g\ \delta^2}{3\mu}\right)=\left(\frac{9g\Gamma^2}{8\mu\rho}\right)^{1/3} \qquad (1.6.4)$$

where Γ is the liquid flow rate per unit width and expressed in terms of the liquid film thickness δ as:

$$\Gamma = \frac{\delta^2 g \rho}{2\mu}$$

Equation 1.6.4 is based on the assumption of negligible interfacial shear. Substituting equation 1.6.4 into 1.6.3 and 1.6.3 into 1.6.2, an expression for K_L can be obtained as follows:

$$Sh = \frac{K_L d_p}{D} = 0.919 (a_p/a_e)^{1/3} Sc^{1/2} Re^{1/3} Gr^{1/6} \quad (1.6.5)$$

Davidson [D1] developed three models based on the Penetration theory to predict the height of transfer unit HTU in packed beds for liquid phase mass transfer. The models were based on the orientation of the packing's surfaces. In the first model, equation 1.6.6, the bed was assumed to consist of a large number of vertical completely wetted surfaces:

$$HTU_L/dp = 0.345 Sc^{1/2} Re^{2/3} Gr^{-1/6} \quad (1.6.6)$$

In the second model equation 1.6.7 the bed was assumed to have been made from a large number with randomly inclined flat surfaces of equal lengths. In the third model equation 1.6.8 the bed was assumed to have been made from a large number of randomly inclined flat surfaces of random lengths. In equation 1.6.7 and equation 1.6.8 the surface lengths of the packing were assumed to be equal dp and dp/2, respectively.

$$HTU_L/dp = 0.244 Sc^{1/2} Re^{2/3} Gr^{-1/6} \quad (1.6.7)$$

$$HTU_L/dp = 0.1833 Sc^{1/2} Re^{2/3} Gr^{-1/6} \quad (1.6.8)$$

1.6.2- Empirical Models.

Vivian *et al* [V1] gave an expression for the volumetric mass transfer coefficient $K_L a$, equation 1.6.9 in which the $K_L a$ is proportional to $g^{0.38}$. In this model both the mass transfer coefficient and the interfacial area were lumped together to avoid any uncertainty in calculating each of the K_L and a separately.

$$\frac{K_L\, a\, d_p}{D} = 0.023\, Sc^{1/2}\left(\frac{g\, d^3\, \rho^2}{\mu^2}\right)^{0.38}\left(\frac{d\, L}{\mu}\right)\left\{1-1.02\exp\left[-(0.15)\left(\frac{d\, L}{\mu}\right)^{0.4}\right]\right\} \qquad (1.6.9)$$

Onda *et al* [O1] were first to express the liquid side mass transfer coefficient correlation equation 1.6.10 which has a gravity term. The K_L was found to be proportional to $g^{1/3}$.

$$K_L\left(\frac{\rho}{\mu\, g}\right)^{1/3} = 0.0051\, Re^{2/3}\left(\frac{a_t}{a_e}\right)^{2/3} Sc^{-0.50}\left(a_t d\right)^{0.4} \qquad (1.6.10)$$

1.7- Gas Side Mass Transfer Coefficient.

Many correlations have been reported in the literature. The value of the mass transfer coefficient K_G was determined by employing different experimental techniques. The systems were purely physical such as evaporation. Shulman *et al* [S2] have used a packing made from naphthalene to measure the evaporation rate. Gamson *et al* [G2] have measured the evaporation rate from a porous packing soaked in water. Onda *et al* [O2] compiled many of the literature data on water and organic systems.

1.8- Rotating Packed Beds.

Podbielniak [P4] tested the application of the centrifugal acceleration in a continuous vapour/liquid contactor. The contactor was used to deodorise fats and oils by using

steam stripping. The rotor's packing was made of pluralities of perforated equally-spaced circular sheets deployed coaxially with the main shaft of the contactor. The perforations permitted the gas to flow inwardly towards the eye of the contactor while the liquid was expelled outwardly to the periphery of the contactor. The circular perforated sheets provided limited surface area resulting poor performance.

Pilo [P5] and Pilo and Dahlbeck [P6] investigated the mass transfer performance of rotating beds in either packed or plated beds. They tested the unit to scrub benzene from town gas. They demonstrated that the unit has lower residence time and tested the unit for the selective removal of instantaneously reacting H_2S from town gas using liquid ammonia as a solvent.

Vivian *et al* [V1] studied the effect of centrifugal acceleration in a gas absorption experiment in a packed bed. The column used was a conventional packed bed, 150mm in diameter and 300mm height and was mounted on a horizontal arm of a large centrifuge. The ratio of centrifugal field to gravity used ($r\omega^2/g$) was varied between 1 to 6.4. They reported that, for desorption of carbon dioxide from water into air, the liquid-side mass-transfer coefficient varied with centrifugal acceleration as follows:

$$K_L a_e \ \alpha \left(\frac{r\omega^2}{g}\right)^p$$

$$0.41 \leq p \geq 0.48$$

ICI (Imperial Chemical Industries) pioneered the HiGee (Hi Gravity) and it holds several patents on this technology [R5,M2,W3,W4]. The unit can operate at high acceleration with packing of high specific surface area. The device was constructed using a doughnut-shaped high surface area packing, figure 1.4. The packing which was mounted on the shaft and the liquid being fed to the bed by a stationary distributor. The liquid is sprayed into the centre 'the eye' of the bed and flows radially outwards

under the action of centrifugal acceleration. On the other hand, the gas is fed from the periphery and flows radially inwards to the centre of the bed due to the pressure difference.

Short [S3] described HiGee and its possible role in the scaling down the height of a distillation column by a factor of ten and mentioned that a slight reduction in diameter is also achieved. He reported that test runs were conducted by ICI in distillation at total reflux. The results have revealed that the theoretical plate height in the distillation runs and the height of transfer unit in the absorption runs varied from 10 to 20mm at a mean acceleration value of 1000g. Fowler [F1] discussed the application of HiGee in water treatment and gas conditioning units.

Ramshaw and Mallinson [R5] were the first to report test results for absorption and distillation using HiGee. Test runs were carried out to determine the gas and liquid volumetric mass-transfer coefficients. For liquid-side volumetric mass transfer coefficients test runs were carried out to absorb oxygen from air into deoxygenated water using two different packing materials; 1mm spherical glass beads and Knitmesh 9031 with specific surface area per unit volume 3300 and 1650 $m^2/m^{3\cdot}$, respectively. For gas-side volumetric mass-transfer coefficients test runs were carried out to absorb ammonia from ammonia-air system (5% by volume) into water using two different packing materials; 1.5mm spherical glass beads and Knitmesh 9031 with surface area per unit volume of 2400 and 1650 m^2/m^3, respectively. A summary of their results is shown in tables 1.2 and 1.3. The results showed an increase of volumetric mass transfer coefficients, in proportion to the rotational speeds, up to several orders of magnitude higher than the reported values for conventional packed beds. The reported values for volumetric mass-transfer coefficients were roughly proportional to the magnitude of the body forces raised to the power ranging from 0.14 to 0.54. The liquid film mass-transfer coefficient was calculated using the following equation:

$$K_L = \frac{Q}{V a_P} \ln \frac{c_{e_1} - c_1}{c_{e_1} - c_2} \qquad (1.8.2)$$

It was assumed that the effective interfacial (active) area for mass-transfer was equal to the specific area of the packing material and the results are given in table 1.2. As can be seen from table 1.2 the values of liquid mass-transfer coefficient are given without any information about the gas flow rates, it is, therefore, difficult to draw any firm conclusion.

The gas film mass-transfer coefficient was calculated using the following equation:

$$K_G = \frac{M_{wt}\, Q(c_2 - c_1)}{V a_p P_t} \left\{ \frac{\ln\left(\frac{y_1 - y_{e_1}}{y_2 - y_{e_2}}\right)}{(y_1 - y_{e_1}) - (y_2 - y_{e_2})} \right\} \qquad (1.8.3)$$

The results are given in table 1.3 where it can be seen that the gas film mass-transfer coefficient increases with increase in the rotational speed.

Fig.(1.4):HiGee Unit of Doughnut-Shaped Packing.

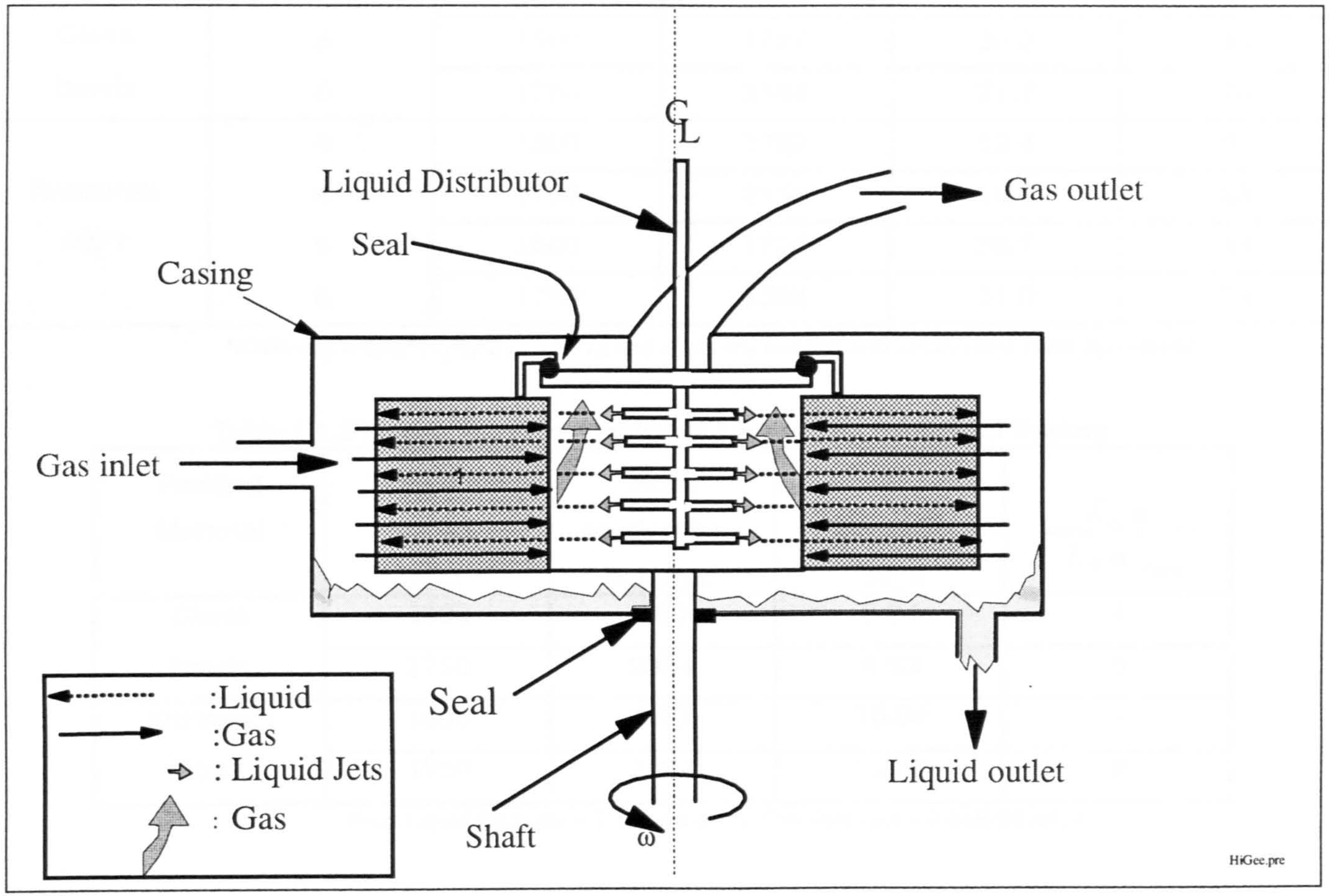

Table(1.2):Mass Transfer coefficients for liquid film controlled System.

Packing material	Water flow rate x10^5 m^3/s	Rotational speed rpm	Mean Acceleration, a_m , m/s^2	k_L x 10^5 m/s	$\frac{K_L a}{(K_L a)_{grav.}}$
1mm Glass beads	3	1250	1197	21.2	37
	3	1500	1727	24.9	42
	5	1500	1727	20.3	41
	5	1750	2354	21.7	44
Knitmesh 9031	4	1500	1727	19.4	27
	4	1750	2354	20.6	28
	6	1500	1727	26.7	29
	6	1750	2354	31.5	34

NOTE: $a_m = [(r_o^2+r_i^2)/2]^{1/2}\omega^2$, r_o and r_i are the outside and inside rotor radii, receptively.

Table (1.3):Mass Transfer coefficient for gas film controlled System.

Packing Material	Rotational Speed, rpm	Mean Acceleration, a_m m/s^2	K_G x10^8 m/s	$\frac{K_G a}{(K_G a)_{grav.}}$
Glass beads	1000	760	3.94	4
	1750	2354	4.83	5
Knitmesh 9031	1000	760	10.08	8
	1750	2354	12.69	9

Note: Liquid flow rate = 0.17E-04 m^3/s, Gas flow rate = 0.84E-03 m^3/s

Ramshaw and Mallinson [R5] have also tested rotating packed beds for distillation methanol-ethanol mixture at total reflux using a small vapour-liquid contactor, the inner and outer radii of which were 6 and 9 cm, respectively. Packing material was made of filaments of stainless steel gauze with a specific area of 1650 m^2/m^3. The bed was run at a feed composition of 70% methanol and 30% ethanol. The feed was first charged to a boiler and the resulting vapour, subsequently fed to the rotating bed and the vapour condensed in a total condenser. The liquid composition leaving the condenser was 9% ethanol and 91% methanol. For comparison with the gravity packed bed, using 12 mm Intalox saddles, the same mixture was distilled, with results as shown in table 1.4. It can be seen that up to a nine fold increase in the gas-side mass-transfer coefficient was achieved.

Table (1.4):Mass Transfer Coefficient for Methanol-Ethanol system.

Vapour flow rate x 10^3 mol/m^2 s	Mean Acceleration., m/s^2	K_Gx 10^5 mol/m^2 s	k_Ga mol/m^3 s
8.60	2147	44	0.72
8.42	9.8	5.4	0.034

Munjal *et al* [M3] investigated the mass-transfer performance for two different rotating models: rotating disk and rotating blades. The Penetration theory and the asymptotic solution for liquid film thickness were assumed to apply. They studied the effect of rotational speed on the enhancement of the volumetric mass-transfer coefficients. They modified Davidson [D1] model to estimate HTU for flat surfaces and indicated that for constant Grashof number values based on the average bed radius and the centrifugal force, the resultant model may be used to estimate the mass transfer coefficient K_L in RPBs. For the gas-liquid mass transfer, they found that both liquid-side volumetric mass-transfer coefficient and interfacial area varied with the rotational speed (ω), at powers of 0.61 to 0.75 and 0.28 to 0.42, respectively.

Munjal *et al* [M4] studied the effect of various operating parameters such as bed volume and rotational speed on the gas-liquid interfacial area in rotating beds. To determine the interfacial area, they used the chemical method which is based on absorption with fast chemical reaction. Carbon dioxide was absorbed in and reacted with sodium hydroxide solution in a bed packed with 3mm glass beads. The gas-liquid interfacial area was found to increase with both the liquid flow rate and rotational speed as follows:

$$a_e \alpha Q_{NaOH}^{0.3}$$

$$a_e \alpha \omega^{0.42}$$

Keyvani and Gardner [K1] studied the operating characteristics of rotating packed beds made of porous rigid foam-like aluminium packing with specific surface areas of 656, 1476 and 2952 m^2/m^3 all having a bed porosity of 0.92. The inside and outside radii of the bed were 12.7 and 22.85 cm, respectively, with an axial height of 4.4 cm. The mass-transfer results were found in close agreement with those obtained by Vivian *et al* [V1].

Tung and Mah [T1] used the penetration theory to describe the mass transfer behaviour in the HiGee process, for two different packing materials: glass beads and copper gauze. The estimation of the mass transfer coefficients was based on the effective interfacial area, which was estimated by two different empirical correlations, instead of the total surface area per unit volume of the equipment. Based on limited experimental data from Ramshaw [R2] it was concluded that the Penetration theory can describe, reasonably well, the mass transfer performance in HiGee process.

Kumar and Rao [K2] studied the mass transfer performance in HiGee using wire mesh packing material having a surface area and porosity equal to 4000 m^2/m^3 and 0.95,

respectively. They obtained higher values of volumetric mass transfer coefficient than those in the conventional packed beds by approximately an order of magnitude.

Sirenko and Kulov [S4] investigated the fluid dynamics and mass transfer in rotating packed beds. Three packing elements were used: corrugated disk, screen type elements and perforated plate sheets having surface areas and porosities of 179, 358, 125 and 0.978, 0.955, 0.995 respectively. Tests were carried out at relatively high speed ranging from 1500 to 5000 rpm, corresponding to centrifugal acceleration of 155 to 1710g respectively, and flow rates were varied from 1.04 to 2.89 kg/m^2s and from 0.354 to 26.5 kg/m^2s for gas and liquid respectively. The screen type packing was used in air stripping of ammonia solution from water and carbon dioxide from water to study the mass transfer with gas phase and liquid phase limitations, respectively. In the liquid film limited system their findings are, however, unusual as it was appeared that the height of transfer unit HTU increased as the gas flow rate increases i.e. there was easier separation. Moreover, in the CO_2-water system, the height of transfer unit was independent of the liquid flow rate. The reported data of HTUs was in the range between 10 to 30mm at 5000 rpm for both the liquid and gas control mass transfer respectively.

Bucklin *et al* [B2,B3] and Schendel [S5] highlighted different features of the HiGee, and reported different commercial applications of the HiGee in natural gas treating facilities. Mohr [M5] has described the HiGee test runs of different systems for a wide range of process conditions and physical properties. Martin and Martelli [M6] reported preliminary results on the distillation of cyclo-hexane and pentane at pressure of 12 atm using rotating packed beds. Using a rotor with a packing depth of 21.2cm they determined an average value of HETP of 22mm. About nine theoretical stages were achieved.

Singh [S6] studied the application of HiGee in VOC removal from ground water. It was claimed that HiGee was prone to fouling, which can be caused by the presence of some inorganic elements in water.

Al-Shaban *et al* [A2] discussed a large scale type of HiGee separator, in which the liquid is the continuous phase, and the rotor's outside diameter was 1m. Up to 4.3 transfer units were obtained. However, they reported an unusual trend in the mass transfer results whereby there was a reduced performance at higher speeds of rotation. These observations were attributed to the size and the maldistribution of the bubbles within the rotor. They also provided some cost data for a 0.5m rotor used in gas dehydration in offshore duties where the gas was the continuous phase. A significant reduction in both weight and cost was reported in comparison with a conventional column.

Zheng *et al* [Z3] highlighted recent progress in the application of RPBs in different processes such as:

1. Water Deareation: a tentative economic comparison, between existing technologies and RPBs, was presented in terms of capital cost, energy consumption, footprint area, weight and height. Apart from the energy consumption which may be in conflict, all other factors showed significant savings.

2. Gas Desulfurisation: to produce ammonium sulphite and bisulphate by absorbing SO_2 in ammonia or ammonium bicarbonate. Significant savings in process time and energy consumption were achieved.

3. Production of Ultrafine Particles (nano scale) using RPBs as a reactive precipitator to produce $CaCO_3$ particles from CO_2 and lime $Ca(OH)_2$. Significant reduction in process time and a tighter and small size distribution were reported.

Xumei *et al* [X1] investigated the application of RPBs in an oxygen consuming fermentation process with liquid film mass transfer limitations. The process was to oxidise, sodium sulphite anhydrous in xanthen gum aqueous (XGA) which is a pseudoplastic non Newtonian fluid, by means of aeration. They investigated the effect of XGA's apparent viscosity and surface tension, for different concentrations, on mass transfer. The volumetric mass transfer coefficient was found to be higher by 5-20 folds than that in a stirred tank reactor.

Liu *et al* [L1] studied the air stripping of ethanol from its solution in water. Enhancement was achieved for the volumetric mass transfer coefficient as a direct result of the application of the centrifugal acceleration. The values of the volumetric mass transfer coefficient were found to vary with the centrifugal acceleration raised to the power 0.25:

$$K_G a \; \alpha \; g^{0.25}$$

The reported pressure drop data were relatively high as the porosity values of the packings used were 0.533 and 0.389, respectively.

Zheng *et al* [Z4] highlighted the relevant progress of the commercialisation of the RPB technology in China. The results of using RPBs in potential target applications such as particulate removal, reactive precipitation, polymer devolatisation, absorption, stripping and bio-oxidation were discussed.

1.8.1-Advantages of Rotating Packed Beds.

RPBs, have several advantages which accordingly can made them desirable units: small size equipment, high intensity providing low height of transfer unit and low residence time, hence less chemical inventory during processing. The first feature can be a

crucial one if the space and weight of particular units, are at a premium as in offshore platforms. Another feature is the low residence time that will make HiGee advantageous in selective removal of acid gases such as the removal of H_2S from natural gas. RPBs can still be favourable to accomplish certain duties because of the compactness of these units even if fabricated from exotic/expensive materials such as titanium or stainless steel.

1.8.2-Disadvantages of Rotating Packed Beds.

RPBs rotate similarly to the widely familiar equipment such as pumps, compressors, and blowers. Also they require the use of seals such as face seals or labyrinth type seals for rotors at modest speeds. Furthermore as only 20~25 stages per machine basket can be achieved, due to distribution consideration, a multiple of machine baskets (either arranged in parallel or sequence depending upon the target duty) may be needed to achieve difficult separations. Pressure drop is relatively high in RPBs, nearer to that in a plate column rather than the packed equivalent. This is largely because of the enhanced frictional pressure drop with the static pressure drop increases as a result of the application of the high centrifugal acceleration environment. A typical liquid velocity at the rotor tip of 50 m/s will incur an energy penalty as a result of the loss of kinetic energy. This may be significant at high liquid flows.

1.9- Packed Bed Design

1.9.1-Mass Transfer Equations in Rotating Packed Beds.

For a differential volume ΔV figure 1.5 the material balance equation can be written as follows:

$$\{mass \text{ in } \} - \{mass \text{ out}\} = \text{ Rate of Stripping}$$

Fig.(1.5): Mass Balance in Packed Bed.

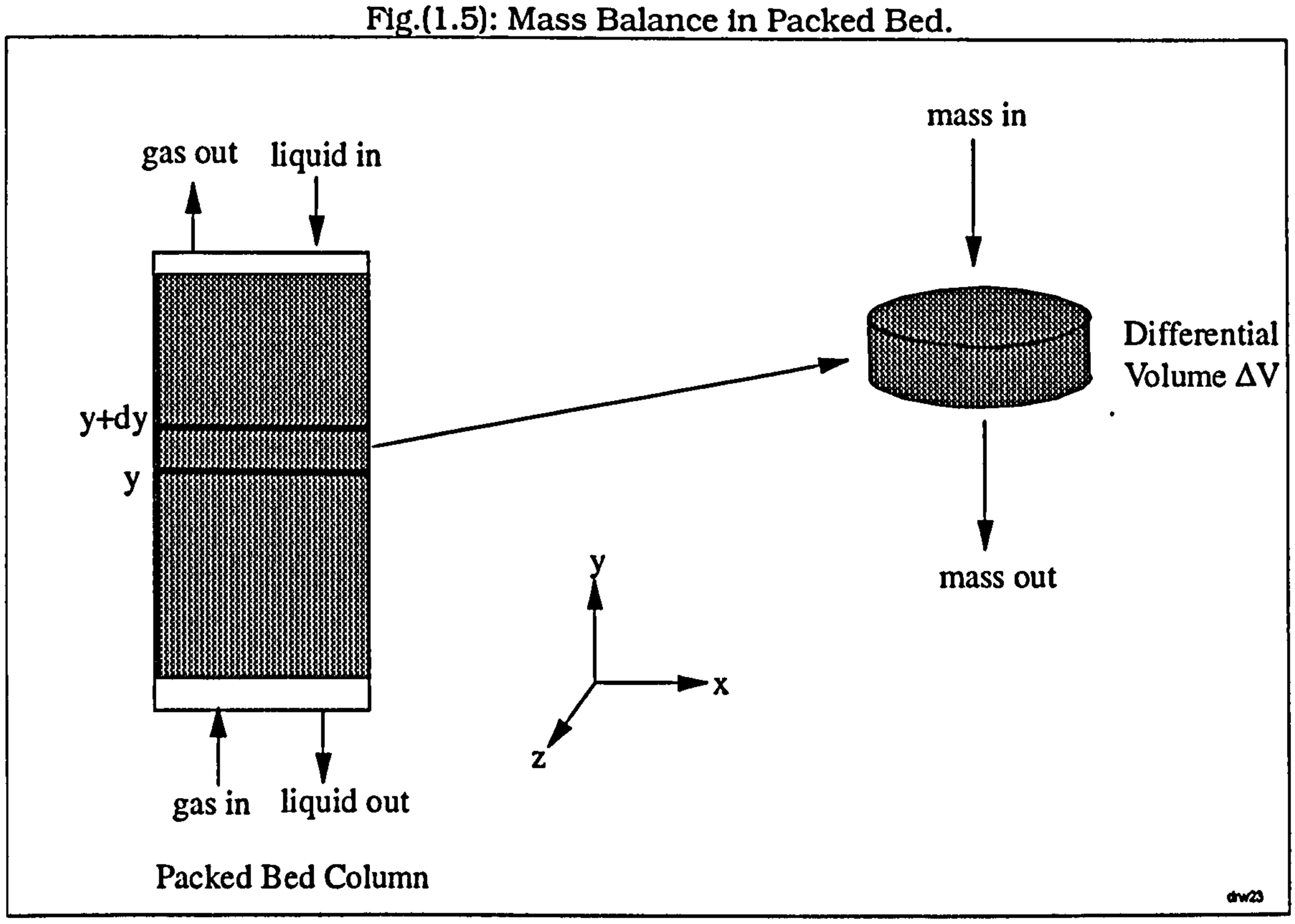

$$d(Q_L\, c) = K_L a(c - c^*)dV \qquad (1.9.1)$$

where a is the interfacial area per unit volume of the packing section and dV is the differential volumn of the packing. Integrating equation 1.9.1 the volume of the bed needed to accomplish a given stripping for liquid phase control mass transfer is given by the following equation:

$$V = \frac{Q_L}{K_L a} \int_{c_1}^{c_2} \frac{dc}{c - c^*} \qquad (1.9.2)$$

For a dilute solutions the above equation can be expressed in terms of the liquid mole fractions as follows:

$$V = \frac{Q_L}{K_L a} \int_{x_1}^{x_2} \frac{dx}{x - x^*} \qquad (1.9.3)$$

Equation 1.9.3 can be expressed in terms of the height of the bed H as follows:

$$H = \frac{Q_L}{A\,K_L a} \int_{x_1}^{x_2} \frac{dx}{x - x^*} \qquad (1.9.4)$$

Equation 1.9.4 can be expressed in the familiar way as:

$$H = \frac{L}{\rho\,K_L a} \int_{x_1}^{x_2} \frac{dx}{x - x^*} \qquad (1.9.5)$$

where A is the cross-sectional area. The integral part in both equations 1.9.3 and 1.9.4 is known as the NTU (Number of Transfer Units) and the terms (Q_L/AK_La) or ($L/\rho K_L a$) represents the Height of a Transfer Unit HTU. For constant values of Henry's or equilibrium constant in a dilute solution, the NTUs for such systems can be expressed as:

$$NTU = \frac{S}{S-1} \ln\left(\frac{\frac{x_{in}}{x_{out}}(S-1)+1}{S} \right)$$

where S is the stripping factor which is defined as the ratio of the between the slopes of the equilibrium and the operating lines as shown in figure 1.5:

$$S = \frac{mG'}{L'}$$

where G' and L' are the molar gas and liquid flow rates respectively and m is the equilibrium constant. The total height of the bed, H, can be found from the following equation:

$$H = HTU \times NTU \qquad (1.9.6)$$

Fig. (1.6) : Mass Transfer Stripping: x-y Diagram for a Dilute System.

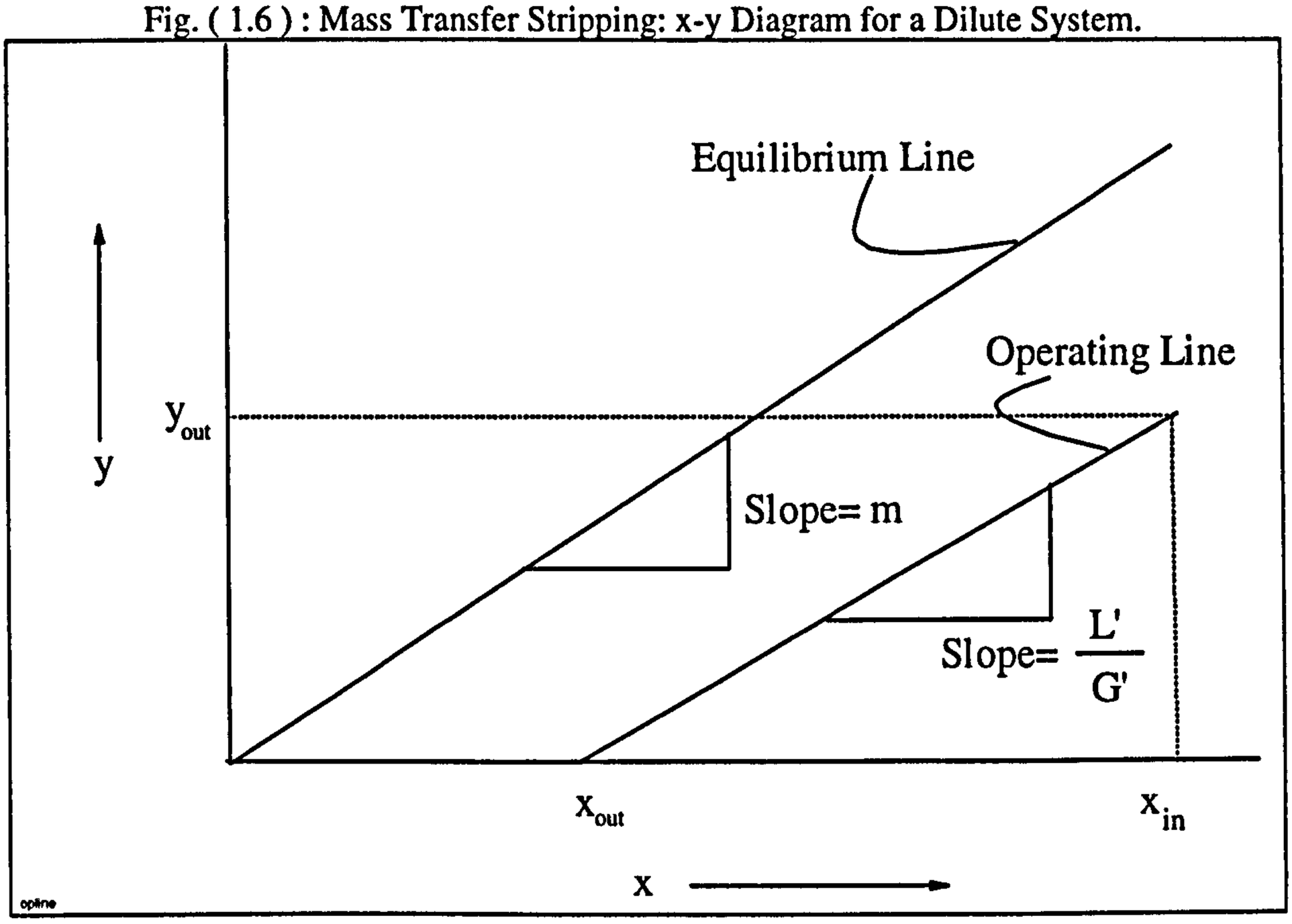

Similarly the performance of RPBs is determined on the basis of: (a) the packed height or radial depth (R_O-R_I), and (b) height of transfer unit HTU or height equivalent to a theoretical plate HETP and therefore the number of transfer unit in RPB can be expressed as follows:

$$NTU = \frac{R_o - R_i}{HTU} \qquad (1.9.7)$$

R_o and R_i were the outside and inside radii of the bed.

1.9.2-Thermodynamic Consideration.

As shown above in figure 1.6, the ratio of the slopes between the operating and equilibrium line will determine the stripping factor and hence the required transfer

units (NTU) for a given separation duty (x_{in}/x_{out}). The equilibrium data can further be used to ascertain more about the driving force ΔP for the solute between the liquid phase vapour pressure, P^{vap} and the gas phase the partial pressure, P^{i} .

1.9.2.1- Phase Equilibria.

At equilibrium in a closed system containing an aqueous phase, an organic phase and a gas phase, the Henry's law constant can be defined as the direct ratio between the compound's vapour pressure to its solubility in the water. Thus at equilibrium the Henry's constant can be expressed as:

$$H = \frac{P^i}{C_l}$$

where:

H, is Henry's constant of the solute (atm-m^3.mol^{-1})

P^i, partial pressure of the solute (atm)

C_l liquid phase solute concentration (mol.m^{-3})

Alternatively, Henry's constant can be expressed in terms of the distribution coefficient: at pressure of 1 atm the weight of 1 m^3 will be 10^6 g, thus,

$$K = \frac{y_i}{x_i} = H \times \left(\frac{atm - m^3}{mol}\right)\left(\frac{1}{1atm}\right)\left(\frac{10^6}{18}\right)\left(\frac{mol\,H_2O}{m^3}\right)$$

The distribution coefficient or Henry's law constant depends on temperature and it can be empirically described by an Arrhenius type equation. Gosset *et al* [G2] discussed several methods and various factors affecting the results of each method. They referred to several experimental methods used to determine Henry's law constant such as batch air stripping and equilibrium partitioning in closed system. Other methods have been

reported such as the direct method of Leighton and Calo [L2] and the Multiple Equilibration method of Munz and Robert [M7].

Usually, solubility data is not available and it may be estimated by using one of the group contribution methods such as UNIFAC (UNIversal Functional group Activity Coefficients) Fredenslund *et al* [F2]. The model is a semiempirical thermodynamic model used to estimate the activity coefficient of a compound in liquid solution and the method can be applied to any system provided its parameters are available.

Leighton and Calo [L2] gave an expression for the distribution coefficient for different chlorinated hydrocarbons, benzene and toluene in the form of K=exp (A-B/T), where T is temperature is in ^{o}K and the temperature range was between 0-30 ^{o}C. For Ethylene Dichloride (EDC) the values of the constant A and B were 16.05 and 3539 respectively. Leighton and Calo[L2] showed that the regressed results for all components investigated have a random error of +/- 0.5 ^{o}C in the temperature range and 5.0% due to the overall experimental error. Furthermore, they showed that UNIFAC model, consistently overestimate the temperature dependence of the activity coefficient.

1.9.3-Determination of the Hydraulic Capacity.

In packed beds, the diameter of the packed bed is determined in terms of liquid, gas mass fluxes and packing surface area and porosity. Using the Sherwood plot, figure 1.1 to determine the flooding gas velocity (U_g), usually 50 to 70% of the flooding velocity is used to determine the diameter because the bed must operate at a velocity lower than that which causes flooding. From the Sherwood plot, it can be seen that if the acceleration 'g' is increased to several g's, by applying centrifugal environment on the bed, then to sustain the equivalent flooding velocity, a more dense packing material can be used providing higher surface area per unit volume for the mass transfer process. Detailed flooding behaviour in rotating packed beds is discussed in chapter 5.

Chapter 2

Experimental Equipment

2.1-Experimental Rig.

In mass transfer runs, air stripping was used to strip ethylene dichloride (EDC) from water. The EDC was used to represent the volatile organic compounds (VOCs) in the air-water system investigated. EDC is immiscible with water above concentration around 2000 ppm, and accordingly, the maximum concentration of EDC used throughout the runs was less than 1000 ppm. Additionally, to meet the University safety regulations, the runs were carried out in a flameproof enclosure equipped with a ventilation system.

Figure 2.1 shows the flow diagram of the test rig. The air was supplied from the departmental compressor, which can supply a maximum flow rate of 5.7m^3/min.. A flameproof pump (0.26kW, model: TOTTON™ Pumps) with a maximum head and flow rate of 8m and 85 L/min., respectively, was used to pump the liquid from the feed tank (capacity ~ 0.45 m^3). A by-pass line was fixed so that the liquid recirculated back to the feed tank. The solute (pure EDC) was introduced from the solute reservoir which

was fixed on top of the steel structure, on which both the feed and discharge tanks were laid. The solute was allowed to flow and mix with the water for about 10 hours which was a sufficient period to ensure equilibrium.

2.1.1-Section Through The Stripper.

Figure 2.2 shows a section through the stripper used throughout this work. The gas was introduced through the rotary union at the rear and flows through the shaft and then enters the bed from the gas plenum via the holes of the back aluminium disc. The liquid enters the bed at centre 'eye' and flows through towards the periphery where it forms a liquid seal that compels the gas to flow counter current to the liquid in the bed.

2.1.2-The rotor.

Figure 2.3 details the rotor dimensions. The packed section has OD = 402mm, ID = 158mm and an axial depth of ΔX = 60mm. The bed is mounted on the back of an aluminium disc with OD = 454mm. The bed was sandwiched between the back disc and the cover, which is made of perspex with ID = 130mm and OD = 450mm. Eight equal cut-outs of 2mm deep were machined out of the perspex cover in order to facilitate the liquid discharge out of the rotor. A peripheral steel lip with 454mm, 450mm and 2mm OD, ID and thickness, respectively, was fixed on the cylindrical shell to help to establish the liquid seal. As the liquid enters the bed it flows through the bed and leaves the rotor through the established liquid seal as shown in figure 2.4. The liquid seal forces the gas to flow towards the eye of the bed. During rotation the gas pushes the inside surface of the liquid seal, and thereby the outside head ($h_{outside}$) of the liquid seal will be greater than the inside one (h_{inside}).

The liquid leaves the rotor and collects at the drain and then flows to the discharge tank. The gas was fed through a rotary union mounted on the rear of the shaft. It flows through the shaft before entering the bed through the seventy gas holes in the back disc. Spacers were mounted at the back of the aluminium disk to form a gas plenum.

Fig.(2.1): Flow Diagram of the Mass Transfer Test Rig

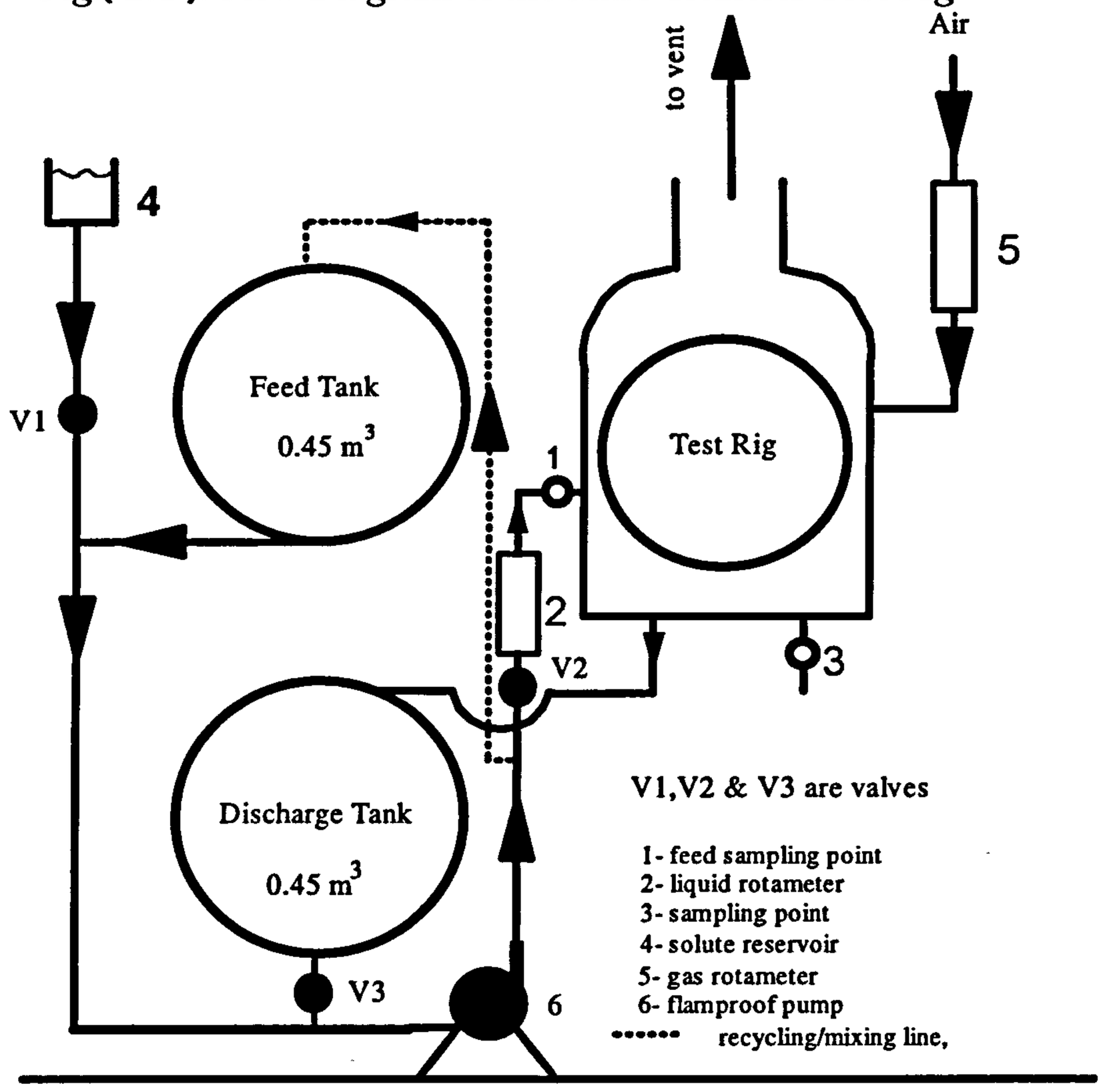

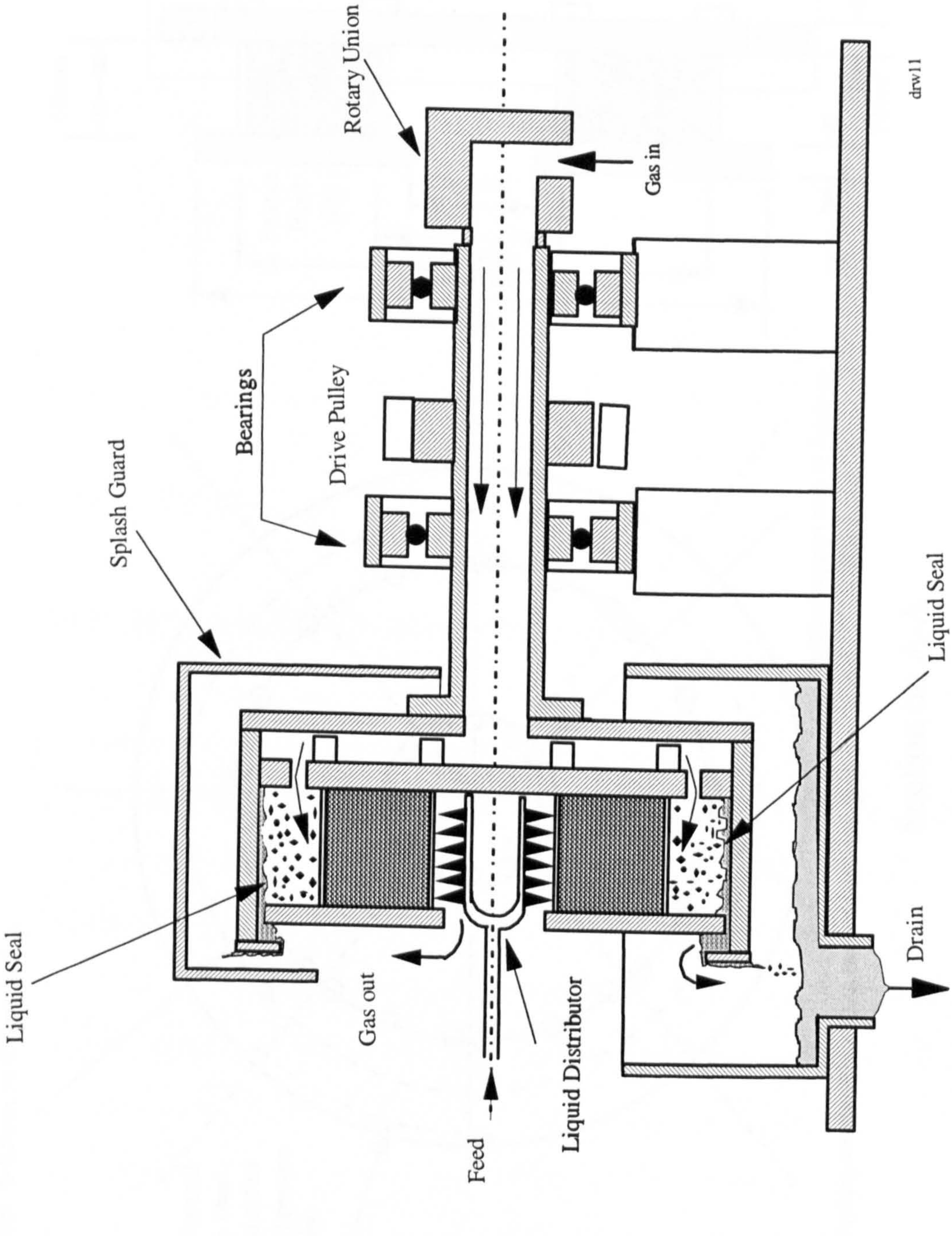

Fig.(2.2): Section Through The Stripper

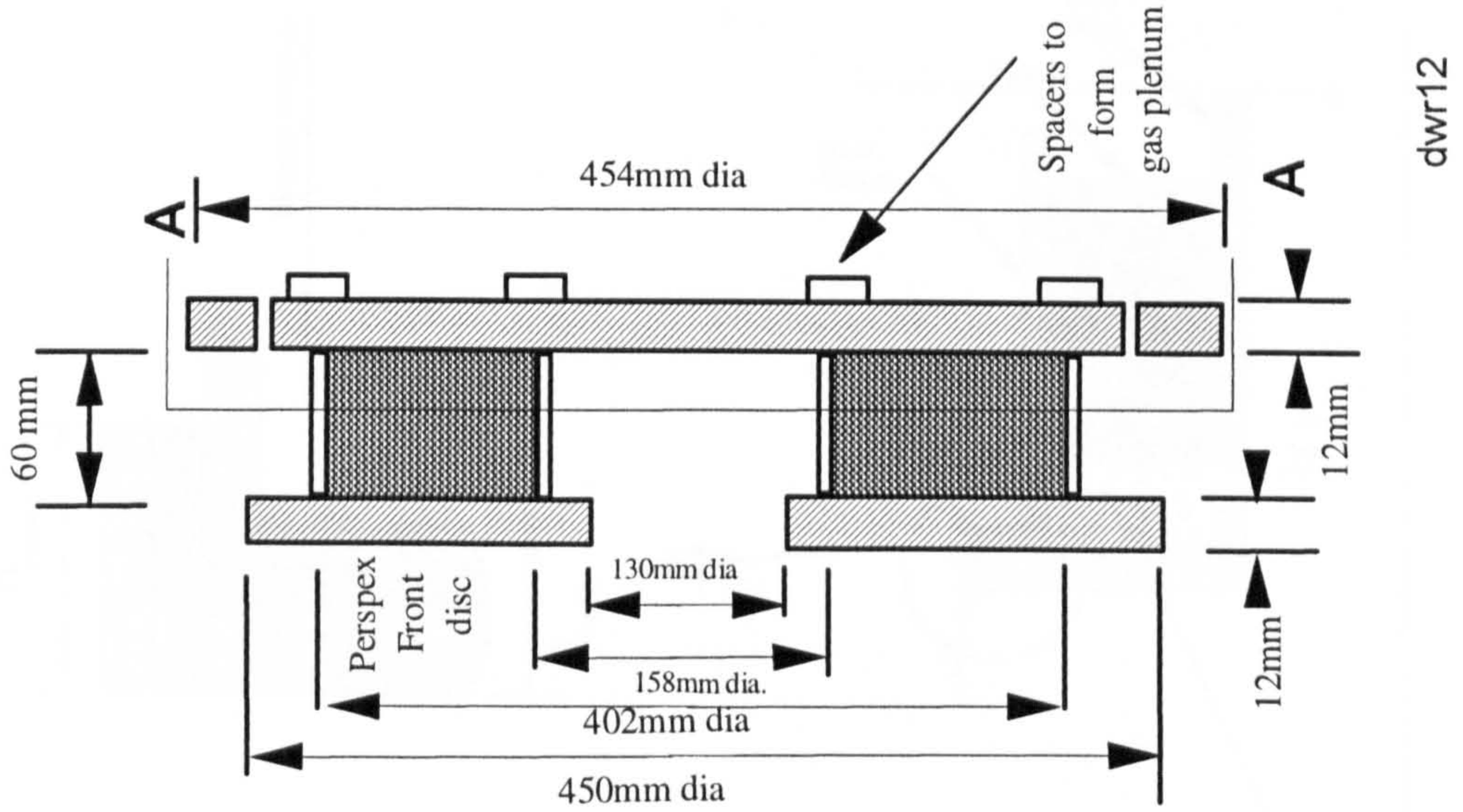

Fig.(2.3): Rotor Details

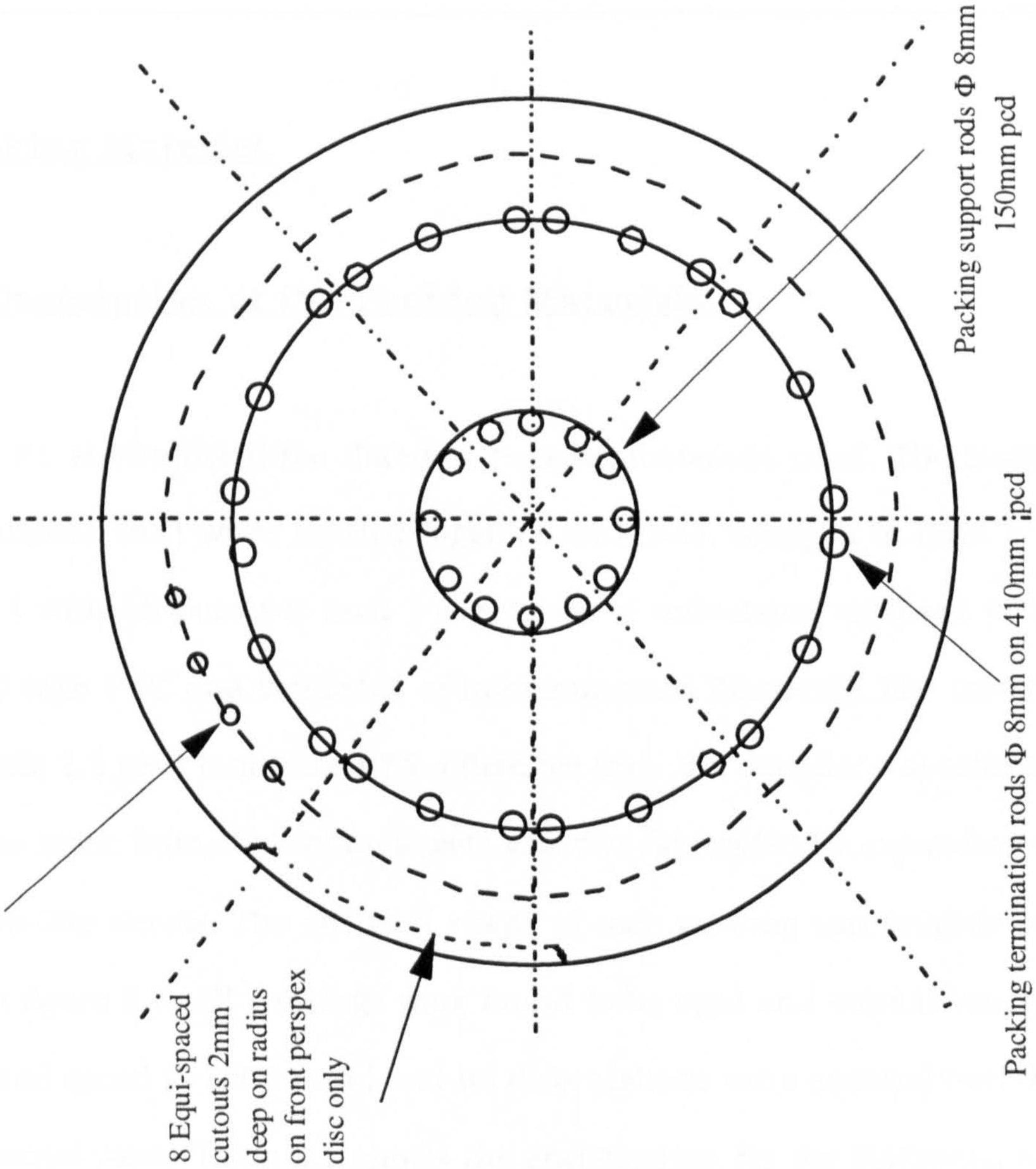

Section on A-A

Fig. (2.4): Liquid Seal Details.

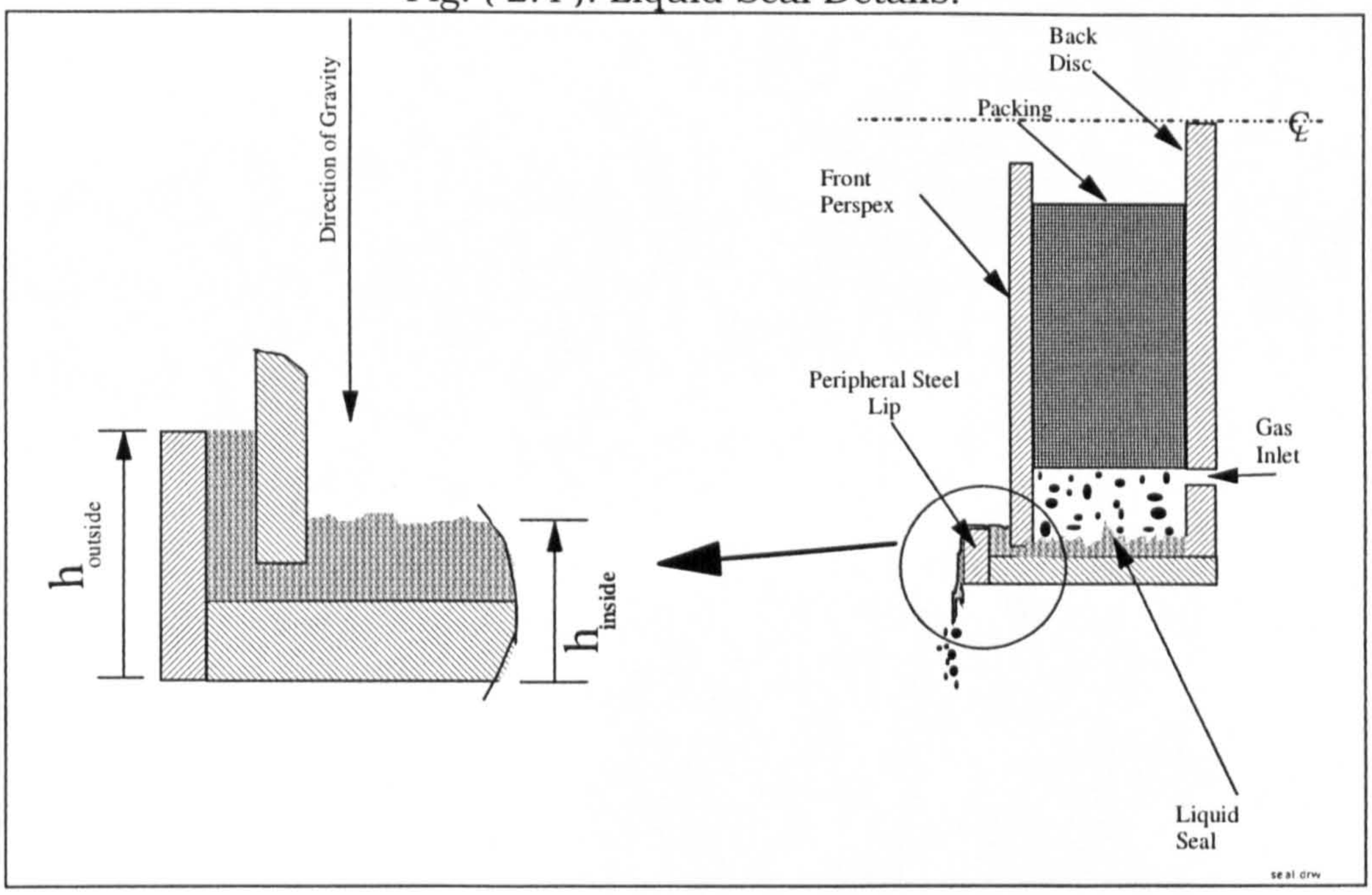

2.1.3-Packing Material.

2.1.3.1- Description of the Packing Materials.

Photograph P1 shows the three different packing materials used. The Knitmesh was made of stainless steel wires knitted together and then wrapped to form a firm tape. The Declon (with 15 pore per inch) was made of reticulated rigidised polyurethane foam coated with PVC and consisted of interconnected filaments. The calculated pore length in table 2.1 gave less than 10% difference from the supplier's specifications. The Expamet was made from aluminium sheets and was fabricated by expanding the sheets to form mesh-like sheets. The skeleton shape of each packing can roughly be depicted as shown in figure 2.5. All packings were found to be rigid and dimensionally stable at high rotational speed (~1500 rpm) and no deformations were encountered throughout the experimental work. Table 2.1 shows the specification for the Knitmesh and Declon filaments and the strand width for Expamet.

Photograph (1)

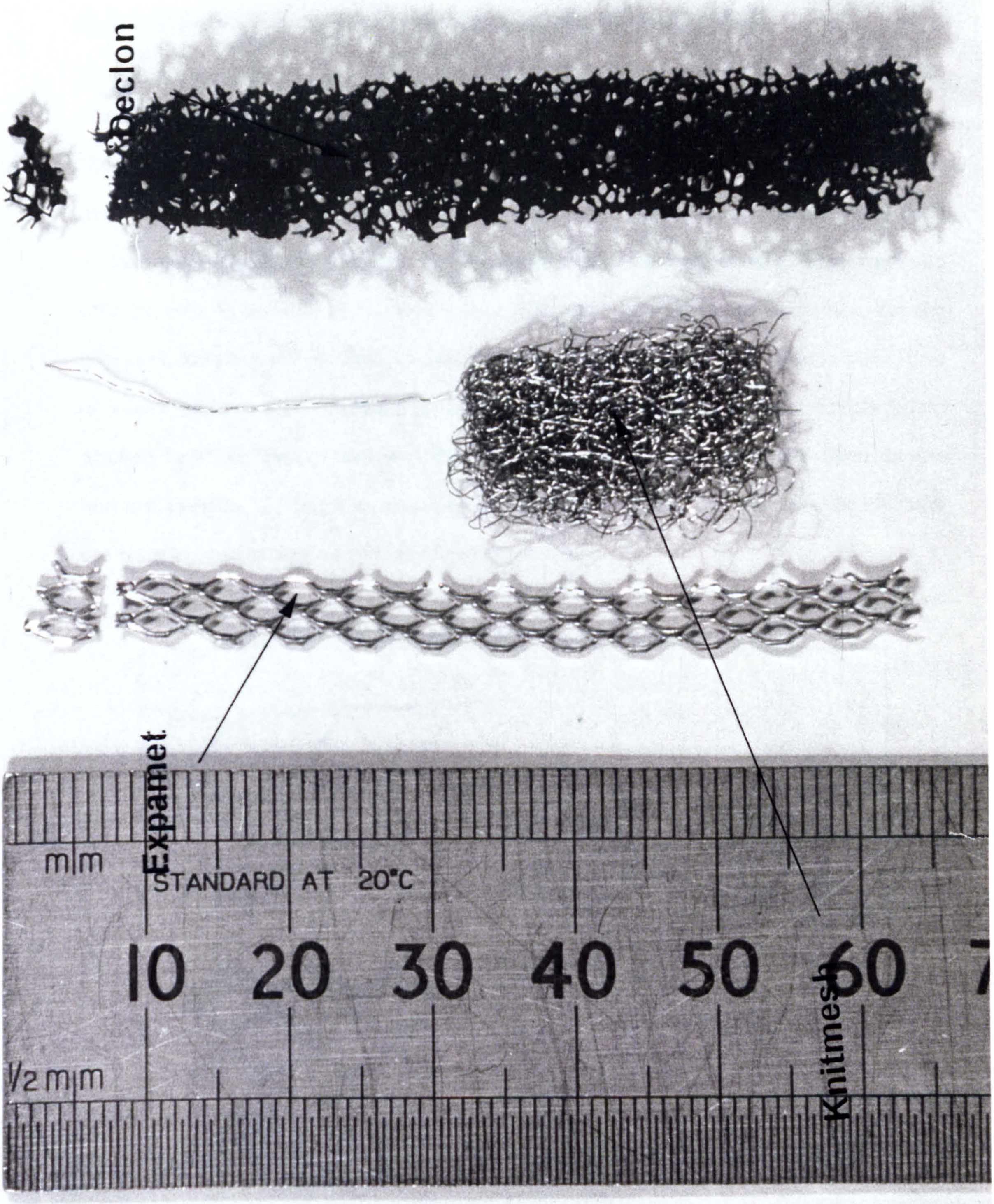

2.1.3.2- Loading of the Packing Materials on the Rotor.

The Knitmesh tape with 60mm thickness was wound on the packing support rods at the eye and the other end of the tape was anchored with the peripheral support rods on dia. 410mm. The Declon sheets were cut according to the bed dimensions and each section had a thickness of 10mm. Consequently, six slices were needed. They were slid into the rotor supported by the fixed packing supporting rods in the back disc. For the Expamet, sheets were cut and placed in similar fashion. Thirty three sheets were used of which sixteen were dimpled thereby forming gaps in between the sheets when stacked together. Each sheet was dimpled in 24 different positions and each dimple had a dimension of 10mm in diameter and 2.5mm in depth. The sheets were slid into the rotor in similar way as with the Declon packing.

Fig. (2.5) The Skeleton Shapes for The Packing Materials.

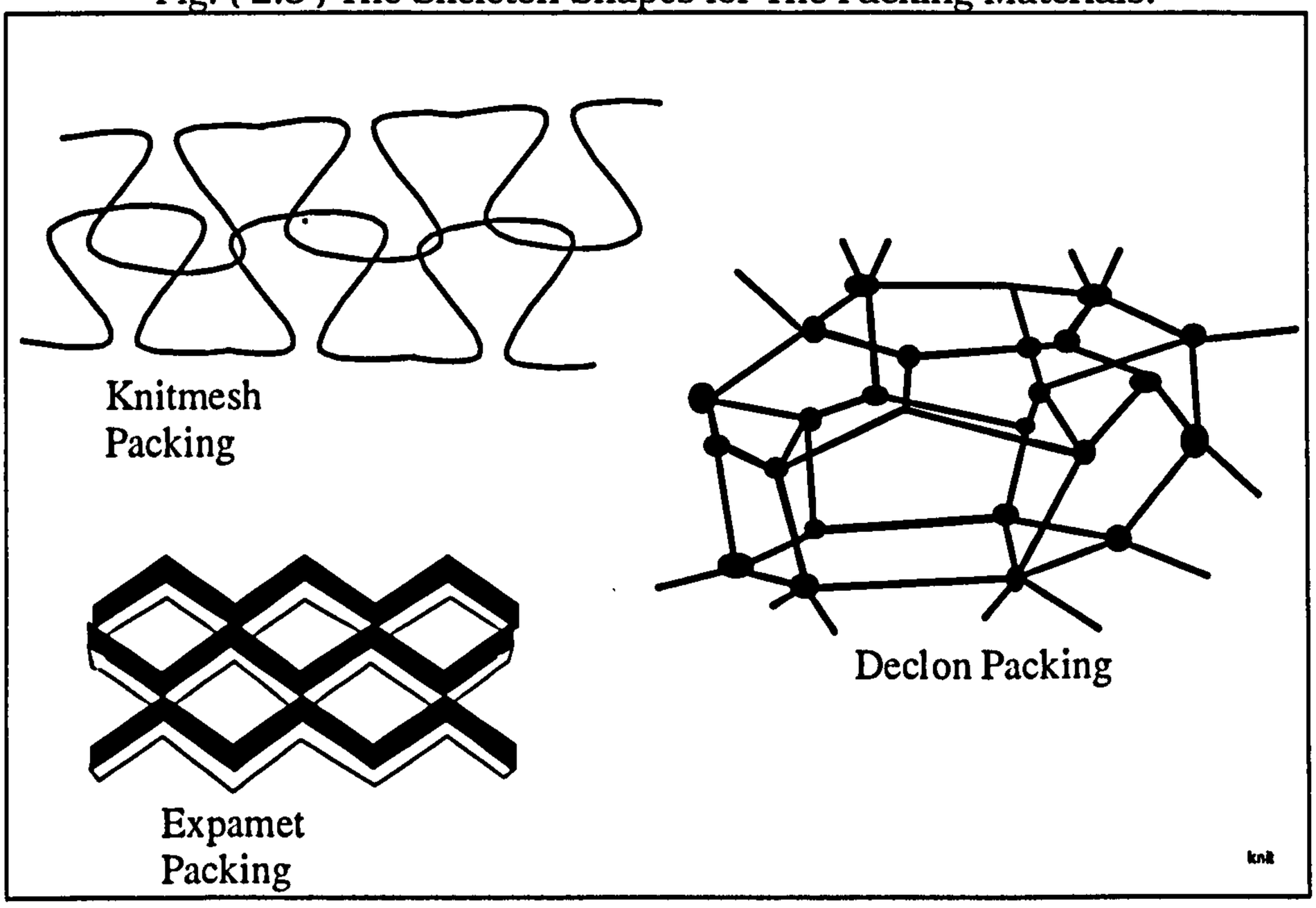

Table(2.1): Specifications for Different Packing Material.

Packing Type	Material	Filament Thickness (μm)	Packing Dry Area (m2/m3)
Knitmesh	Stainless Steel	150	2300
Declon	Polyurethane Foam	230	870
Expamet	Aluminium	500*	1400

2.1.4- The Motor.

A flameproof electrical motor (Brook Crompton 1.5kW model; AE100LB) with variable speed, was used to drive the bed. The motor was connected to the shaft by a belt, which connected the pulley on the shaft with that on the motor.

2.1.5-Liquid Distribution.

Photograph P2 and figure 2.6 show the two different liquid distributors used to distribute the liquid. Stable liquid jets, with a minimal entrainment at the inlet 'eye' of the bed were maintained. The single pipe distributor had (24 x Φ 2.3mm) holes drilled in each of the eight equal surface zones on the circumference. In every zone three holes were machined in one array. The holes were threaded so that they could be plugged if the injection velocity needed to be changed. The other distributor was designed to have an armed configuration (i.e. 4 arms) and in each arm a number of holes with the desired diameter were drilled. Contrary to the single pipe distributor, in the armed distributor the liquid jets had a shorter trajectory to hit the bed than from the single pipe distributor. However, experimental findings showed that the single pipe distributor had higher values of HTUs than the armed distributor. One explanation for the above finding was that for the multi-arms distributor, the deployment of the liquid jets along

Four Arms Disributor

Cylindrical Distributor

Photograph (2)

Photograph (2)

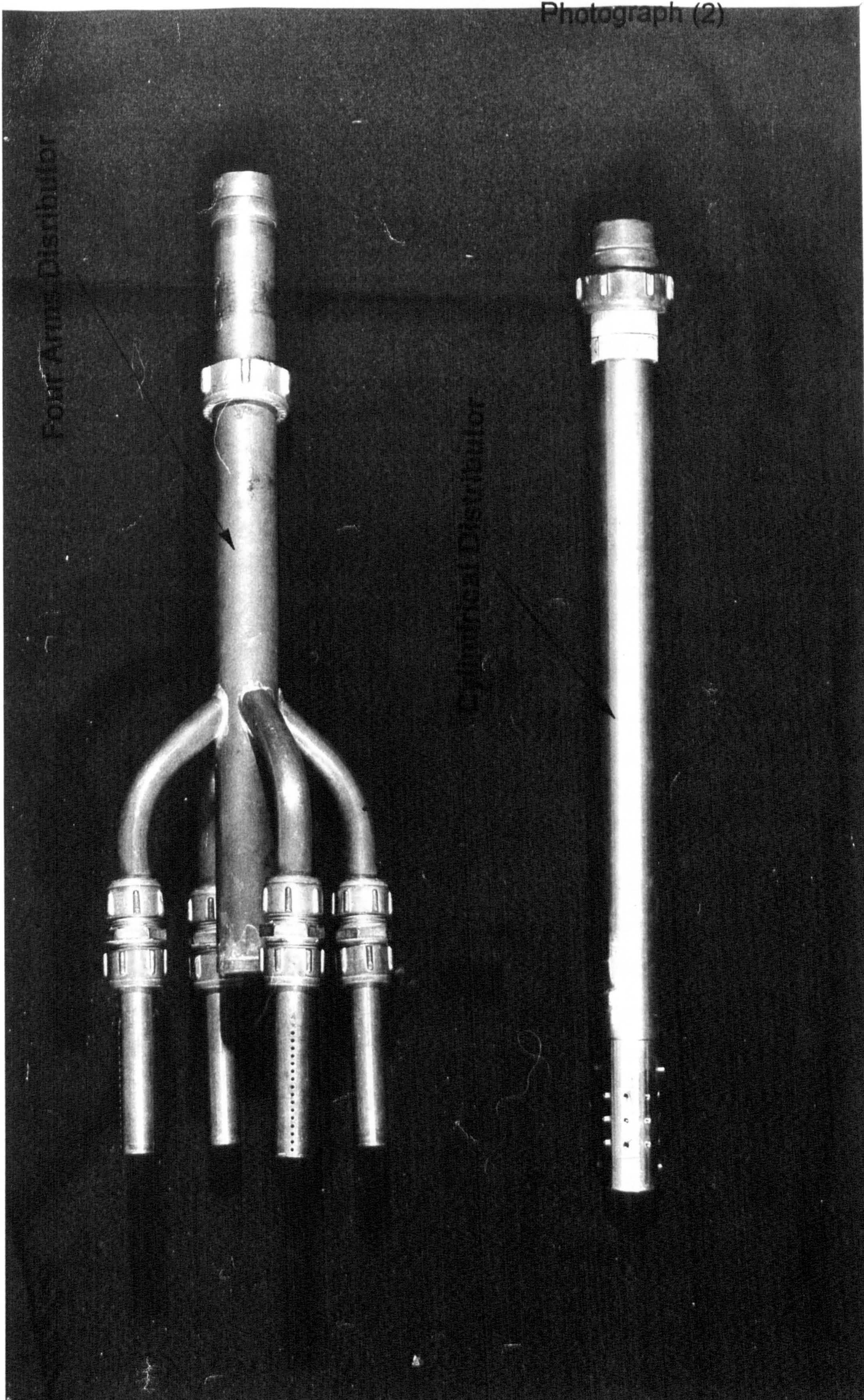

the axial length of the bed was better than the single pipe distributor by which only the central 3 cm of the 6cm axial packing depth was irrigated by the liquid jets.

2.2- The Liquid Sampling Point Positions.

For the mass transfer experiments, the liquid samples were taken from different positions as shown in photographs P3, P4 and figure 2.7. The samples were taken from:

1- Feed sampling point.

2- Peripheral sampling point.

3- Splash guard sampling point.

4- Direct liquid sampling from the liquid seal.

It is worth pointing out that while the bed spins, the removal of a representative liquid sample from the liquid seal was not so easy. After several trials, a direct liquid sampling procedure from the liquid seal was developed. In this procedure a stainless steel tube (1.5mm in diameter) was laid out into the liquid seal, deep into the gap between the frontal perspex and the steel peripheral lip to scoop the liquid samples from the seal. A PTFE extension to the tube was used to help to fill the sampling vials. The scooped liquid was allowed to flow for about 2 minutes before any sample was taken, to ensure a steady state condition was established during every sampling procedure. For the other sampling points, the sampling was straightforward. Feed samples were collected from the feed line before the distributor using a check valve mounted on the line. For every run, a feed sample was taken to account for any concentration changes. The liquid samples leaving the rotor were taken with the aid of the sampling arm shown in photo. 4 and figure 2.7 which could be positioned in such a way to be closer to the periphery of the rotor.

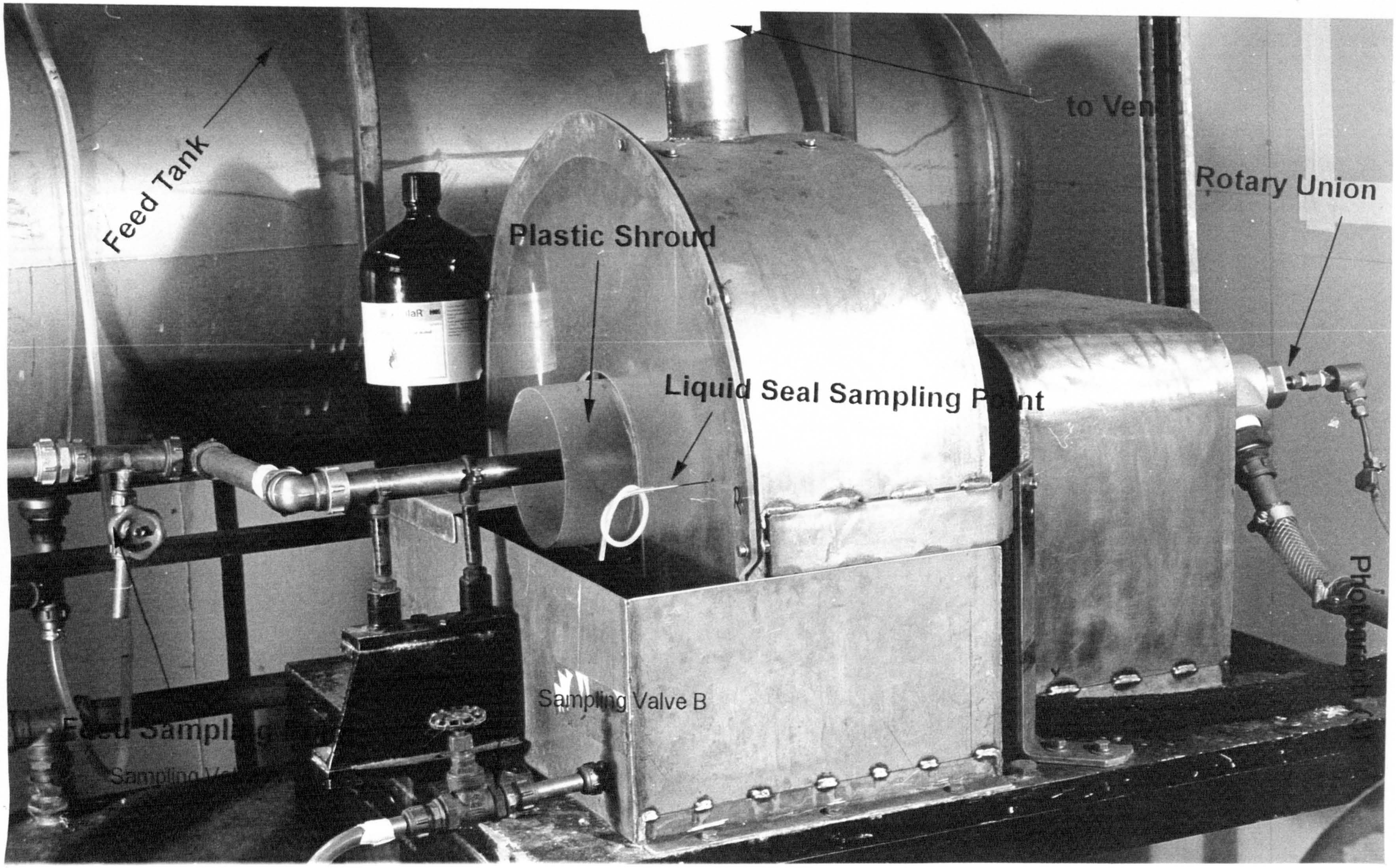
Feed Tank
to Ven
Rotary Union
Plastic Shroud
Liquid Seal Sampling P nt
Sampling Valve B

Photograph (4)

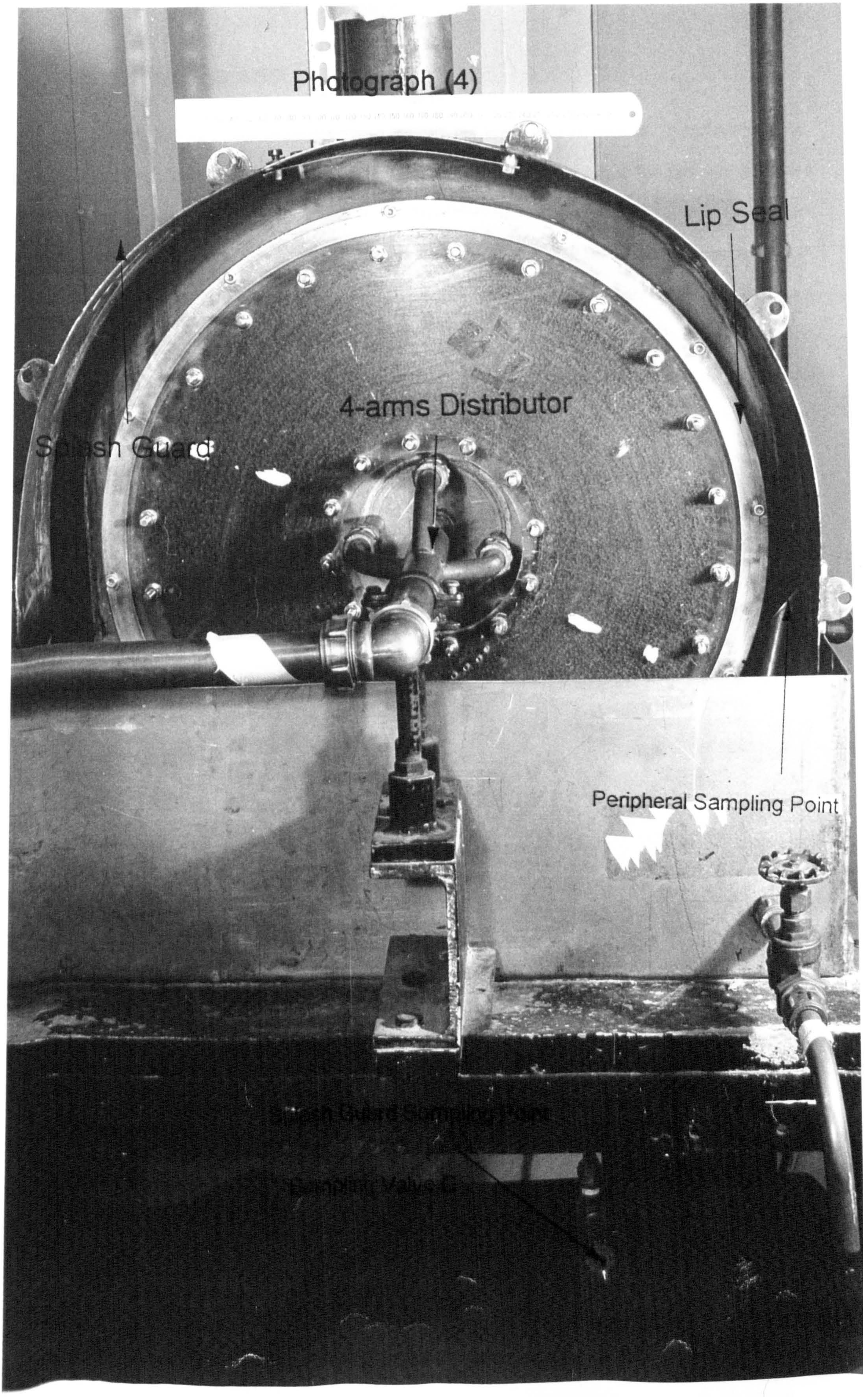

Photograph (4)

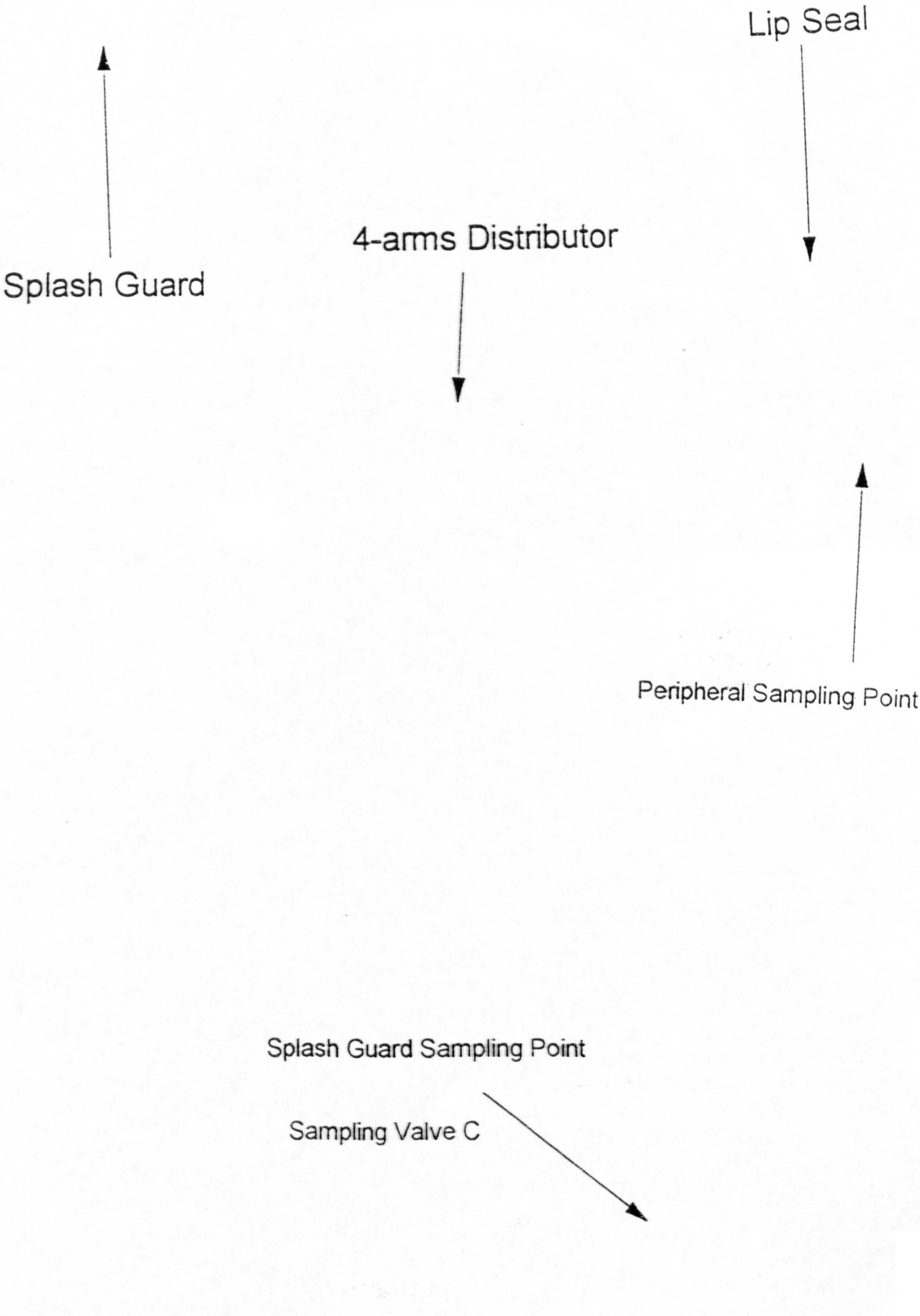

To close the material balance, a gas sample for every run is needed. Details of the gas sampling procedure is given in appendix (C). For every few runs, the gas was analysed and an accepting limit between 5 - 10% error in the mass balance was set for the inclusion of such run in the mass transfer calculation. A few runs were excluded in further consideration and in most of the excluded runs the source of error turned out to be either in the gas sampling procedure such as a gas leak from the gas sampling vessel (before mounting the two Teflon rotoflo™ valves) or gas chromatography misrepresentation of the liquid samples as a result of CG column deterioration. Accordingly, GC calibration was frequently carried out to alleviate any source of error.

Fig.(2.6): Single Pipe and Multi-arm Distributors.

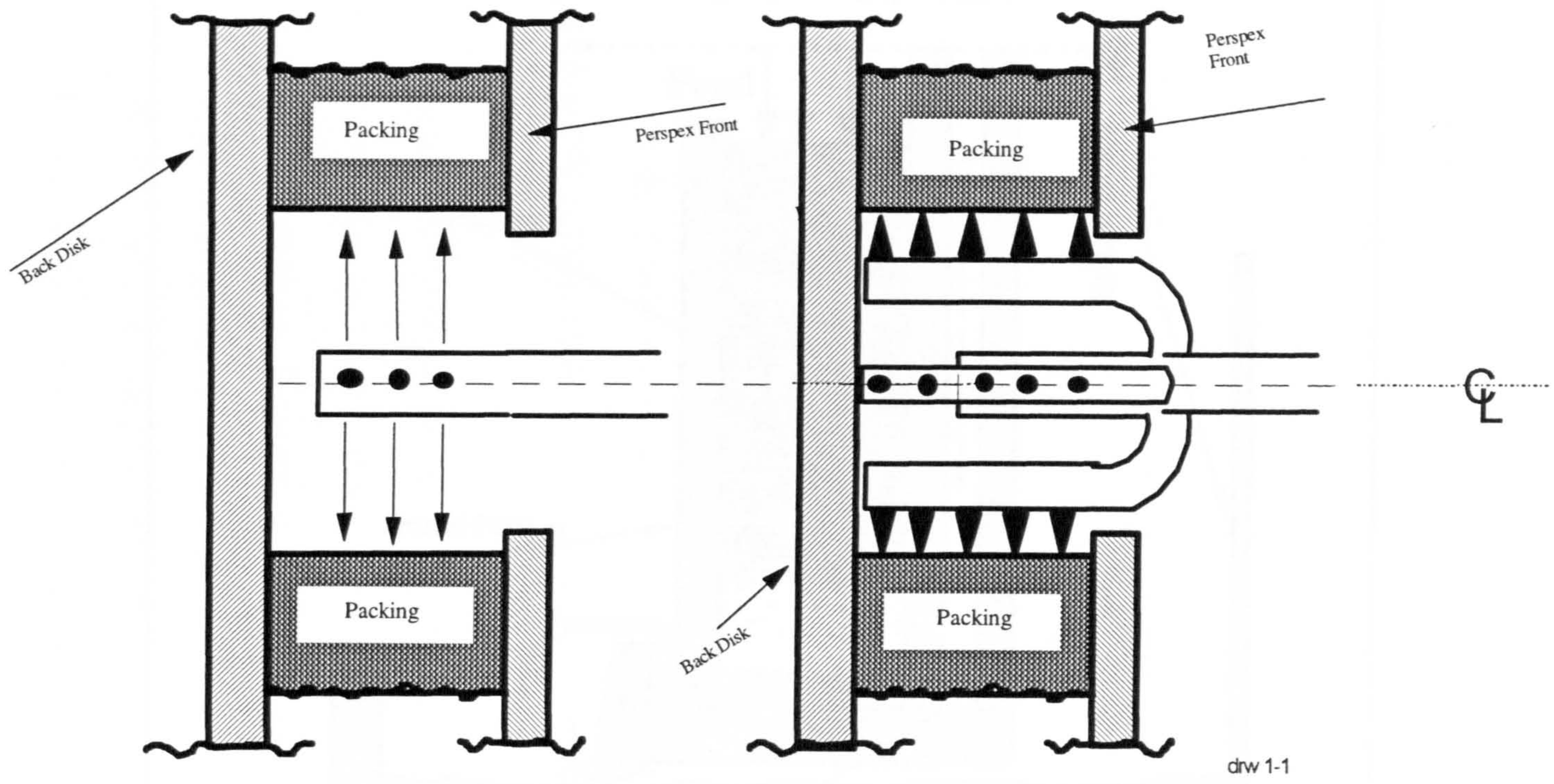

Single Pipe Distributor

4-Arms Distributor

Fig.(2.7): Position of Sampling Points.

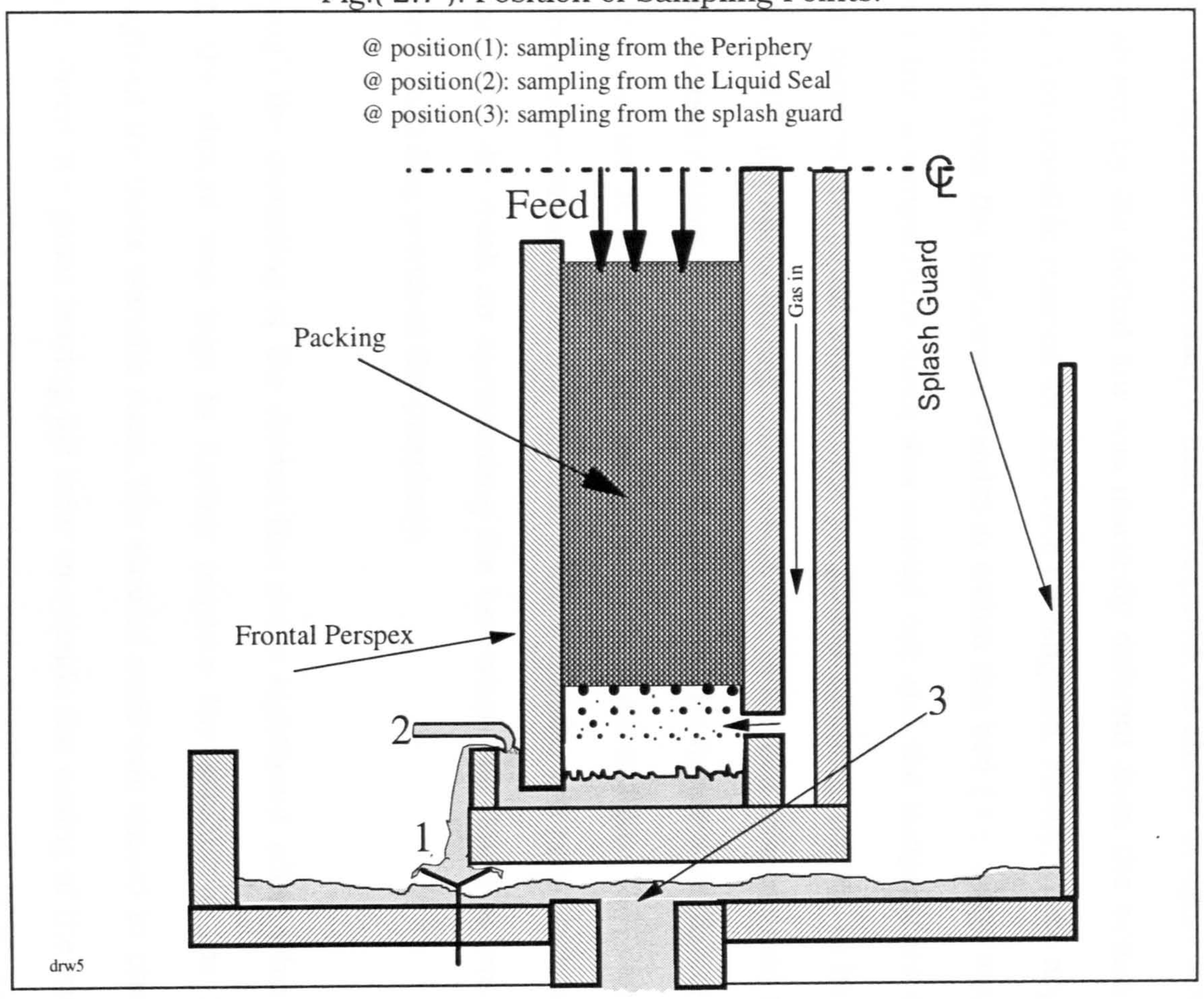

2.3-End Effect.

Normally if there is no gas flow and only liquid is flowing through the bed, at a prevailing rotational speed, the concentration difference between the eye (inlet) and the peripheral sampling points (outlet) should be negligible. However, an unexpected trend was experienced contrary to that anticipated. As shown in figure 2.8 the expected trend shown by the dotted line was markedly different from the actual experimental results. Two possible reasons for this were investigated. Firstly, there might have been a deviation from the isothermal condition within the bed (i.e. some evaporation took place), but a temperature check was carried out and the temperature difference was found, between the liquid feed and the peripheral sampling points, to be less than 1.2 ^{o}C. Secondly, the above finding could result due to the bed rotation and the end effect. When the bed rotates it acts as a centrifugal pump and hence a negligible (or zero) net gas flow cannot be achieved. The end effect, as shown in figure 2.9, can contribute to the above observation in such a way that a mass transfer will take place as result of the contact with the fresh air surrounding the bed when the liquid is sampled from the different sampling points at the periphery.

Although the mounting of the shroud has not a significant effect when the gas was used, the shroud was kept to further improve the quality of the liquid sample throughout the mass transfer runs. The shroud used was shown in photograph P3 to help to divert the gases leaving the rotor to outside the casing of the rotor in order to minimise contact with the liquid leaving the bed at the periphery. It can be seen that there was a noticeable difference between the value of the HTU at every sampling point. Therefore, it is clear that sampling points at the periphery and splash guard incorporated a substantial end effect. It is also clear that the liquid leaving the liquid seal to the splash guard and the liquid collected from the splash guard are all contributing to the end effect of the rotor.

Fig(2.8) End Effect, Φ 1mm, 4 arms Distributor, Gas Off
@ 500 rpm, Q_L = 6.5 L/min.

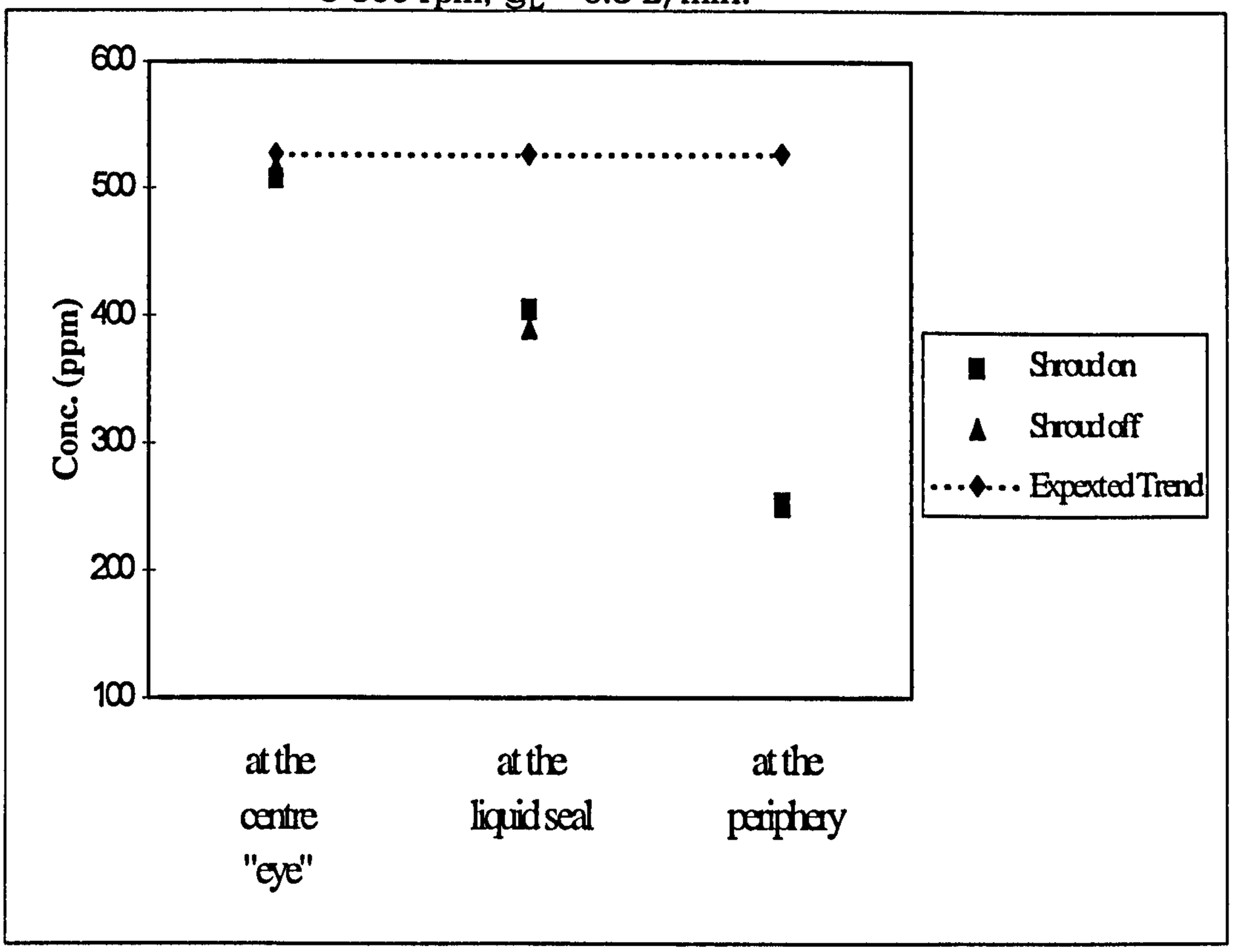

Fig(2.9): End Effect, Different Sampling Point Position, 4 arms Distributor Q_L= 6.5 L/min., @ 500 rpm <T> 21.2 °C.

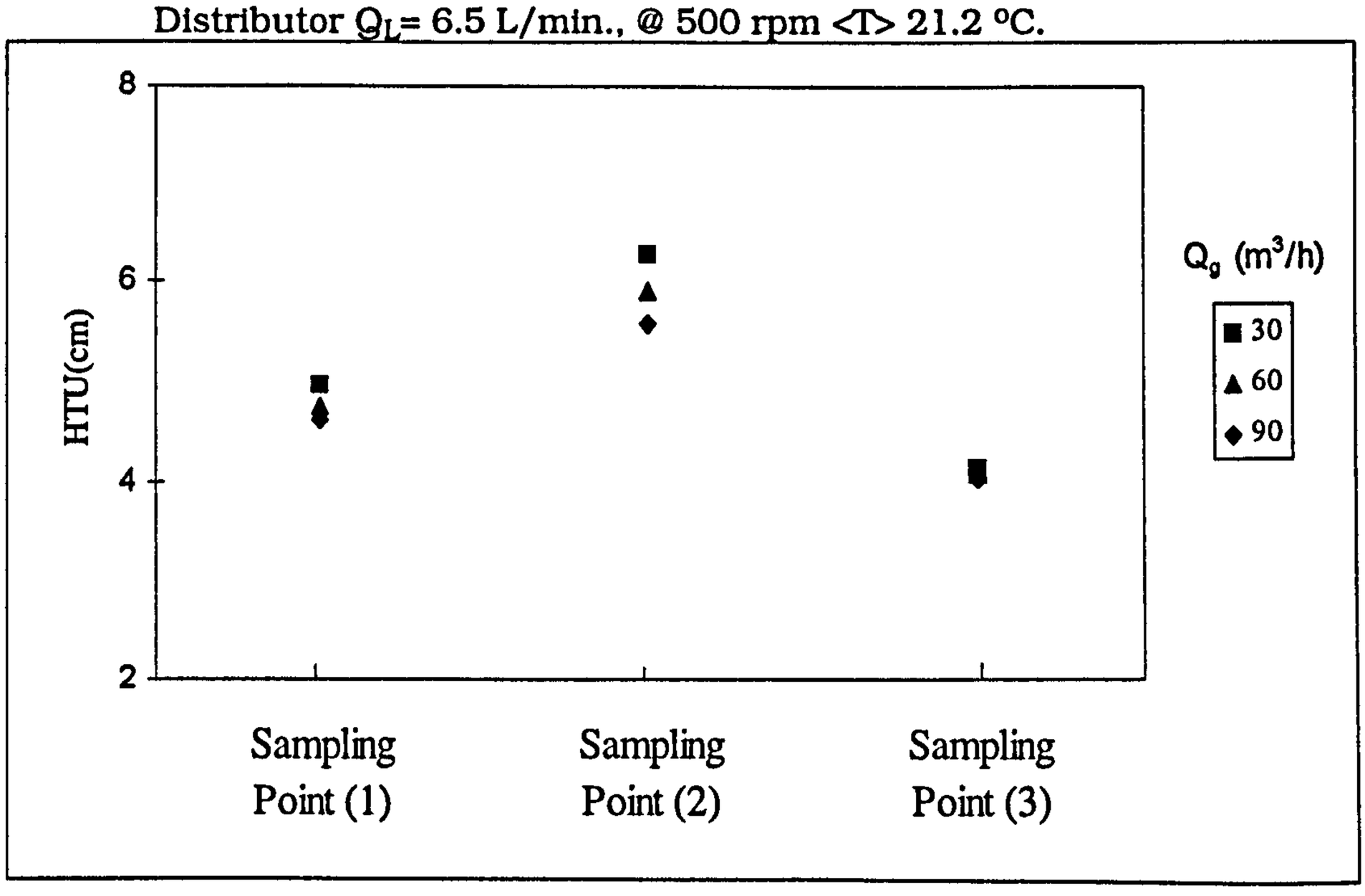

Figure 2.9 shows different HTU values for each sampling point shown on figure 2.7 at three different gas flow rates. The concentration differences observed between sampling points 1,2 and 3 were as a result of the mass transfer that took place because of the direct contact outside the rotor with the air surrounding at the three sampling points. The Liquid seal sample (sampling point 2) which was the most reliable, possibly incorporated some degree of end effect as shown by figure 2.9. Accordingly, all the subsequent HTUs quoted were on the basis of the concentration values at point 2 as shown in figure 2.7 and therefore represent the most conservative estimates possible.

Chapter 3

Mass Transfer: Results and Discussion

3.1- Introduction.

This chapter contains the experimental values of the height of transfer unit obtained using three different packings; the Knitmesh, Declon and Expamet. Comparison between the experimental HTUs and the estimated performance using different mass transfer models is also given. The effective surface area estimation was based on different correlations, namely, the Onda and Mada. Both correlations relate the liquid surface tension and the gravitational force acting on the system to the interfacial area of the packing. To test the importance of the characteristic dimension (in this case the packing's filament length instead of the thickness) in improving the prediction of the HTU's, two additional characteristic lengths for each packing are assumed. Some results with constant (L/G) for higher liquid and gas loadings, using Declon and Expamet are also discussed.

3.2 Mass Transfer Results.

Experimental HTU values have indicated that the height of transfer units varies with the gas flow rate, at constant rpm and liquid flow rate, for the three packings tested. The

experimental HTU values using the multi-arms distributor are shown in figures 3.1 through 3.3. It can be seen that at constant liquid and gas flow rates, the height of transfer unit decreases with an increase in rotational speed and hence this observation would demonstrate that the separation performance was improved as a result of using higher centrifugal acceleration. Furthermore, figures 3.1 through 3.3 show that, as the gas flow rate increases, the height of transfer unit decreases at constant liquid flow rate and rotational speed.

Figure(3.1): Mass Transfer Results for Declon: 4- Arms Distributor.

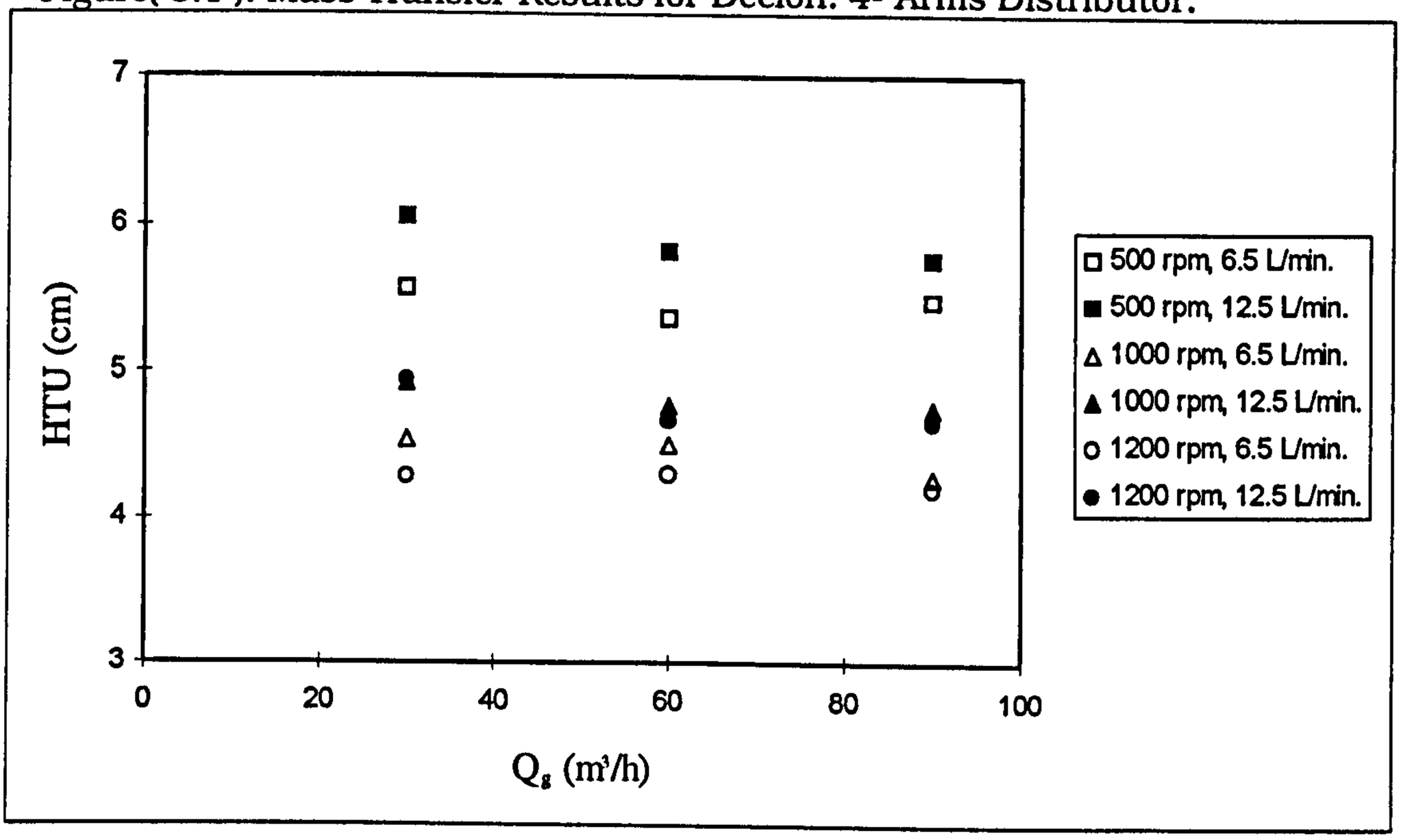

Figure(3.2): Mass Transfer Results for Expamet: 4- Arms Distributor.

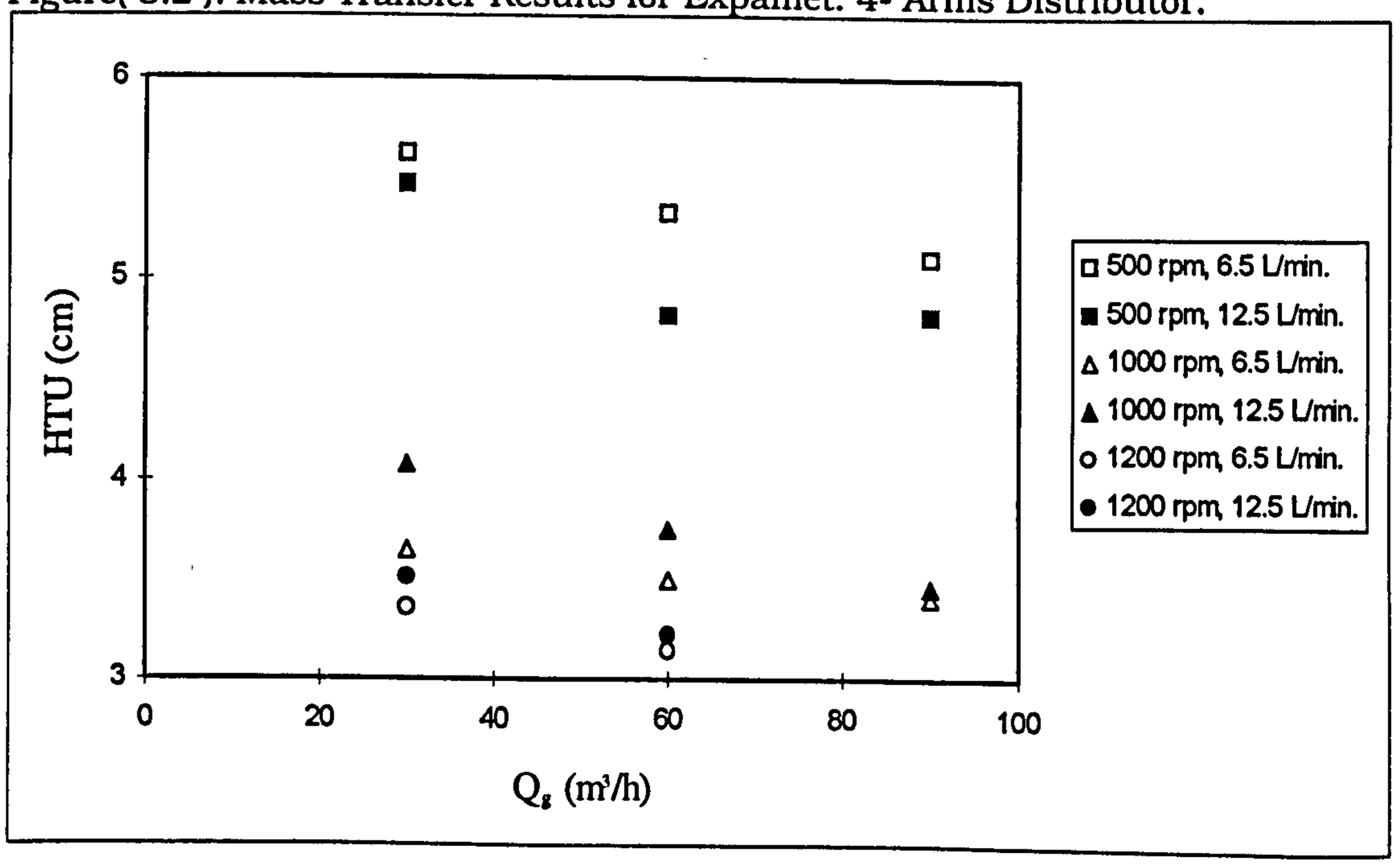

Figure(3.3): Mass Transfer Results for Knitmesh: 4- Arms Distributor.

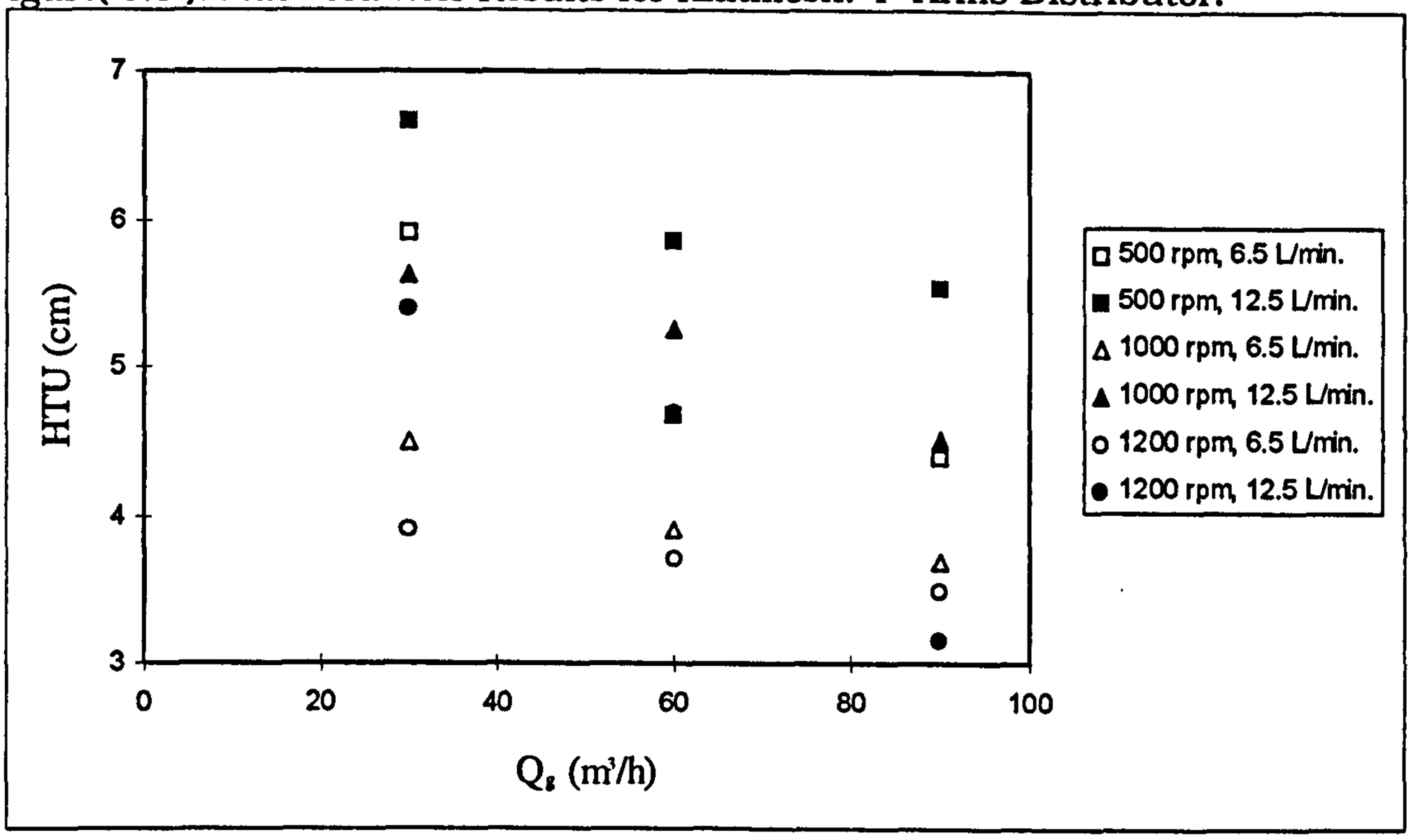

3.3- Effect of Rotor Speed on HTU.

At the extreme, when the liquid distribution is not limited by the number of liquid source points, which can be deployed onto the bed to create well irrigating liquid films (i.e. the packing is wettable), then the effective area of the packing a_e will be equal to the bed dry surface area a_p and, as a result of that, the packing will be considered a good packing. However, because of the inherent liquid maldistribution in any packed bed, the actual local liquid flow in packed beds can be different from a uniform thin liquid film flow, instead the liquid progresses in a series of stable rivulets which have lower surface area compared to thin films, therefore regions within the bed will remain dry or partly wet.

Bremer and Zuiderweg [B1] investigated the liquid distribution and spreading in packed beds using different liquid systems with different surface tension values. They found that the wettability of the packing had no effect to help to spread the established liquid rivulets. They concluded that in packed beds liquid would tend to trickle down through the bed in a form of rivulets rather than a series of films. Therefore for any packed bed, no matter the liquid wetting condition may be, it can not improve the separation performance of such bed

and, consequently, it is not unreasonable to assume that the liquid partly wets the packing.

Since the mass transfer theories such as the Penetration and Davidson models assume that the packing is completely wet by the liquid films, they may not be adequate to predict the performance in rotating beds. Theoretical models as the Penetration and Davidson models and empirical models as the Onda and Vivian correlations were used to estimate the HTU and compared with the experimental values. The surface area per unit volume was calculated from equations 1.5.1 and 1.5.3. The characteristic dimensions of the packing material used were the measured filament size for each packing given in section 2.1.3.

In the calculation below the filament thickness for Knitmesh and Declon and the strand width for Expamet were assumed to be the characteristic dimension, as they form the skeleton of each packing. Additionally, these filaments and strands were further assumed to be crossed, perpendicular to the filament axis, by the liquid (i.e. cross over liquid flow). The Onda's correlation equation 1.5.1 was used to predict the a_w wetted surface area, which is equal to the interfacial area on the basis that the static hold up in rotating beds can be assumed to be very low (i.e. lower film thickness at higher acceleration) analogous to a conventional bed run at 1g with packings having a large size. Tables D1 through D6 - Appendix D show the comparison between the experimental and calculated HTU values using the above models.

From figures 3.4 through 3.9 shown below it can be seen that the experimental HTU values deviated significantly from the models predictions. The Penetration and Davidson models have grossly underpredicted the whole spectrum of the experimental values, while the Onda and Vivian correlations overpredicted the HTU values.

Fig.(3.4): Prediction for Knitmesh, Q_L= 12.5 L/min., <T> 23.2 °C

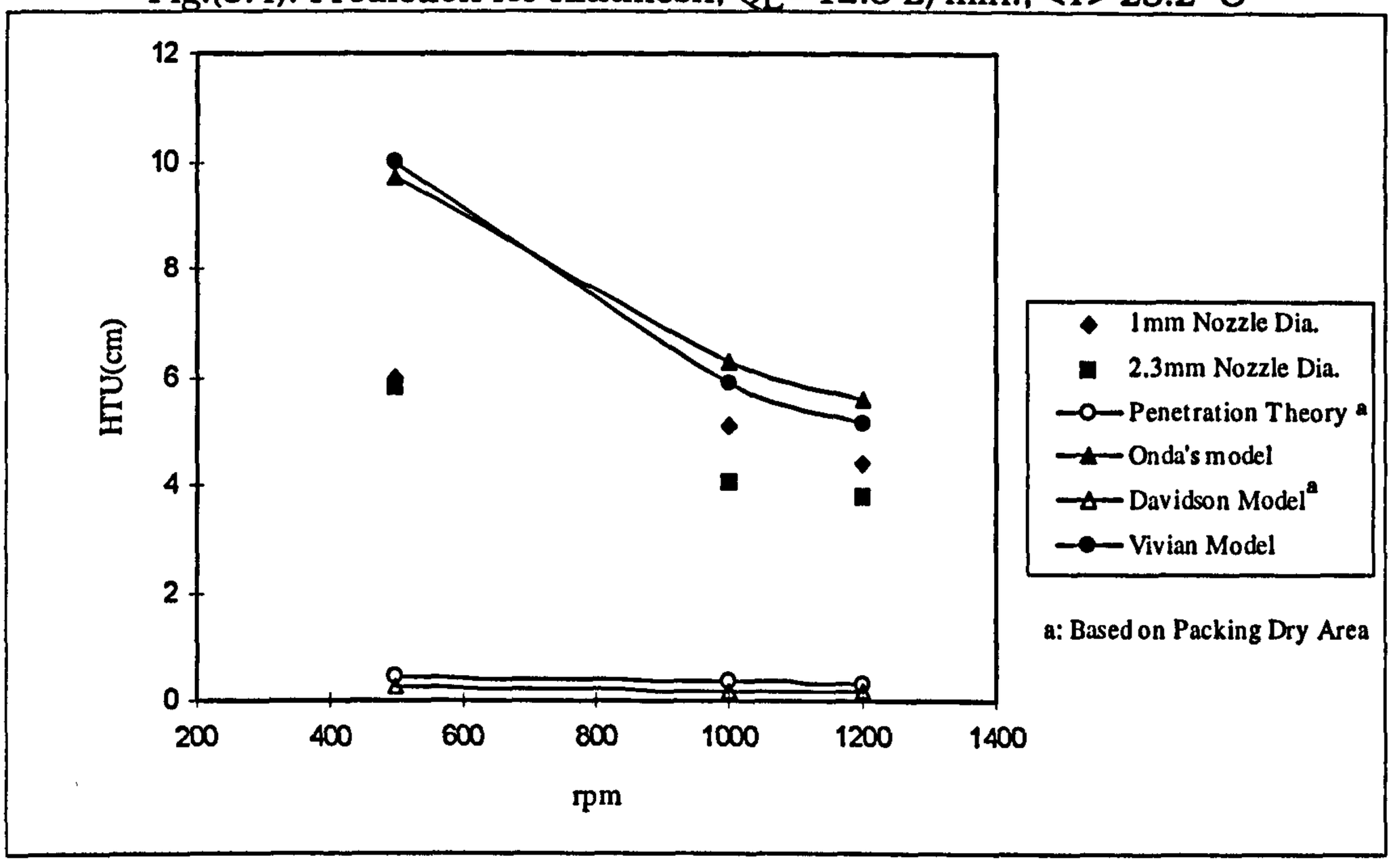

Fig.(3.5): Prediction for Declon, Q_L= 12.5 L/min., <T> 21.4 °C

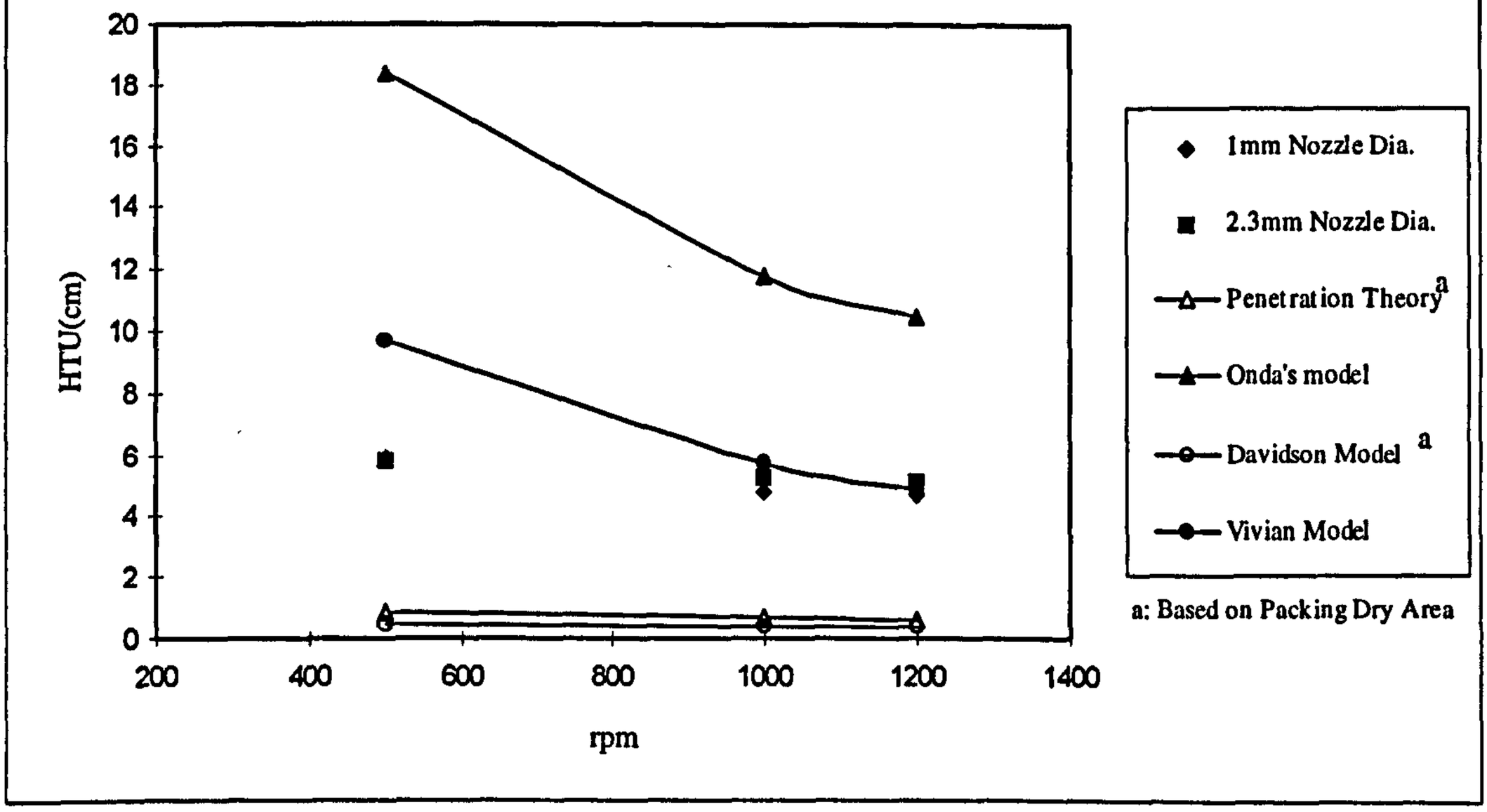

Fig.(3.6): Prediction for Expamet, Q_L= 12.5 L/min., <T> 22.4 °C

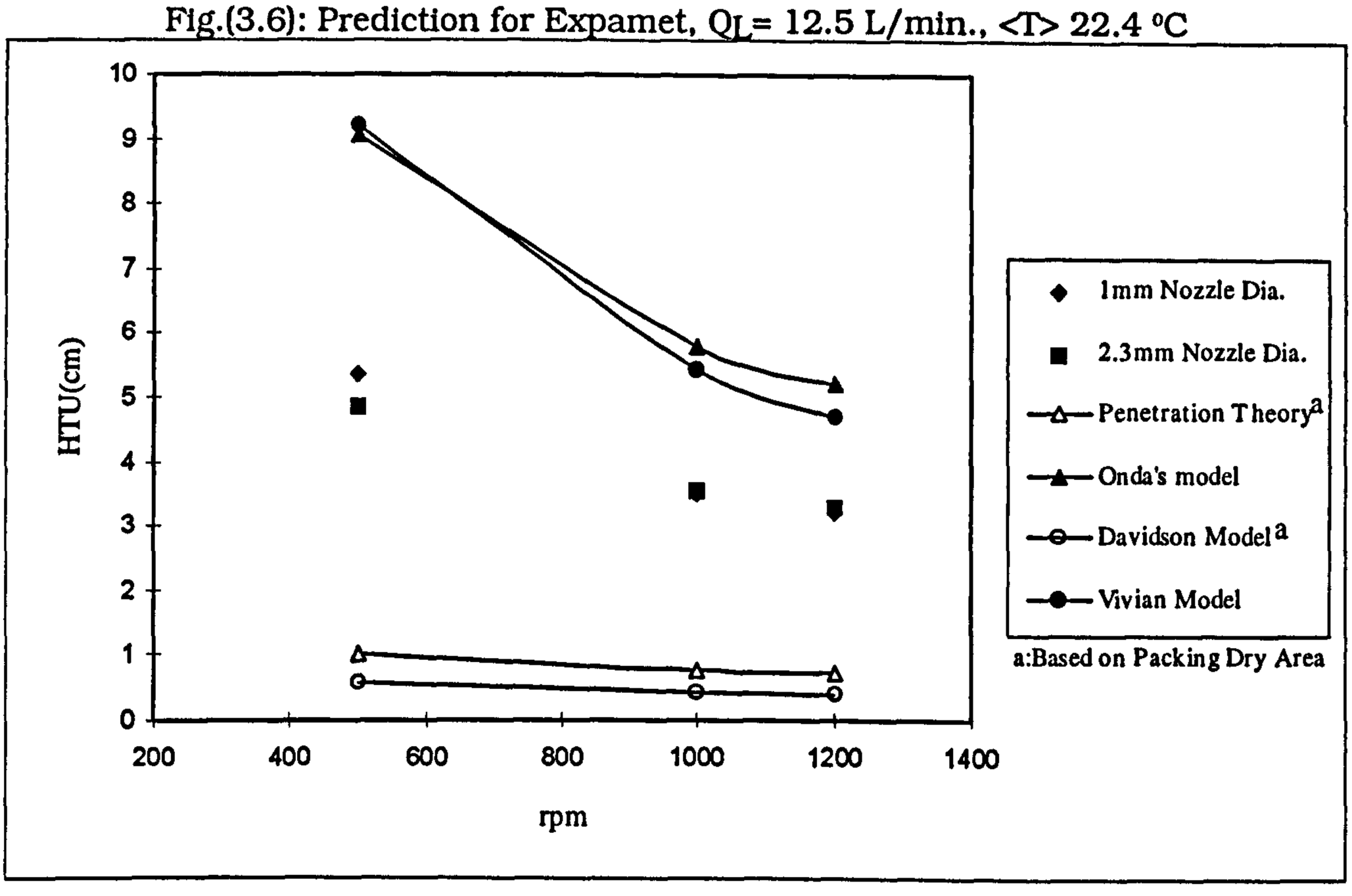

Fig.(3.7): Prediction for Knitmesh, Q_L= 6.5 L/min., <T> 19.9 °C

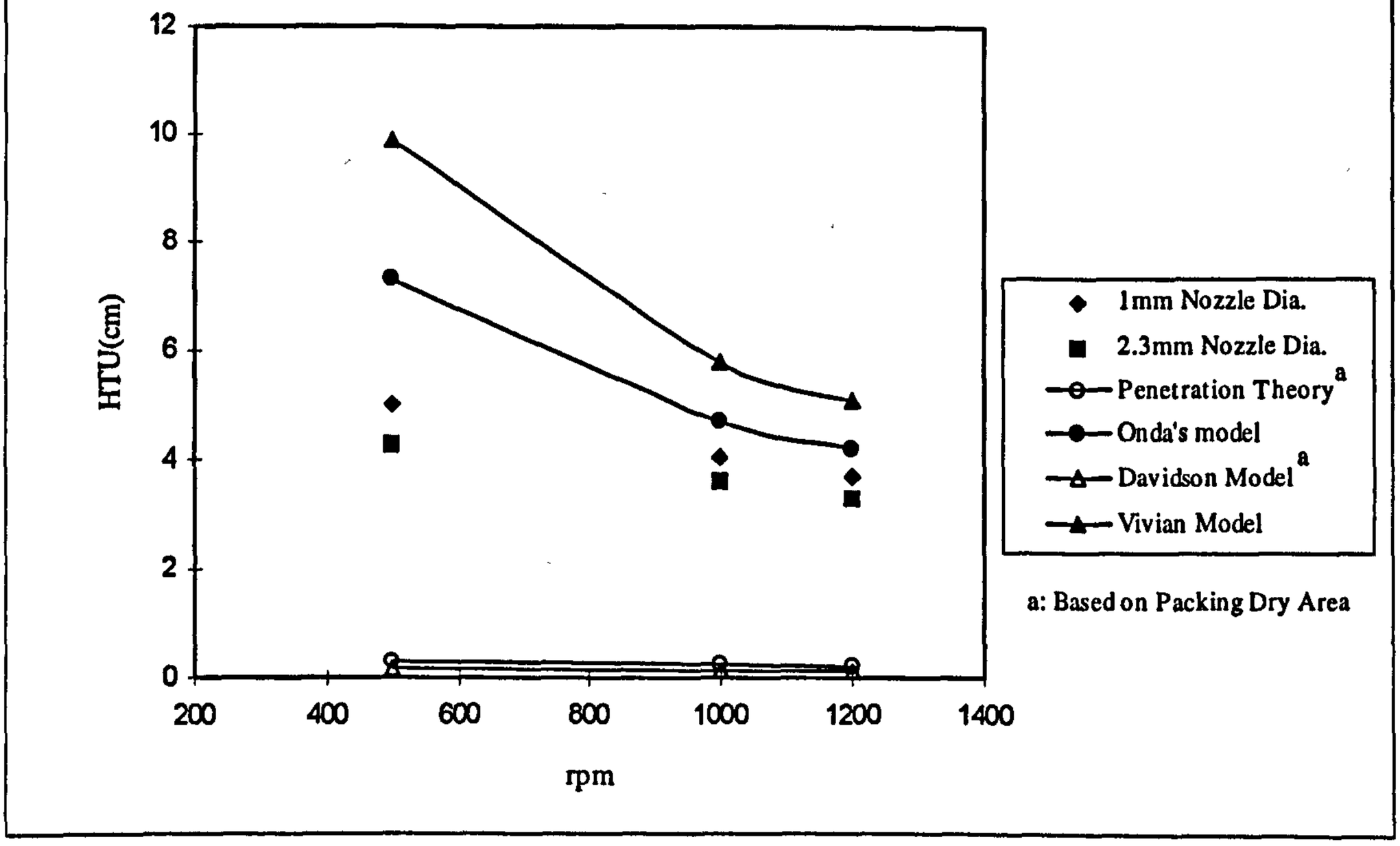

Fig.(3.8): Prediction for Declon, Q_L= 6.5 L/min., <T> 24.2 °C

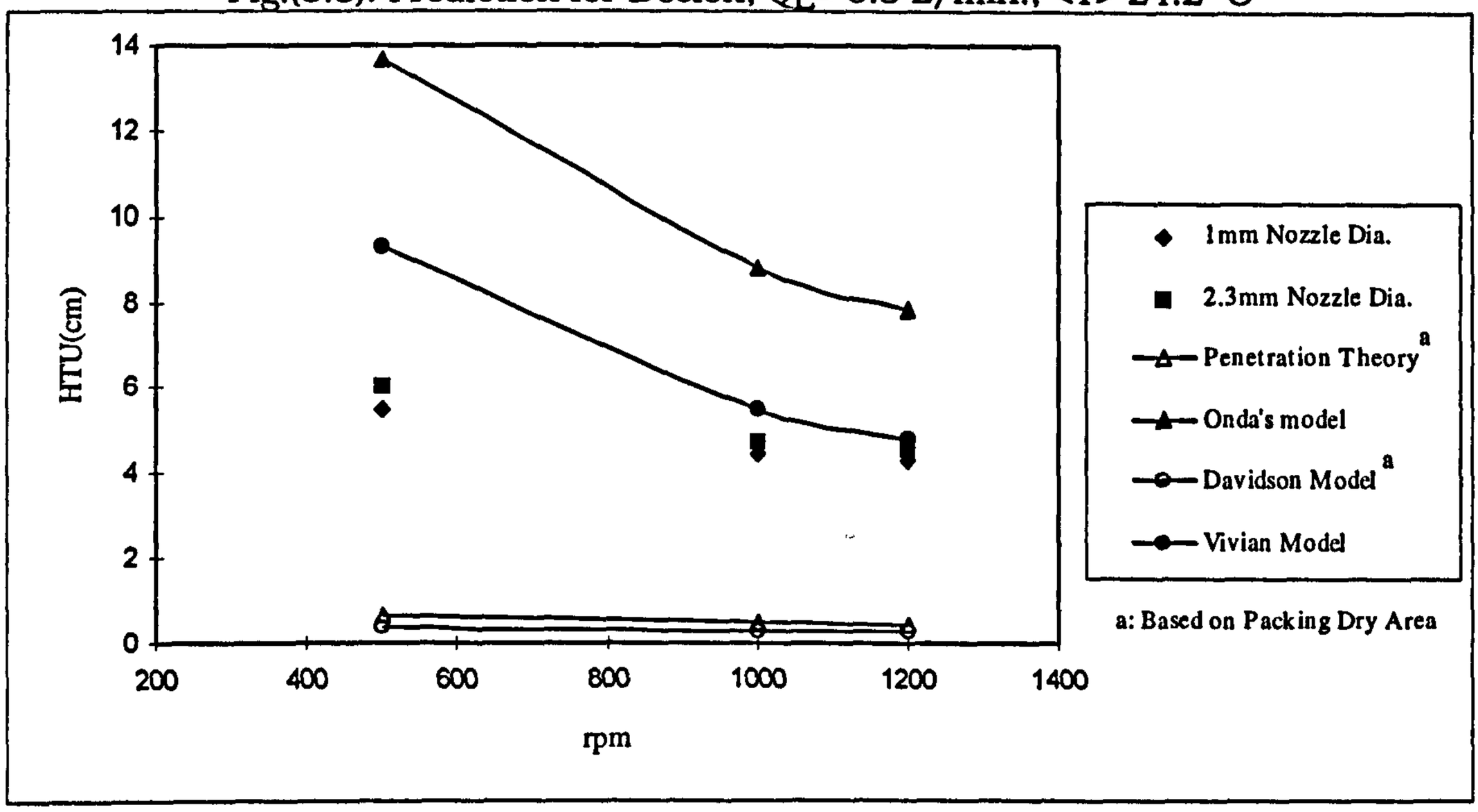

Fig.(3.9): Prediction for Expamet, Q_L= 6.5 L/min., <T> 22.6 °C

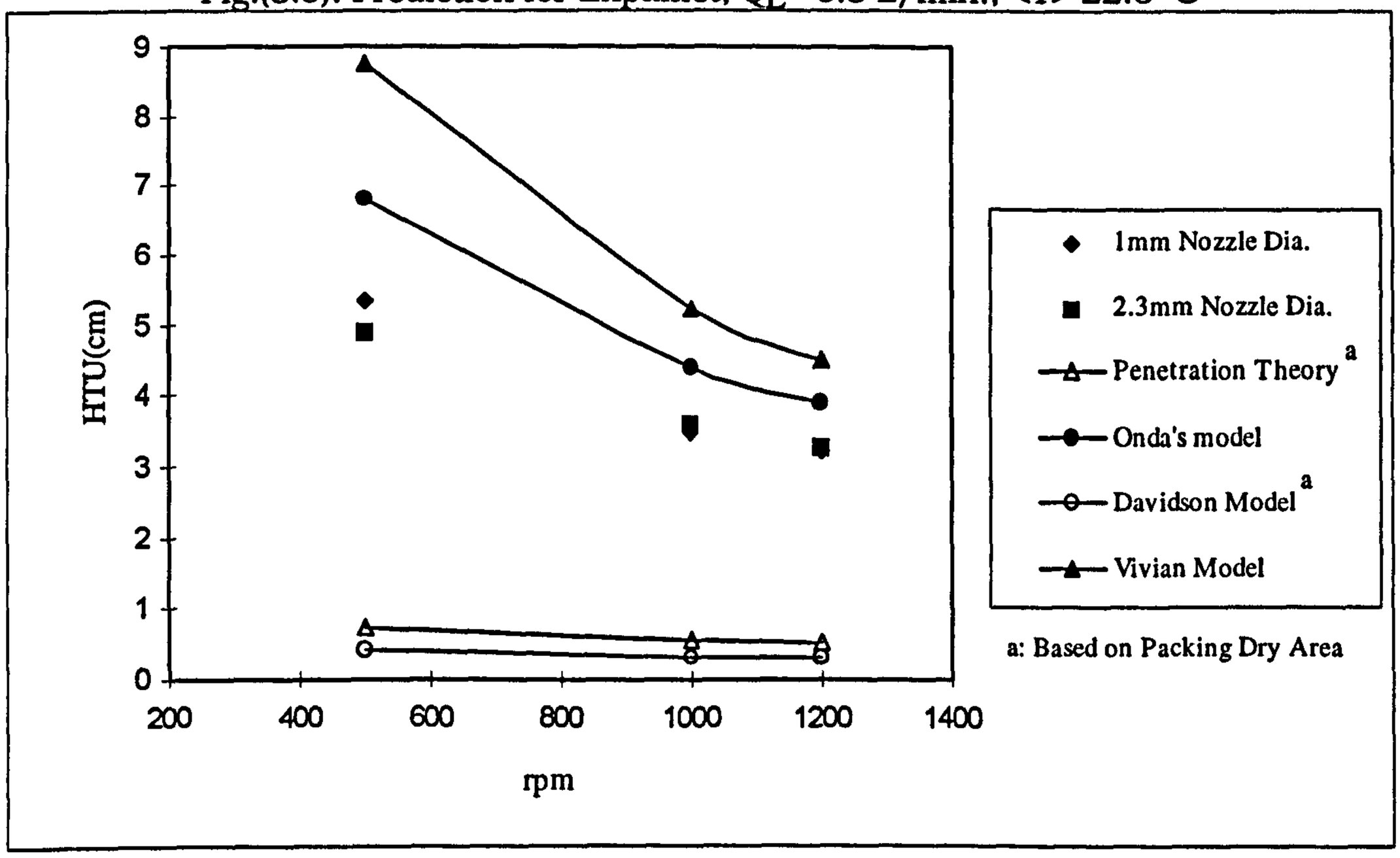

The relationship of the experimental HTU and volumetric mass transfer coefficient and the centrifugal acceleration ' g ' for all packing can be expressed respectively as:

$$HTU \alpha\ g^{-\beta}$$

$$K_L a \alpha\ g^{\beta}$$

It was expected that increasing the rotor speed (i.e. g's) would increase the volumetric mass transfer coefficient, hence yielding lower HTU values. The range of experimental values of β are shown in table 3.1.

Table(3.1): β -Values for all packings

Knitmesh	Declon	Expamet
0.133 - 0.244	0.111 - 0.167	0.227 - 0.278

In order to study the mass transfer performance, the HTU values were compared with the theoretical models as follows:

1-For example, in the case of Expamet and assuming that the $K_L \alpha\ g^{0.167}$ (the Penetration model eq. 1.6.4). However, it can be seen from figures 3.4 through 3.9 that the estimated HTU based on the Penetration model did not match with the experimental values. Therefore it will not be safe to assume that the flow pattern of the liquid through the bed was similar to that in the Penetration model.

2- From table 3.1 it can be seen that some of the value of the exponent β changes with g by values less than the theoretical value of 0.167 proposed by the Penetration and Davidson models. Therefore this relationship could indicate the complex nature of the liquid flow through the bed. The liquid was maldistributed and was flowing through the bed possibly

in a series of thick rivulets whereby the whole area was not taking part in the mass transfer process.

As shown above it was difficult to ascertain how the higher centrifugal acceleration employed can affect the mass transfer coefficient K_L and the interfacial area a separately. Therefore the enhancement in the mass transfer performance should be attributed to the effect of the centrifugal acceleration on the volumetric mass transfer coefficient K_La However, the obtained enhancement in mass transfer may not reinforce the assumption that the liquid was well distributed and wetted the whole packing at higher acceleration.

3.4- Effect of Packing Characteristic Length and Surface Area Estimation of HTU.

In the following calculation the significance of the characteristic dimension (filament length) in the prediction of the experimental HTU values was investigated for each packing using any particular mass transfer model.

It was assumed that the bed was randomly packed with filaments which have different length with flat surfaces, figure 3.10. The liquid film flow was along the surface of the filament and not perpendicular to the filament axis. The assumed packing lengths were double and triple the filament thicknesses shown in table 2.1 for each packing.

In these calculations the theoretical models was used to test the mass transfer performance on the basis of the assumed new arrangement of the packing material. An additional equation (eq. 1.5.3) which takes into consideration the surface tension and the inertia of the liquid was also used. Equation 1.5.3 estimates directly the effective interfacial area rather than the wetted area. The Weber number We in this equation depends on filament length d*p*.

Fig. 3.10: Details of the Filament Length

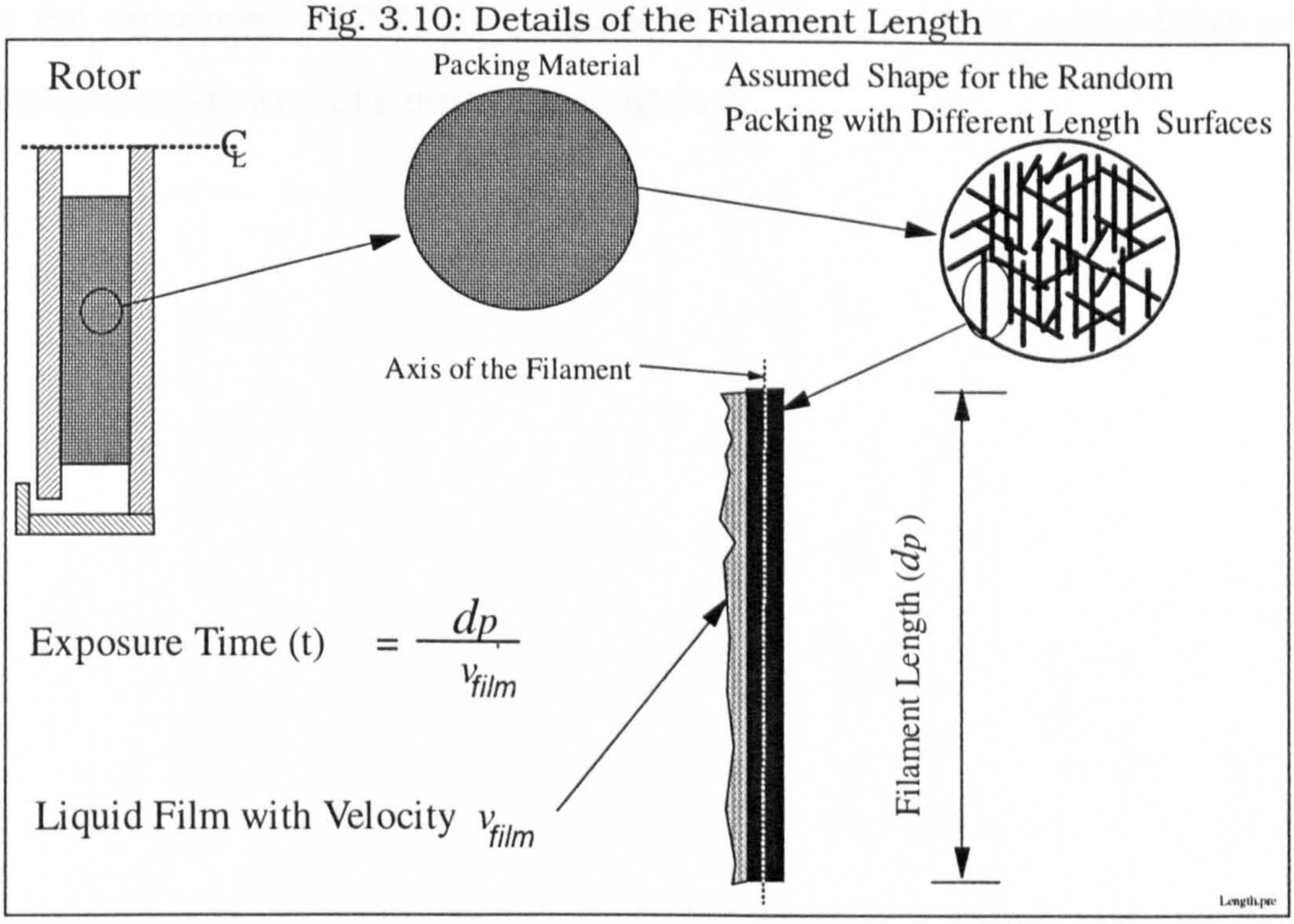

The estimated values of the interfacial area for packings, Knitmesh, Declon and Expamet were found to be as low as 4, 6 and 16% of the total specific interfacial area, respectively.

Tables 3.2 through 3.4 show results of using equation 1.5.3 along with the assumed packing lengths for each packing. For Knitmesh, the estimated HTU values using the Penetration, Davidson and Onda models underpredicted HTU values for d*p* values, while Vivian model overpredicted the experimental HTU values. For Declon, Onda correlation gave good match with the experimental values for both liquid flow rates for the two values of d*p* values (460 and 690 μm). With regard to Expamet packing for all values of a_e and a_w, the Penetration and Davidson models underpredict HTU experimental values while, Vivian model overpredict the experimental values and Onda's model has showed good agreement with some of the HTU experimental values.

In general, the Penetration and Davidson models underpredicted the whole spectrum of the experimental data for the three packings. However, the Onda and Vivian models gave better

agreement with the experimental HTUs compared to the estimated HTUs on the basis of the filament thickness as shown in figures 3.4 through 3.9.

Table (3.2): Prediction of HTU for Knitmesh, 4-arms Distributor (hole's size 1mm).

Liquid Flow (L/min.)	Filament Length (μm)	rpm	Experimental HTU (cm)	Penetration Theory (cm)	Onda Correlation (cm)	Davidson Model (cm)	Vivian Model (cm)	a_e, Mada Correlation (m^{-1})	a_e, Onda Correlation (m^{-1})	< T >, Average Temperature (°C)
6.5	300	500	5.29	1.5	2.91	0.91	9.07	88	581	21.2
		1000	3.92	0.80	2.31	0.46	5.36	178	617	
		1200	3.72	0.66	2.18	0.38	4.66	213	627	
	450	500	5.29	1.42	2.90	0.82	8.70	142	581	
		1000	3.92	0.71	2.30	0.41	5.17	285	617	
		1200	3.72	0.59	2.16	0.31	4.50	478	627	
12.5	300	500	6.31	2.12	3.88	1.22	9.40	110	725	24
		1000	5.33	1.06	3.08	0.61	5.53	220	767	
		1200	4.51	0.88	2.90	0.51	4.82	248	779	
	450	500	6.31	1.89	3.86	1.09	9.20	177	725	
		1000	5.33	0.95	3.06	0.54	5.40	354	767	
		1200	4.51	0.79	2.88	0.45	4.70	425	779	

Table (3.4): Prediction of HTU for Expamet, 4-arms Distributor (hole's size 1mm).

Liquid Flow (L/min.)	Filament Length (μm)	rpm	Experimental HTU (cm)	Penetration Theory (cm)	Onda Correlation (cm)	Davidson Model (cm)	Vivian Model (cm)	a_e, Mada Correlation (m^{-1})	a_e, Onda Correlation (m^{-1})	< T >, Average Temperature (°C)
6.5	1000	500	5.92	1.56	4.06	0.90	8.30	226	417	21.2
		1000	3.97	0.78	3.22	0.45	4.91	457	442	
		1200	3.34	0.65	3.03	0.37	4.28	542	449	
	1500	500	5.92	1.40	4.04	0.80	8.19	362	417	
		1000	3.97	0.70	3.20	0.40	4.80	725	442	
		1200	3.34	0.58	3.02	0.33	4.21	870	450	
12.5	1000	500	5.86	2.09	5.42	1.20	8.90	280	517	22.4
		1000	4.21	1.04	4.30	0.60	5.24	561	547	
		1200	3.78	1.70	5.65	0.97	4.60	517	554	
	1500	500	5.86	1.86	5.40	1.07	8.82	450	517	
		1000	4.21	0.93	4.38	0.53	5.20	901	547	
		1200	3.78	0.78	4.03	0.45	4.53	1082	554	

3.6-Discussion.

It has been demonstrated that in RPBs higher values of the volumetric mass transfer coefficients and hence lower height of transfer unit values can be achieved at higher centrifugal acceleration. The lower height of transfer units values would contribute to the significant reduction of the equipment size.

The higher centrifugal acceleration environment was not only enhancing the mass transfer coefficient but it also enhanced the effective surface area hence producing higher volumetric mass transfer coefficients. This also, however, tend to imply that better mixing was achieved within the packing as a result of higher centrifugal acceleration.

The estimated height of transfer units values shown earlier suggest that the theoretical models; the Penetration and Davidson models can not be used to predict the mass transfer coefficient K_L in RPBs, and that was largely because both models the mass transfer coefficient varies with g by the theoretical exponent of 0.167. Thus, in RPBs the enhancement in the mass transfer performances, for given separation duties, were as a result of using higher centrifugal acceleration.

The experimentally determined effect of the magnitude of the specific surface area of a packing material on the height of transfer units seem to be insignificant. For example, by comparing HTUs values between Knitmesh and Expamet, which has an area as low as two third the area of Knitmesh there can be no significant difference, despite the fact that both packings are, structurally and materially different. The Expamet has exhibited good performance with the centrifugal acceleration $(0.227 \leq \beta \geq 0.278)$. The Expamet was found to perform as well as the Knitmesh particularly at lower liquid flow rate. The Declon packing which has a reticulated structure similar to the Knitmesh but with about one third the surface area, has shown reasonable results compared to both Knitmesh and Expamet.

It has been shown that on the assumption of liquid film flows along the filament and using the theoretical and empirical models, section 3.4, the models produced some improvement but they still cannot be reliable to use to design RPBs. The empirical models, however, showed some improvement but like the theoretical models cannot also be used for design purposes. This will clearly reflect the complex nature of the liquid flow behaviour within the bed. As mentioned above the flow within the bed will disintegrate into preferential flow paths which will drastically reduce the effective surface area during the mass transfer process.

Chapter 4

Liquid Distribution

4.1-Introduction

In rotating packed beds, it is possible that with the increase of the rotational speed, a higher surface area per unit volume could be generated as a result of the formation of thin films and smaller droplets. Therefore, on this basis, enhancement in the separation performance could be achieved.

Good liquid distribution is likely to enhance the separation performance for any packed bed. However as rotating packed beds make use of different types of packing material, they are susceptible to liquid maldistribution. It has been demonstrated that rotating packed beds exhibit some degree of liquid maldistribution Burns [B4]. The liquid maldistribution was found to have a strong dependency on the rotor speed. In section 4.4 the liquid maldistribution in rotating packed beds is discussed with the help of some photographic evidences.

4.2-Initial Liquid Distribution.

In order to test the initial liquid distribution, at the eye of the bed, and its effect on the separation performance in RPBs two sets of experiments were conducted. In the first set, the aim was to study the effect of the angled liquid distribution whereby the liquid was distributed either in the direction of the rotation of the bed (co-rotation) or opposite to the direction of the bed (counter-rotation). In the second set, the aim was to study the effect of the injection velocity of the liquid jets. Throughout these experiments the multi-arm distributor was used.

4.2.1-Effect of Angled Liquid Distribution on HTU.

In this test the effect of angled liquid distribution on the mass transfer performance was examined. When the liquid jets hit the packing material a relatively intense shearing zone is created on the impact. The arms of the distributor were positioned in the eye of bed as shown in figure 4.1. The distributor arms had to be laid, eccentrically with the axis of rotation in such a way that the liquid jets hit the bed with the desired angle as shown in figure 4.2. Two packing materials were used in these test; the Expamet and Declon. In this test, the four arms were used with each arm having 16 holes, spaced evenly and each hole had a diameter of 1×10^{-3} (m), giving a holes' cross-sectional area of 5.02×10^{-5} (m^2). The liquid jets were positioned so that most of the axial depth of the bed was irrigated. Since the I.D. of the bed was 15.8 (cm) and the distance between any two arms facing one another was 11 (cm) giving an offset distance of 5.5 (cm), therefore, angled jets with a 54^{o} relative to the radial direction can be fixed. Figure 4.2 shows the liquid source points (solid circles) and their direction as indicated by the arrows. Tests were carried out at liquid flow rate of 6.5 (L/min.) at two rotational speeds of 500 and 1000 rpm. At such flow rate the average jet injection velocity was 2.16 (m/s) having radial (V_{radial}) and tangential jet (V_{θ})

velocities of 1.27 and 1.75 (m/s), respectively. The tangential component of the liquid when it hits was equivalent to 22.2 (rad/s).

The comparison for each packing material was based on the position of the arms as whether they were angled in position co-rotating, counter-rotating or normal to the bed. It can be seen from figures 4.3 and 4.4 that both the angled liquid injection and normal liquid injection had almost the same HTUs. Using the angled distributor there was no marked change in the HTUs even when the bed's tangential velocities of 4.13 and 8.27 (m/s) at 500 and 1000 rpm, respectively, were higher than the jets' tangential velocity component (= 1.75 m/s),

Fig:(4.1), 4-Arms Liquid Distributor.

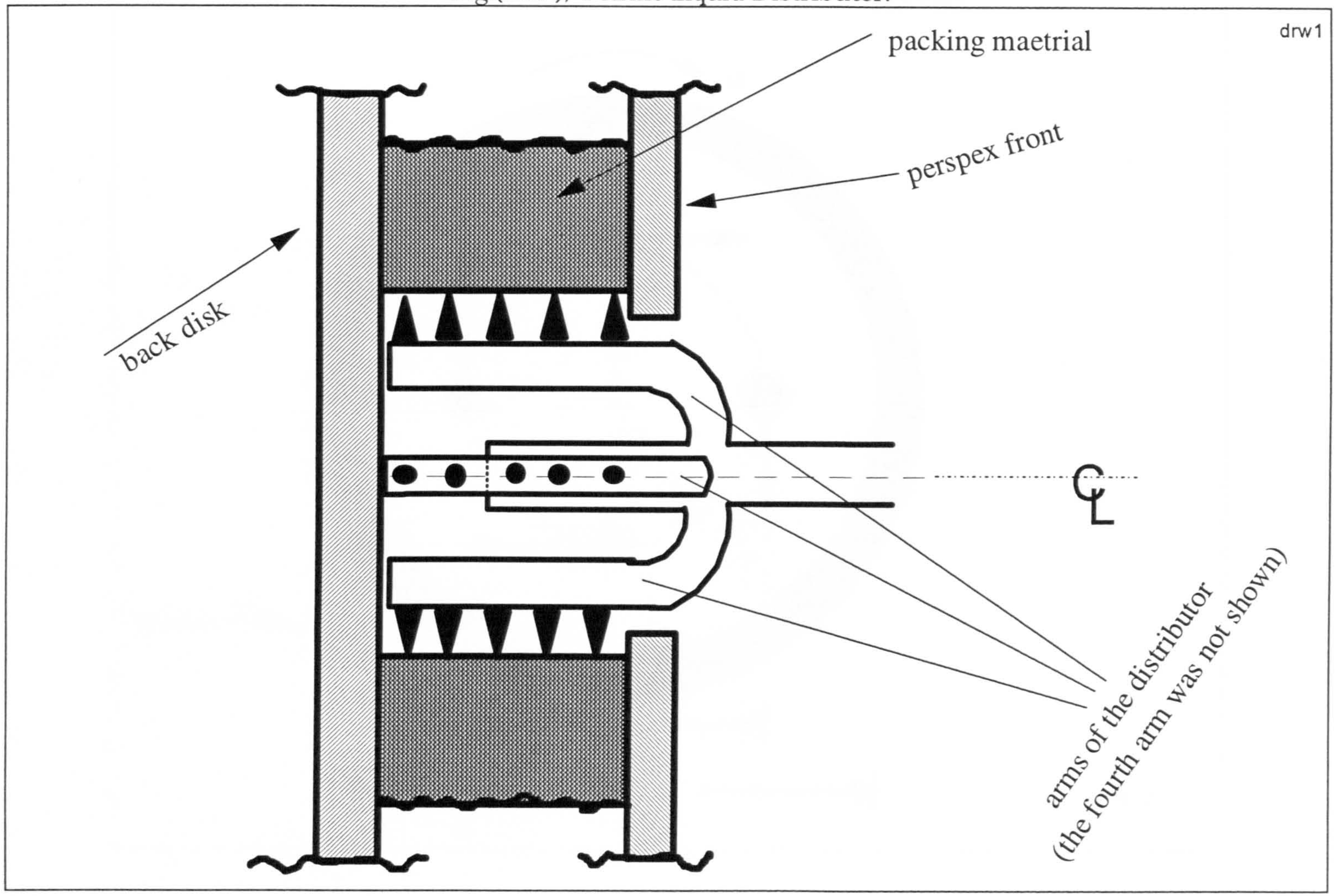

Fig.(4.2): Co-rotational Angled Liquid Distribution.

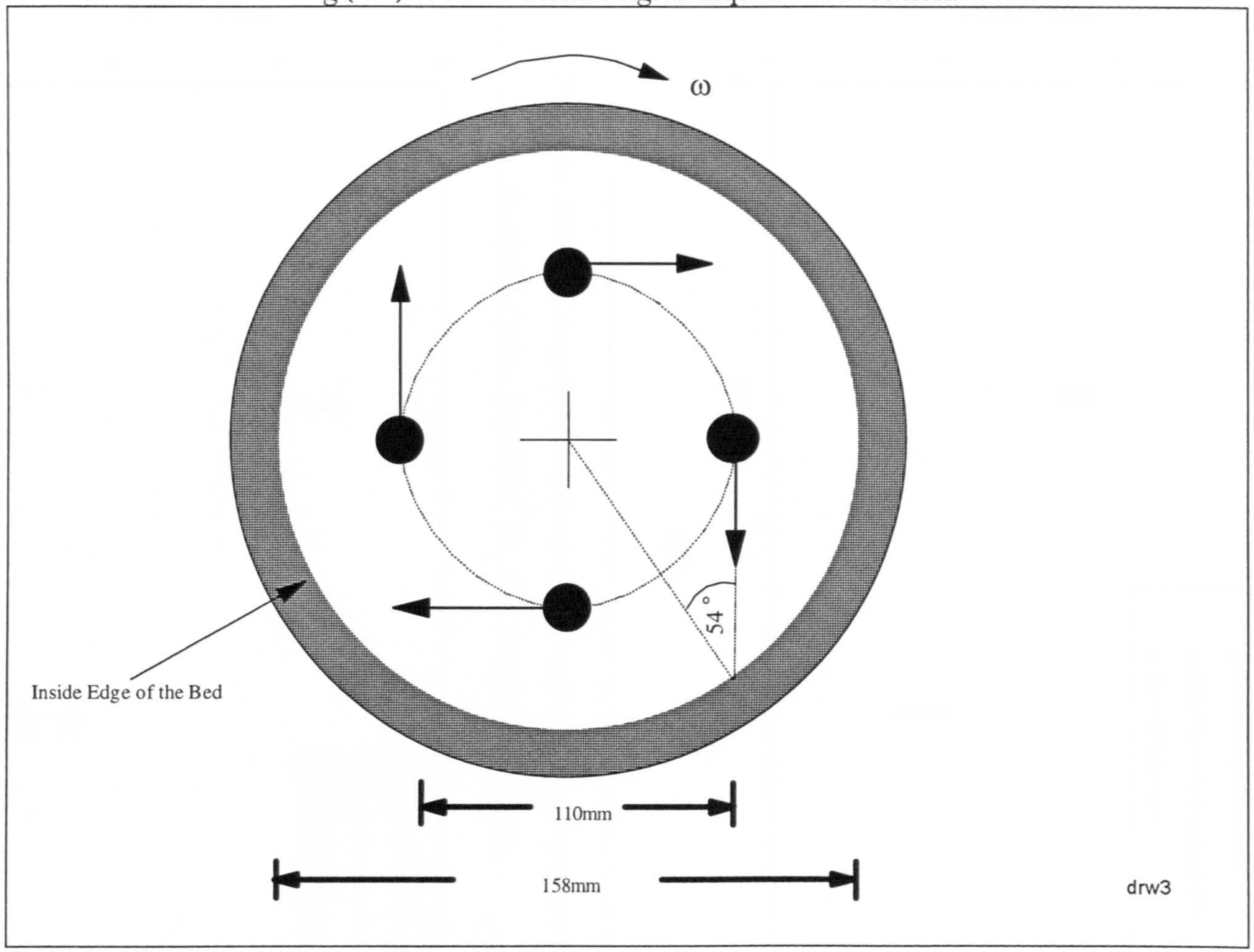

Fig.(4.3): Effect of Angled Distribution, Φ 1mm 4-arms Distributor,
Q_L= 6.5 L/min., Q_g = 60 m^3/h, <T> 26 °C, Declon.

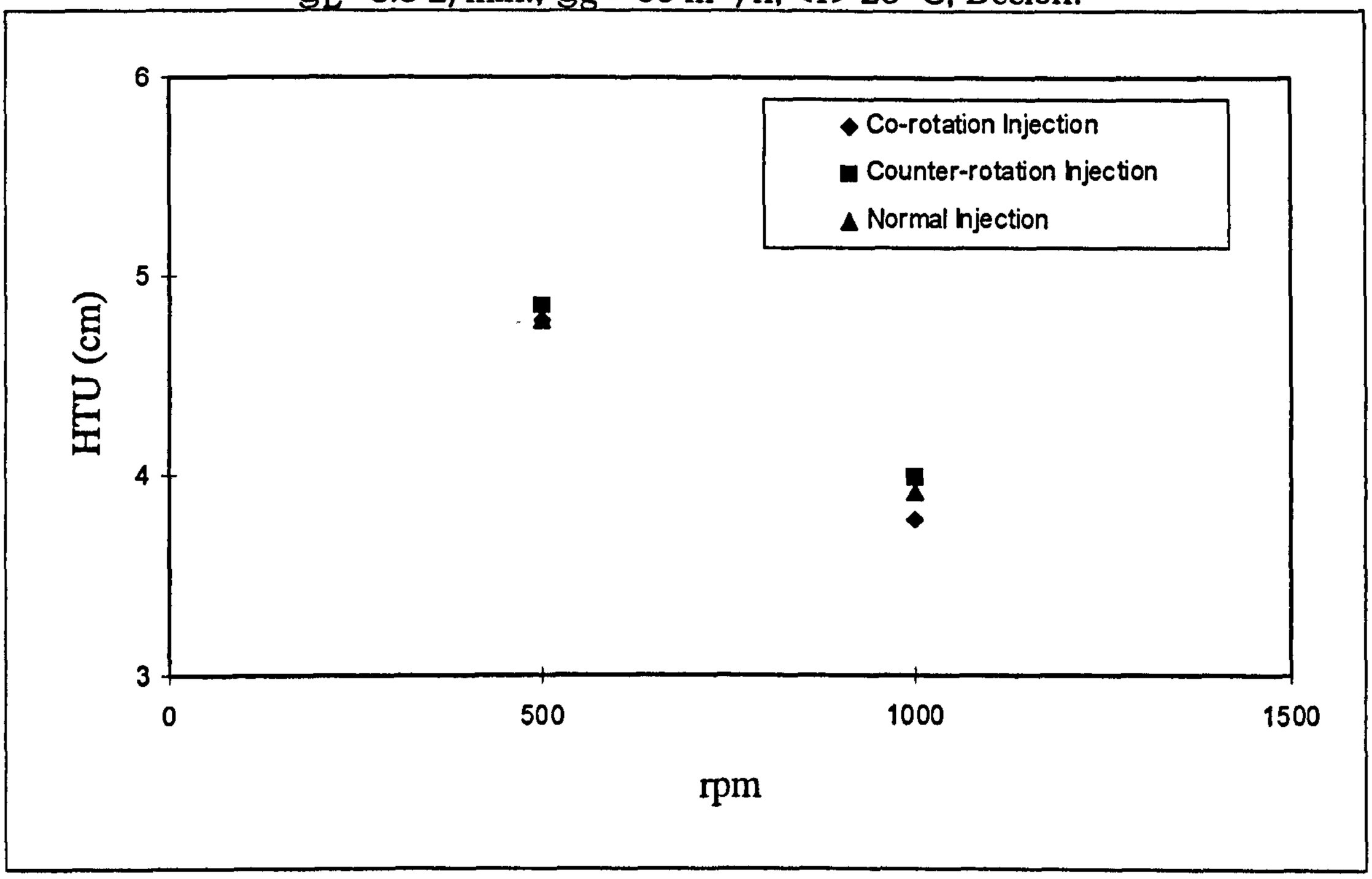

Fig.(4.4): Effect of Anguled Distribution, Φ 1mm 4-arms Distributor,
Q_L=6.5 L/min., Q_g=60m^3/h, <T> 19.3°C, Expamet.

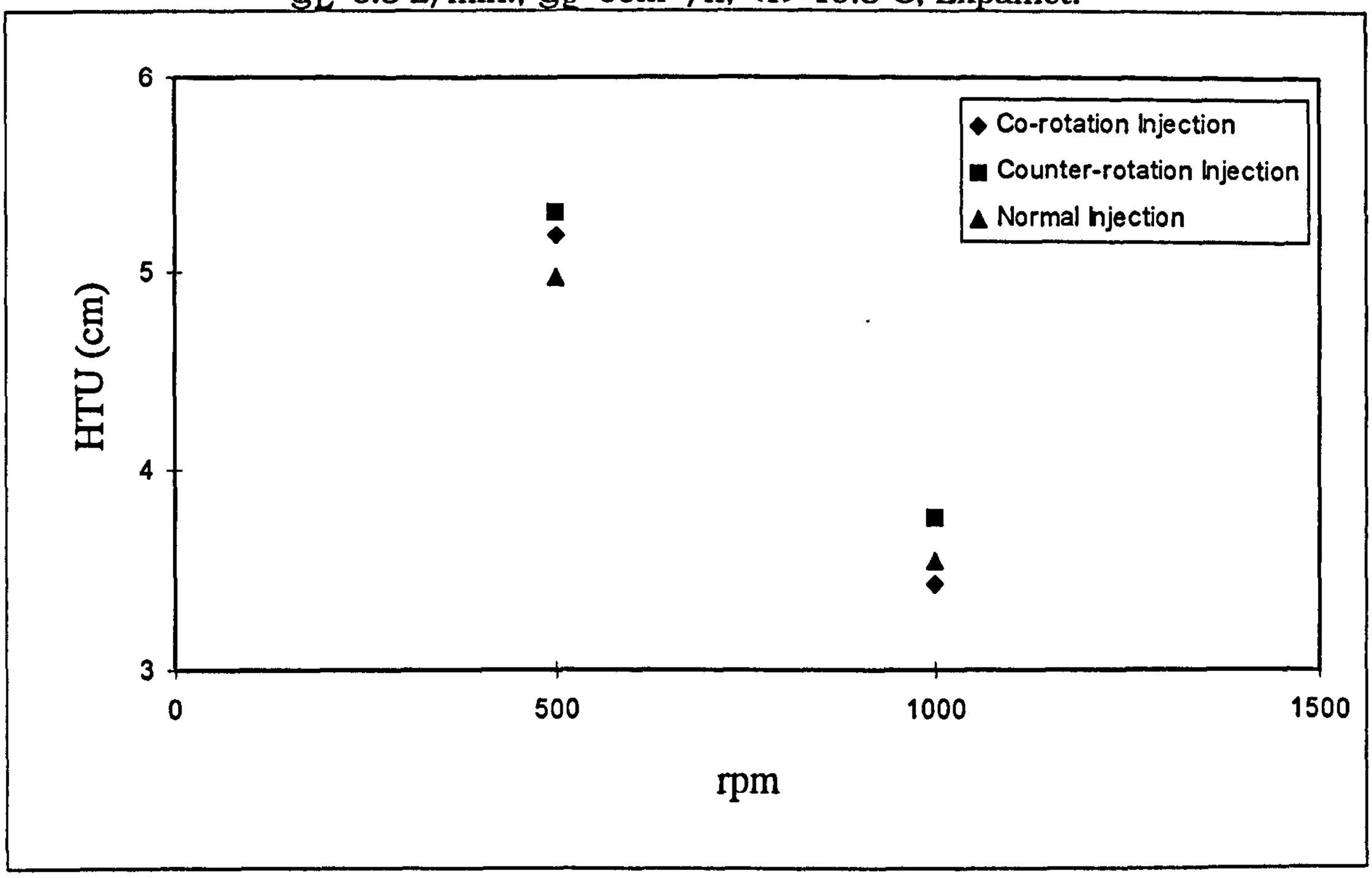

4.2.2- Effect of Injection Velocity on HTU.

In the following test the effect of the injection velocity (V_{inj}) on the mass transfer performance of the bed was studied. For each run a constant liquid flow rate was maintained while the number of arms for the distributor (4-arms distributor) was changed so that for a higher injection velocity fewer arms were used. In this test the direction of the jets was normal to the bed. Table 4.1 shows the number of arms and the corresponding average injection velocity for each case. The effect of the injection velocity on the performance for the three packing materials was shown in figures 4.5 through 4.7.

Table(4.1): Injection Velocity for Different Configurations, Q_L= 0.13 Kg/s.

No. of Arms	4	3	2	1
V_{inj}, (m/s)	2.65	3.53	5.30	10.6

It can be seen that at constant rotational speed for the Knitmesh and Expamet the higher the injection velocity the lower the HTUs, and hence the better the separation performance. The HTU values for Expamet were as good as those of the Knitmesh packing. However, the Declon packing showed the same trend but with HTUs values tend to level off as the injection velocity increases. In general, for the three packings used, the bed gave good HTU values even when liquid distribution quality (i.e. number of jets deployed over unit area) was impaired in the case where the number of arms and the injection velocity were simultaneously changed.

Fig.(4.5): Effect of Injection Velocity, Φ 1mm 4-arms Distributor, Q_L=8 L/min, Q_g = 60 m^3/h, <T> 21 °C, Knitmesh.

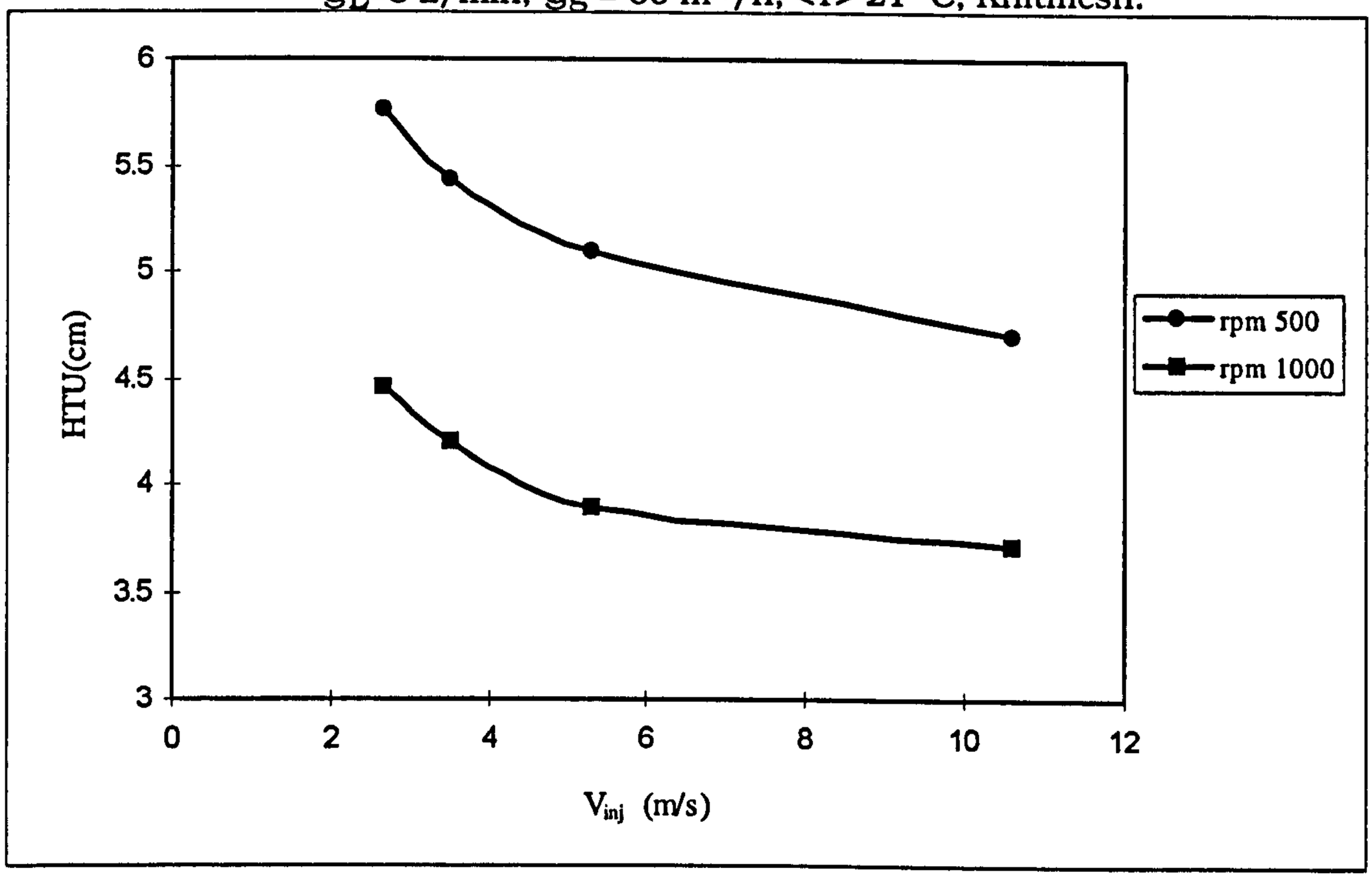

Fig.(4.6): Effect of Injection Velocity, Φ 1mm 4-arms Distributor, Q_L= 8 L/min., Q_g = 60 m^3/h,<T>21 °C, Declon.

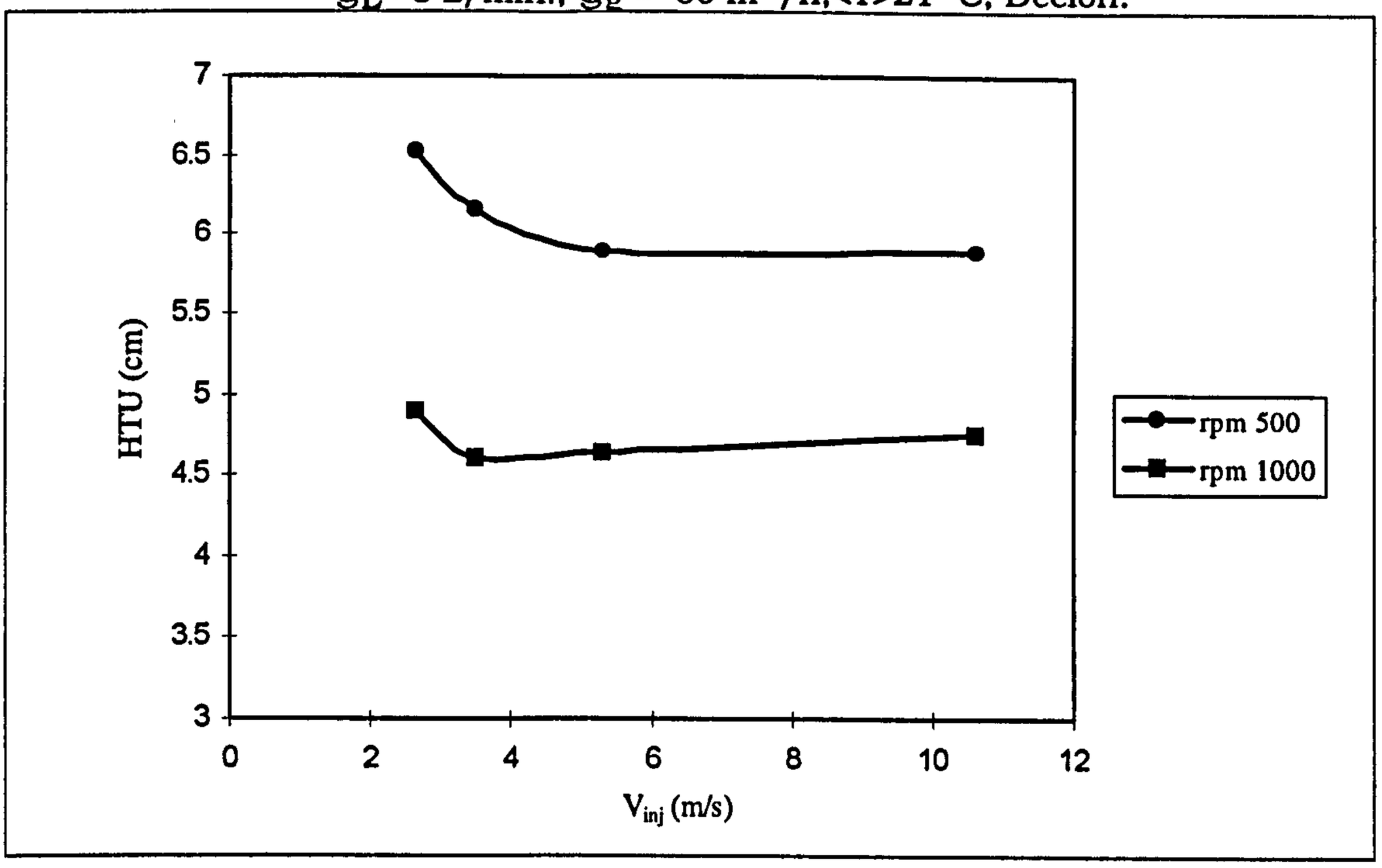

Fig.(4.7): Effect of Injection Velocity, Φ 1mm 4-arms Distributor, Q_L= 8 L/min., Q_g = 60 m^3/h,<T>21 °C, Expamet.

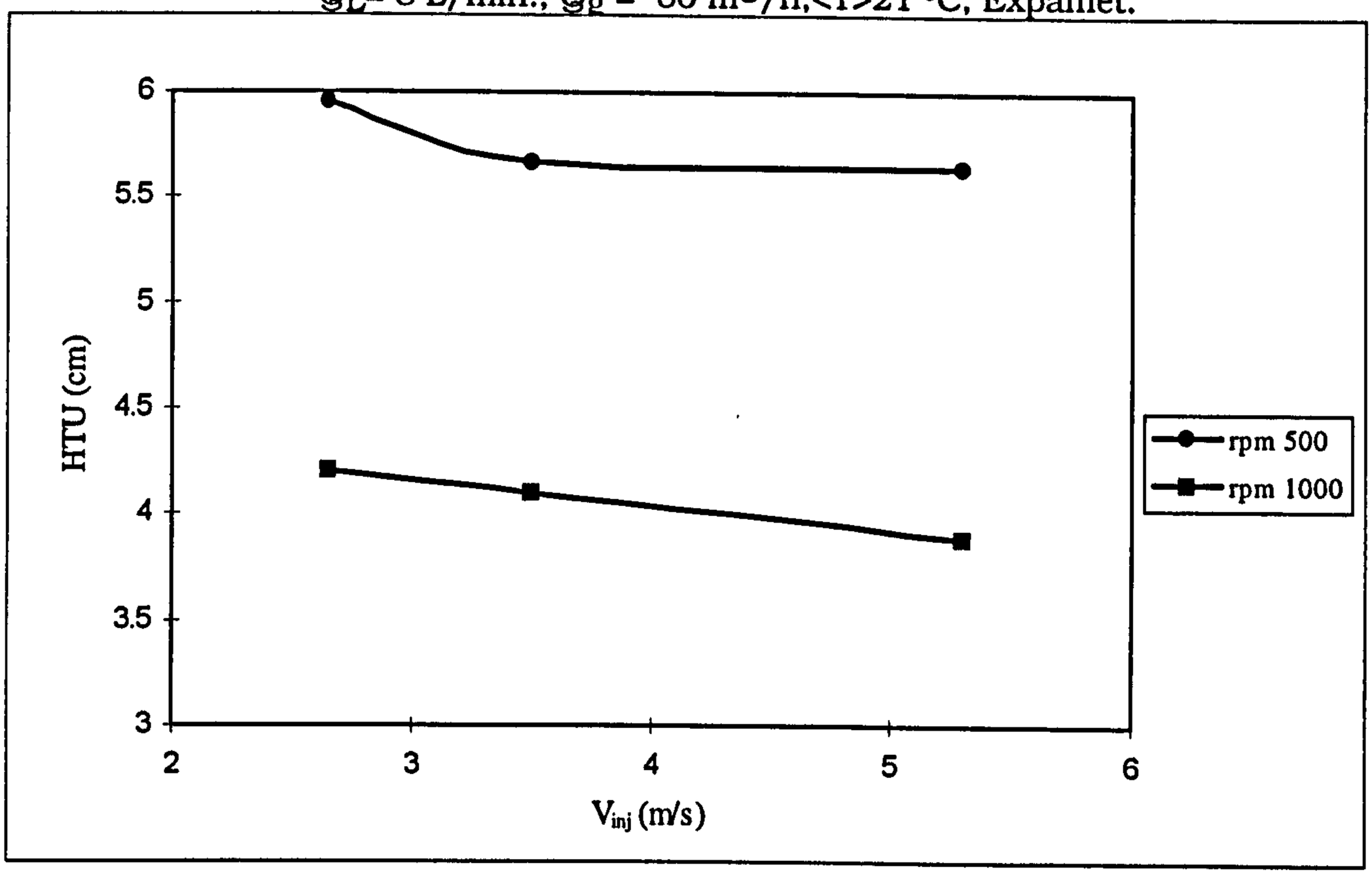

4.2.3-Effect of Distributor's Hole Size on HTU.

Figure 4.8a through 4.8d show the effect of hole size on the mass transfer performance at two different liquid flow rates for constant injection velocity. In this test, the four arms distributor was used with two different hole sizes; 1mm and 2.3mm and the corresponding injection velocities were; 2.2 and 4.2 (m/s) for the liquid flow rates 6.5 and 12.5 (L/min.) respectively, for both hole sizes. In general, it can be seen from figure 4.8 that there were not noticeable changes in the HTU values, and hence this would imply that the bed would perform normally no matter the quality of the jets and/or the droplets sizes involved. Accordingly, it is quite probable that the centrifugal acceleration environment has helped the bed to perform in a normal way as long as the liquid injection velocity was high enough to reach the bed (i.e. no entrainment at the eye of the bed).

(a)Declon Packing at 6.5 L/min.

(V_{inj} = 2.2 m/s)

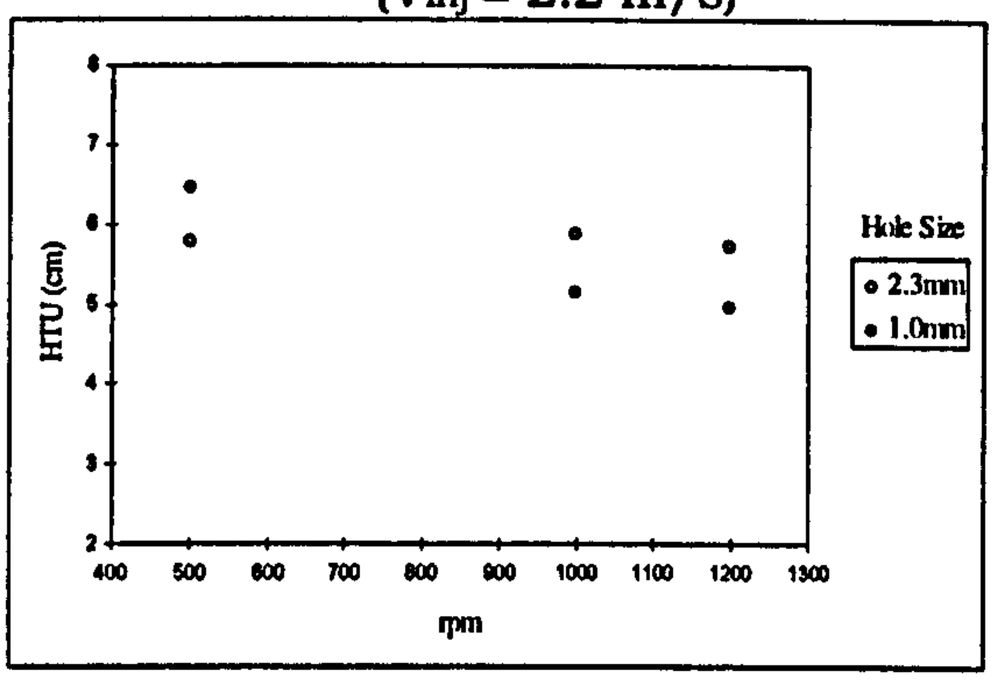

(b) Declon Packing at 12.5 L/min.

(V_{inj} =4.2 m/s)

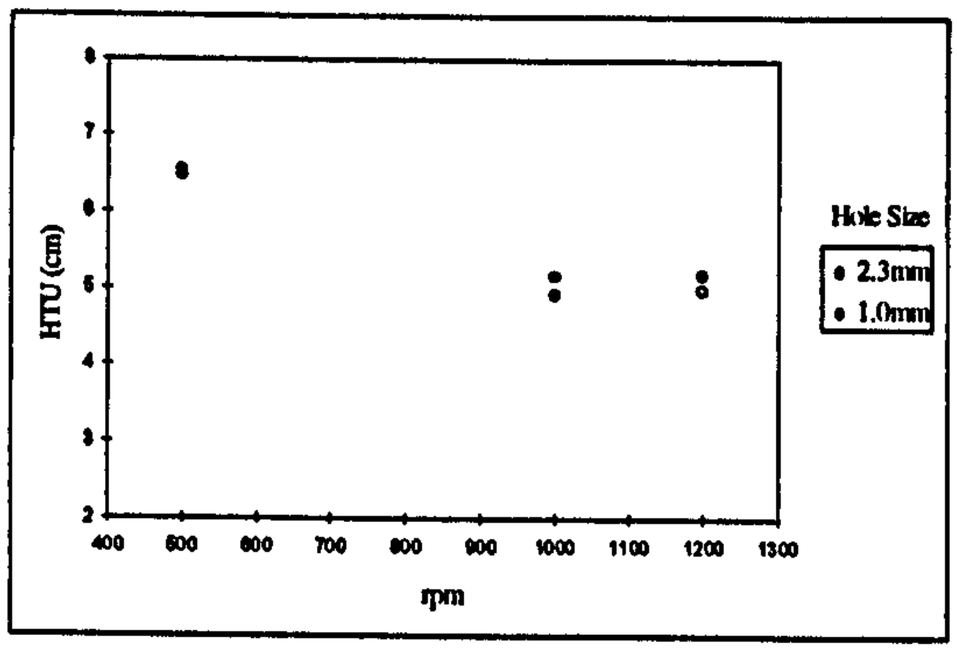

(c) Knitmesh Packing at 6.5 L/min.

(V_{inj} = 2.2 m/s)

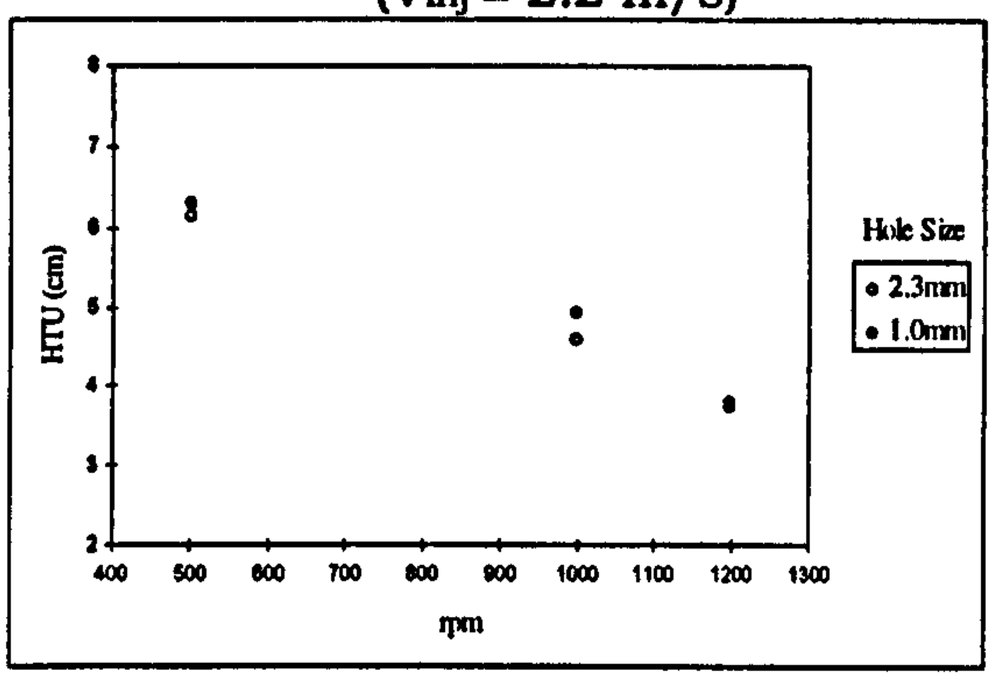

(d) Knitmesh Packing at 12.5 L/min.

(V_{inj} = 4.2 m/s)

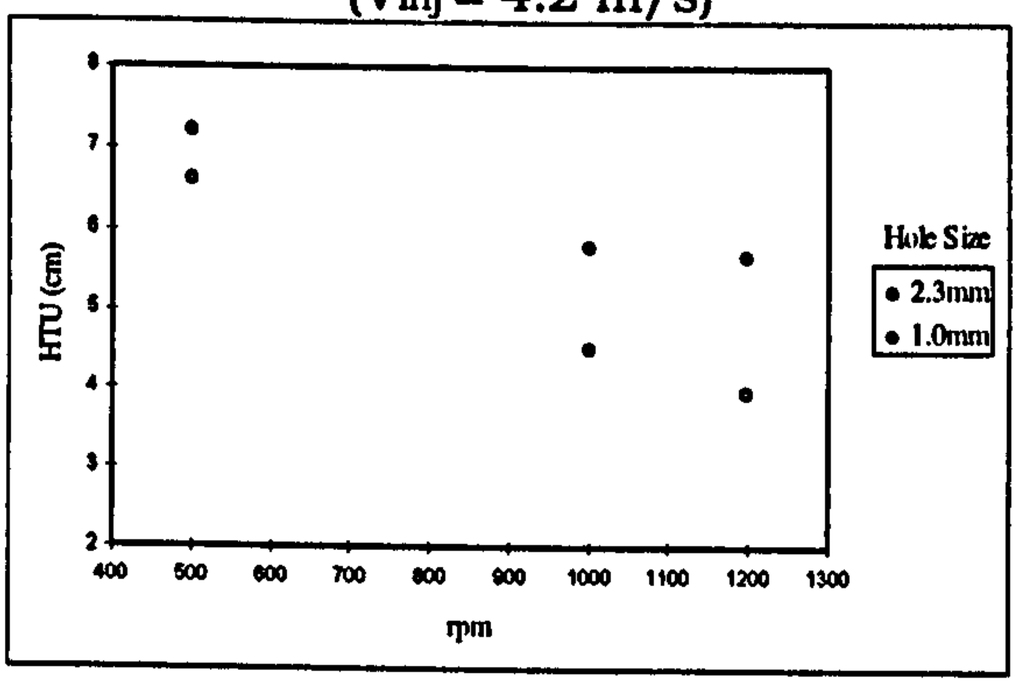

(e) Expamet Packing at 6.5 L/min.

(V_{inj} = 2.2 m/s)

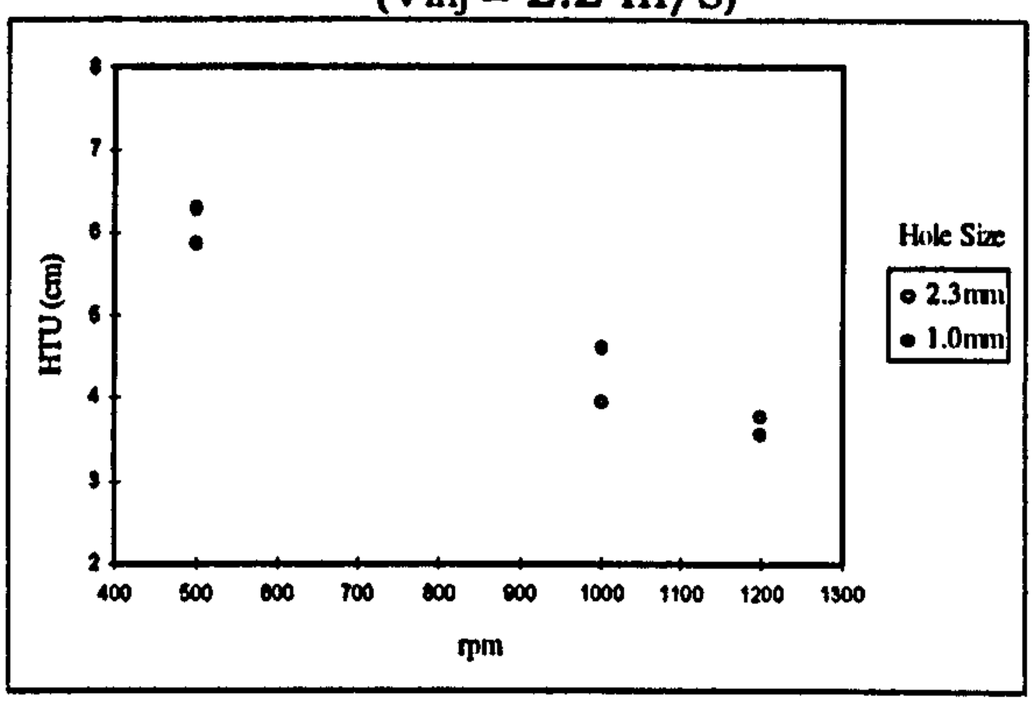

4.4-Discussion.

As shown above a distributor with a high injection velocity performs satisfactory even though the apparent quality of the distribution was degraded (in case of the 4-arms distributor, when using one arm instead of 2,3 or 4 arms). Lower HTUs were obtained at higher injection velocities. Of the three packings, Expamet gave good performance which only slightly dependent of the range of the injection velocity used.

As mentioned earlier that the liquid does have a tendency to maldistribute in RPBs, as shown in the following photographs. The photographs also explain why the theoretical mass transfer models (Penetration and Davidson) cannot mirror the physical situation of the liquid film flow, and why they are so poor in predicting the mass transfer performance as discussed in chapter 3. Photographs P5 through P9 are shown with kind permission from Burns [B4].

Photograph P5 and P6 show how the liquid was distributed in RPBs. A multipoint distributor was used to distribute the liquid onto the packing, and thereby ensuring the time needed to replenish any point at the inner rim of the bed was minimised. But as it can be seen that the liquid was maldistributed. Photograph P7 and P8 show the flow pattern within the bed was far different from a thin liquid film flow assumed by the Davidson model. The liquid rather tend to agglomerate and flows through the bed in preferential paths resulting in varieties of flow patterns such as droplet flow, rivulet flow and film flow. However, photographs P9 and P10 show that more liquid spread was achieved at constant liquid flow rate by using higher rotational speeds, thus it is quite probable that the flow pattern of the liquid was strongly dependent on the amount of rotational speed employed.

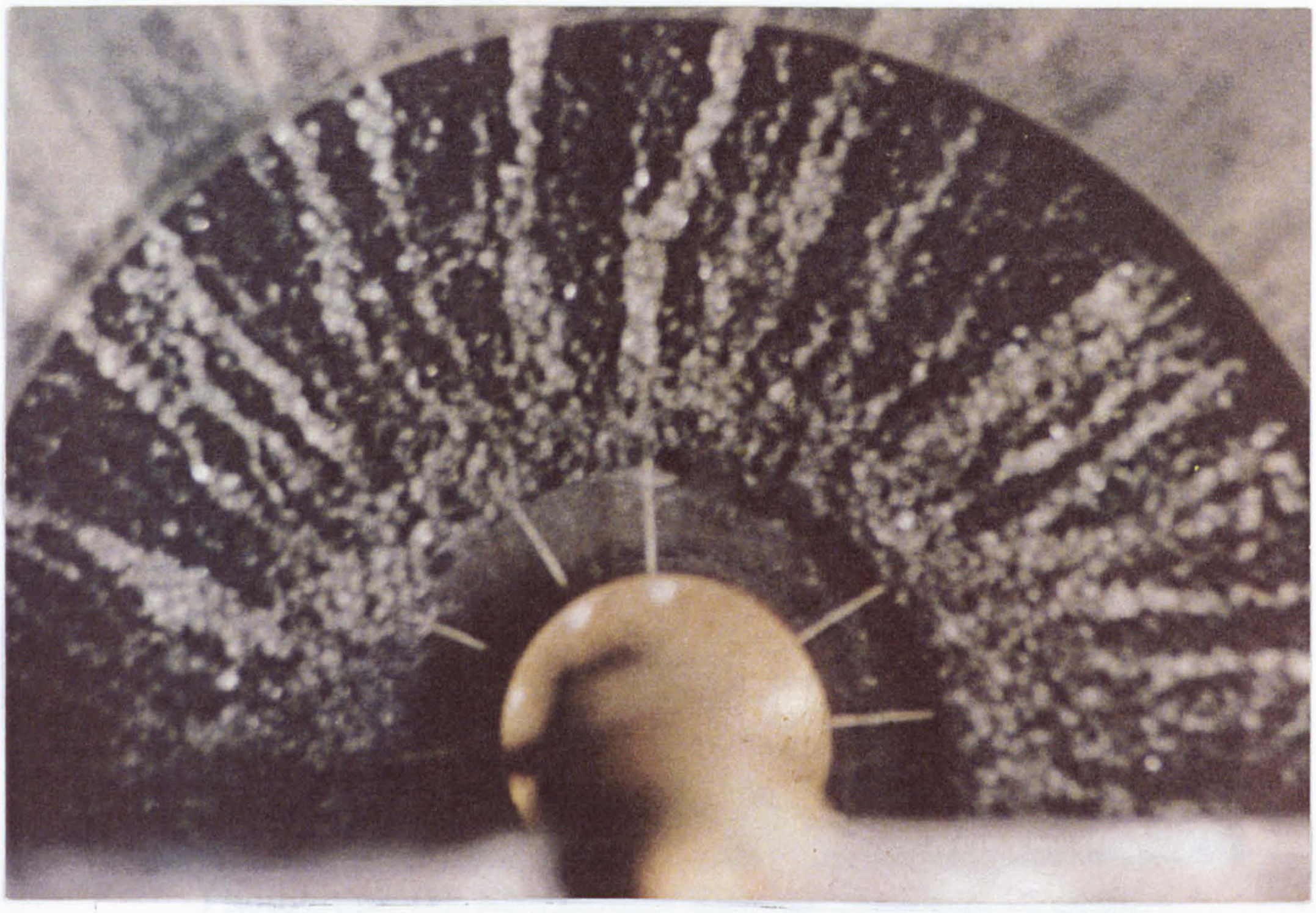

Photograph (5): Radial liquid flow pattern through exposed packing.
12 point liquid distributor with 2.0 L/min. at 400 rpm.

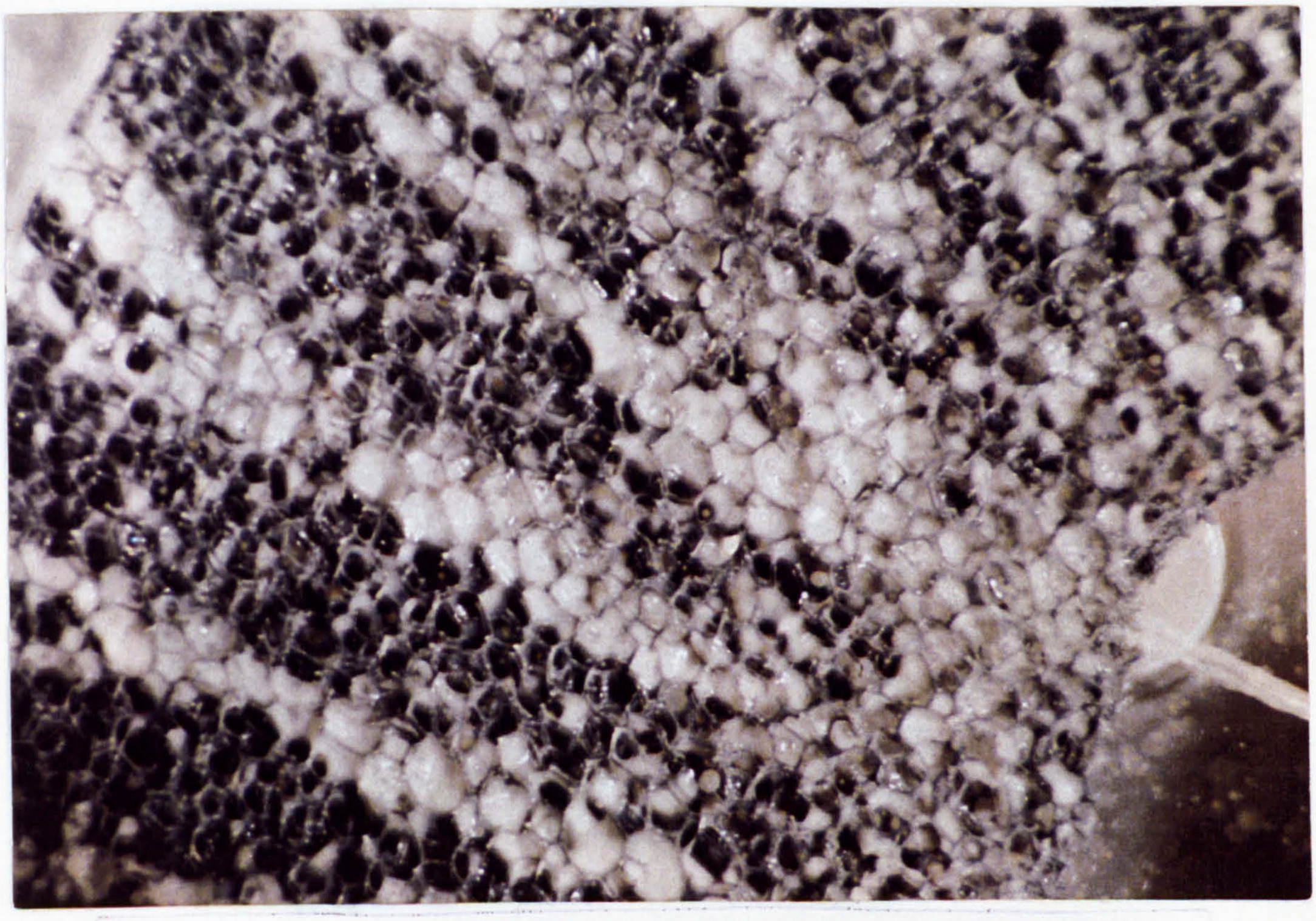

Photograph (6): Radially oriented rivulet flow through exposed packing.
12 point liquid distributor with 2.0 L/min. at 497 rpm.

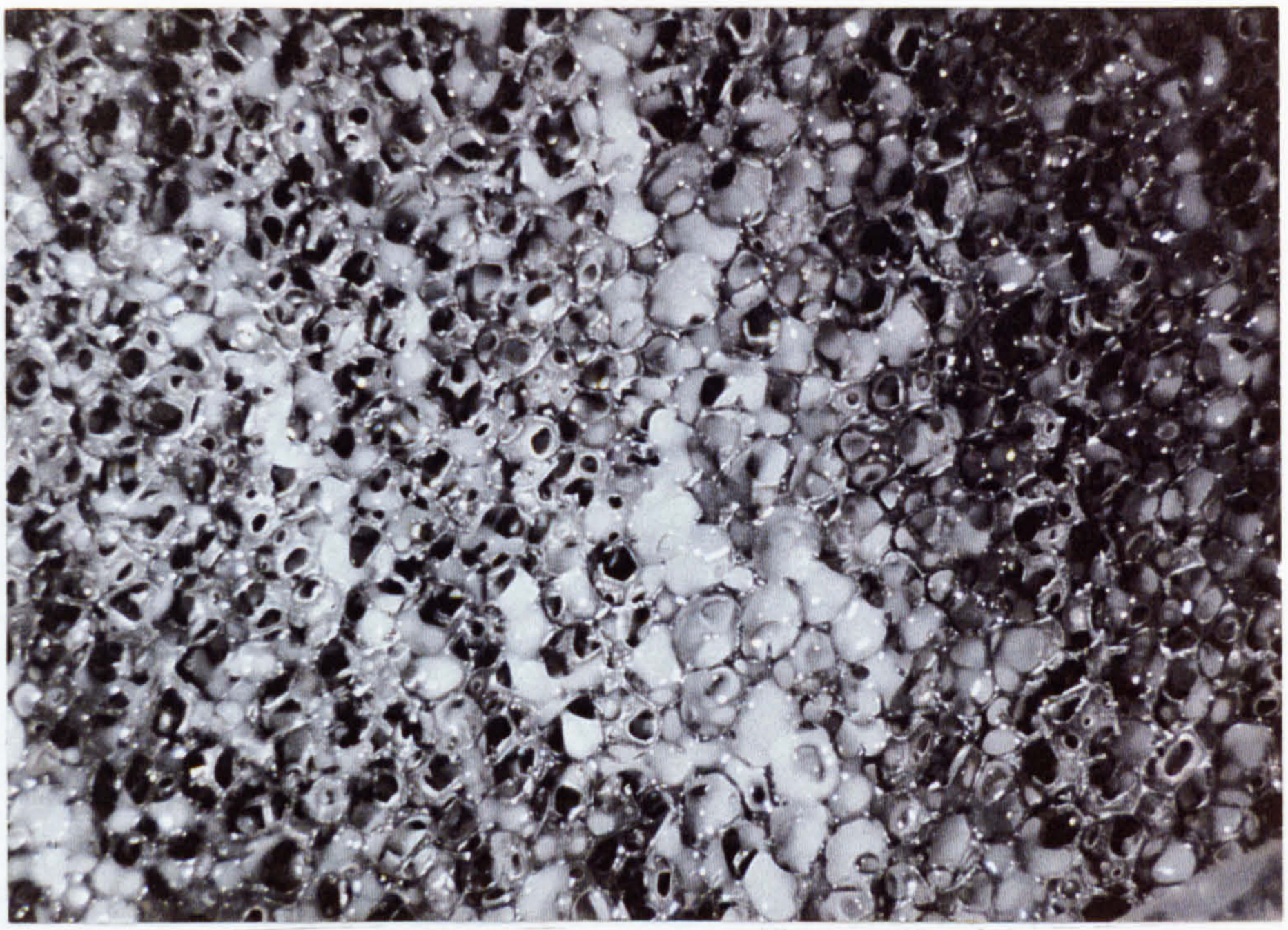

Photograph (7): Rivulet flow through packing. 16 point liquid distributor with 6.4 L/min. at 468 rpm.

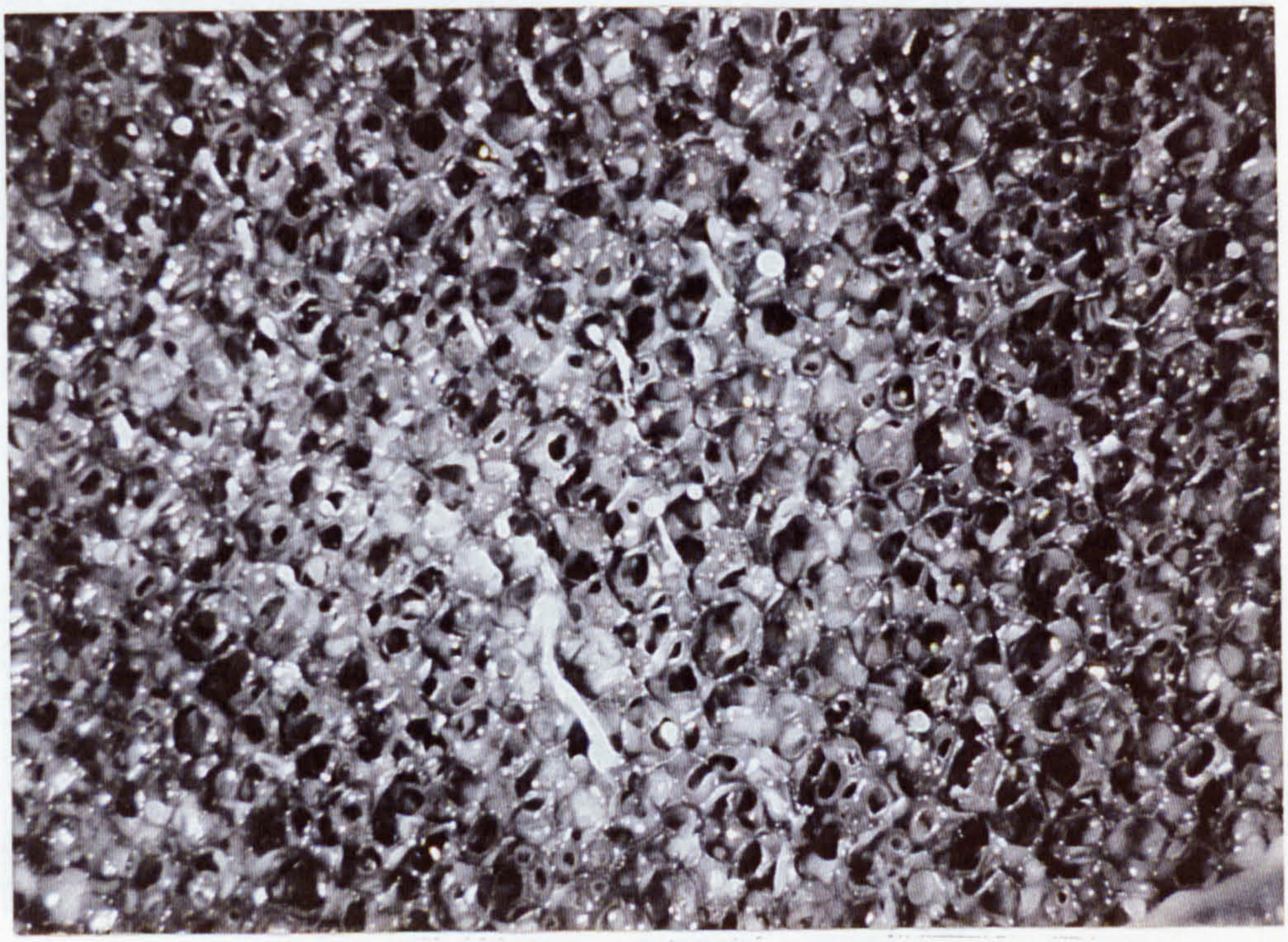

Photograph (8): Change from rivulet flow to droplet flow. 16 point liquid distributor with 6.4 L/min. at 907 rpm.

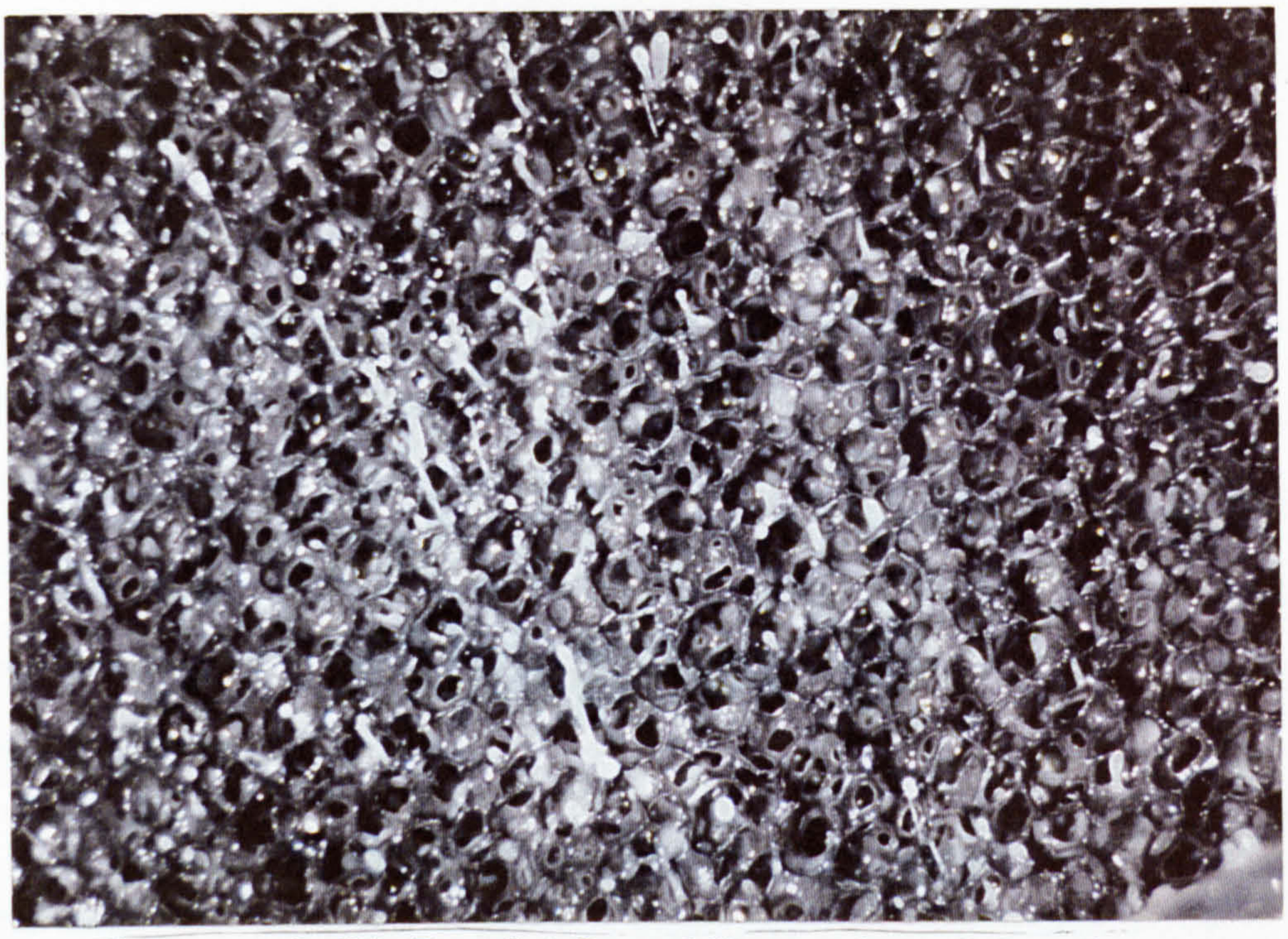

Photograph (9): Droplet flow. 16 point liquid distributor with 6.4 L/min. at 1200 rpm.

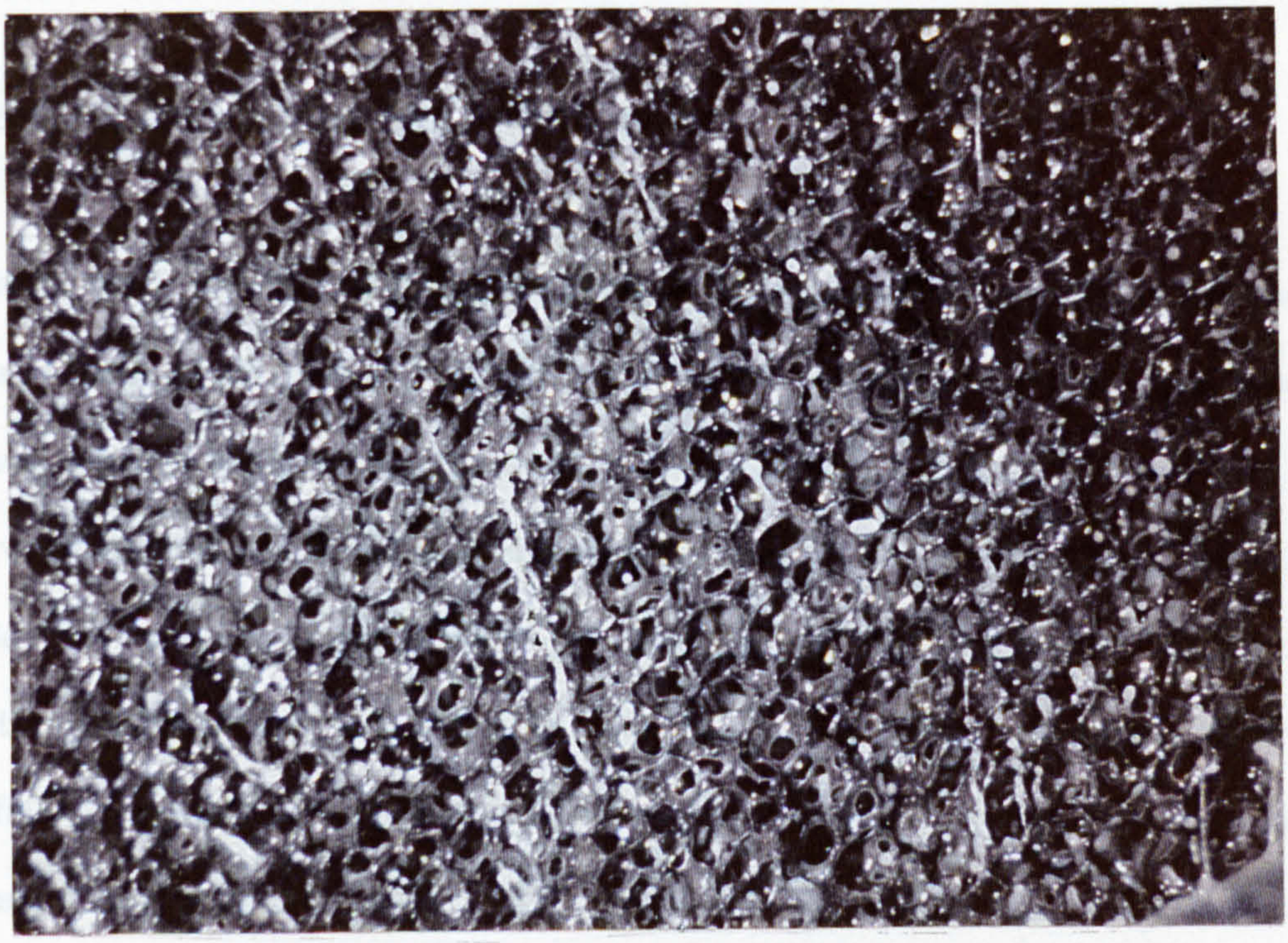

Photograph (10): Droplet flow. 16 point liquid distributor with 6.4 L/min. at 1500 rpm.

Chapter 5

Flooding Behaviour

5.1-Introduction.

This chapter details the flooding behaviour in rotating packed beds. A mathematical model was proposed to predict the pressure drop across the bed.

5.2-Flooding Behaviour in Packed Beds.

The research work conducted to study the flooding mechanism in packed beds is very limited, and most of the research was focused on the wetted wall columns. It has been established that, in wetted wall columns, the interaction between the gas and liquid and the resultant instability of the liquid film determines the flooding point. Hewitt and Hall-Taylor [H4] reported that prior to the onset of the flooding point, the interfacial shear at the gas liquid interface has little effect on the liquid film thickness. However, if the gas flow rate increases, a wavy film flow is established as the flooding point is approached. Shearer and Davidson [S10] studied the behaviour of the liquid film for a stationary wave at the flooding point and verified their model to estimate the flooding velocity. The model defines the flooding gas velocity when the amplitude of the wave

becomes colossal. The calculated flooding velocities can reasonably predict the experimental flooding gas velocity in wetted wall column.

The flooding point in packed beds has been defined in many ways [S7]. Sherwood *et al* [S8] have introduced the very well-known flooding correlation in packed beds, in which different irrigating fluids with different densities, viscosities and surface tension were tested. Approaching flooding point the liquid holdup in the packed bed increases, and therefore, the available area for the gas to flow decreases and a rise in the pressure drop through the bed takes place.

Figure 5.1 shows the behaviour of the pressure drop in countercurrent packed beds at different liquid flow rates. At low liquid flow rate, the available area for the gas to flow will be equivalent to that as if the bed was not irrigated. If the gas flow rate is increased, the pressure drop will increase and its magnitude will vary with gas flow rate. If the gas flow rate is further increased both the pressure drop and the liquid holdup would increase and consequently forcing the liquid to be blown out by the gas leaving the bed. At this condition the gas velocity is called the flooding velocity. Accordingly, the bed must operate at gas flow rate far lower than that on the flooding condition.

Leva [L2] discussed the loading and flooding conditions in packed beds for different types of packing materials and irrigating fluids other than water. A density parameter ($\Phi = \rho_w/\rho_L$) has been introduced to the ordinate values given by Sherwood *et al* [S8]. The density parameter was found to improve significantly the prediction of the flooding velocity in packed beds.

Szekely and Mendrykowski [S9] investigated experimentally the flooding behaviour on packed beds by using a modification to Sherwood correlation as suggested by Leva [L2] for different types of packings using high density and surface tension materials.

Fig.(5.1): Pressure Drop Behaviour in Packed Beds.[P7]

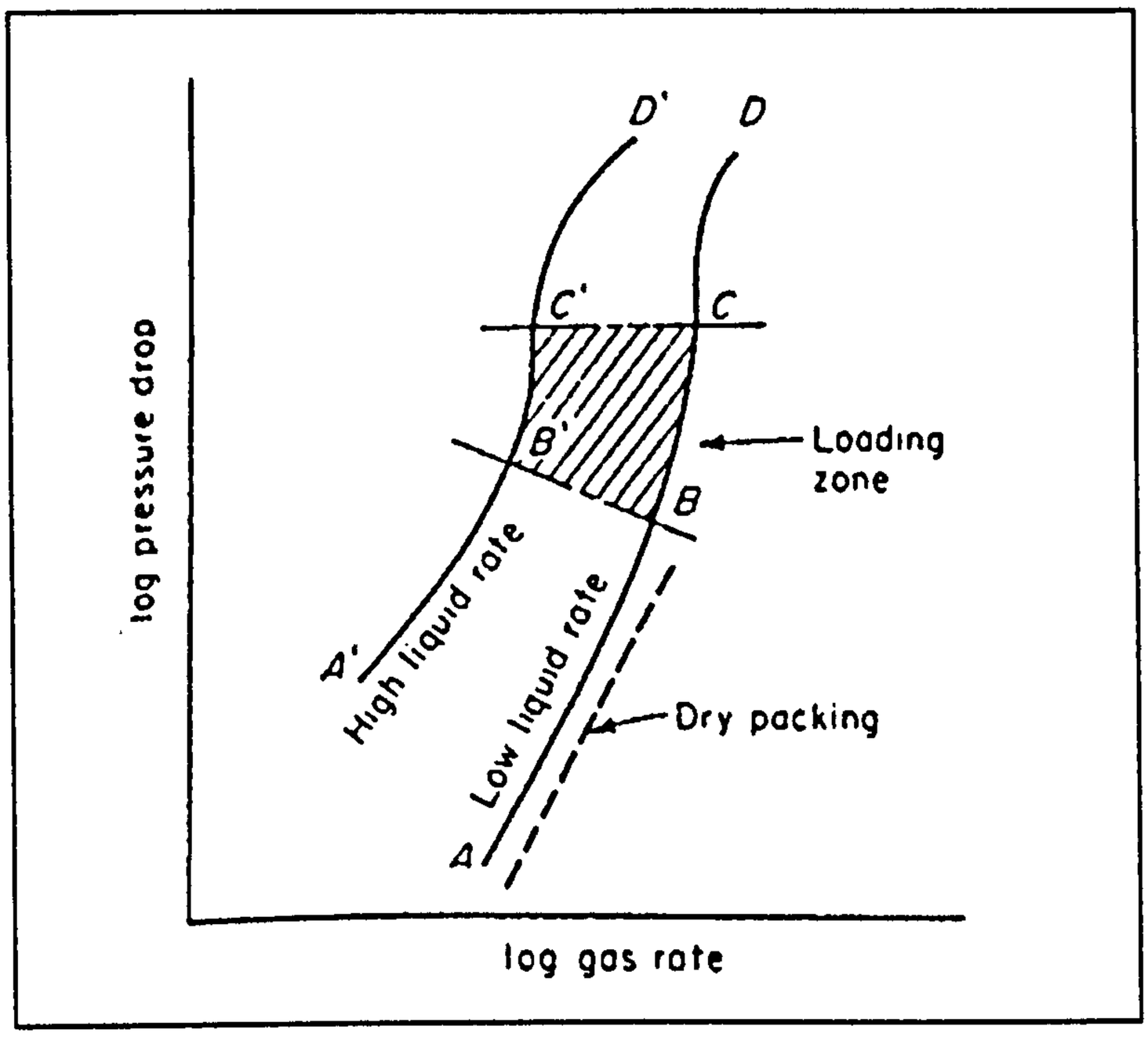

They showed that the modification introduced by Leva for the density parameter ($\Phi = \rho_w/\rho_L$) was the main reason to overpredict their experimental findings as the liquid density effect was overcompensated. On the other hand, the original Sherwood flooding correlation appeared to be in good agreement with their experimental results. They concluded that, despite the strong dependency of hold-up on surface tension, it is unlikely that the prediction of the flooding velocities for liquids with surface tension up to 500 dyne/cm will be affected.

Hutton *et al* [H3] investigated the mechanism of flooding in conventional packed beds. They developed two models; gravity-viscosity model for low liquid Reynold number and gravity-inertia model for high liquid Reynold number. They defined the flooding point as occurring when the derivative of liquid flow rate with respect to hold-up at constant gas flow is zero, i.e. $(\partial L/\partial h)_G = 0$. Their expressions, which can predict the liquid flow rate at the flooding point in terms of pressure gradient and liquid hold-up, were found to overpredict the liquid flow rate value at flooding.

5.3-Flooding Behaviour in Rotating Packed Beds.

Flooding in RPBs occurs only at the centre area 'eye' of the bed which has the lowest centrifugal acceleration compared with that at the bed periphery. In addition, the divergent nature of the flow implies that L and G are higher at the rotor centre. The higher hydraulic capacity behaviour in rotating packed beds can be explained on the basis of Sherwood correlation. Under the action of high centrifugal acceleration, higher gas and liquid velocities can be achieved thereby allowing much higher gas and liquid throughputs.

It is worth pointing out the fundamental difference between the behaviour of the liquid holdup in conventional and rotating packing beds. As shown in figure 5.2 the holdup in the bed will change rapidly for a small increase in liquid loading. The flooding condition is represented by point (A), which has been widely used in the description of the flooding mechanism in conventional packed beds, Billet [B5] and Hutton *et al* [H3]. However as noted above, in the present work flooding occurs within a narrow zone on the inner rotor surface. Excess liquid is rejected by the rotor and can no longer reach the outer (non-flooded) radial point. More detailed discussion of liquid holdup in RPBs is given by Burns[B4].

Fig.(5.2): Liquid Holdup Behaviour in conventional Packed Beds[B5].

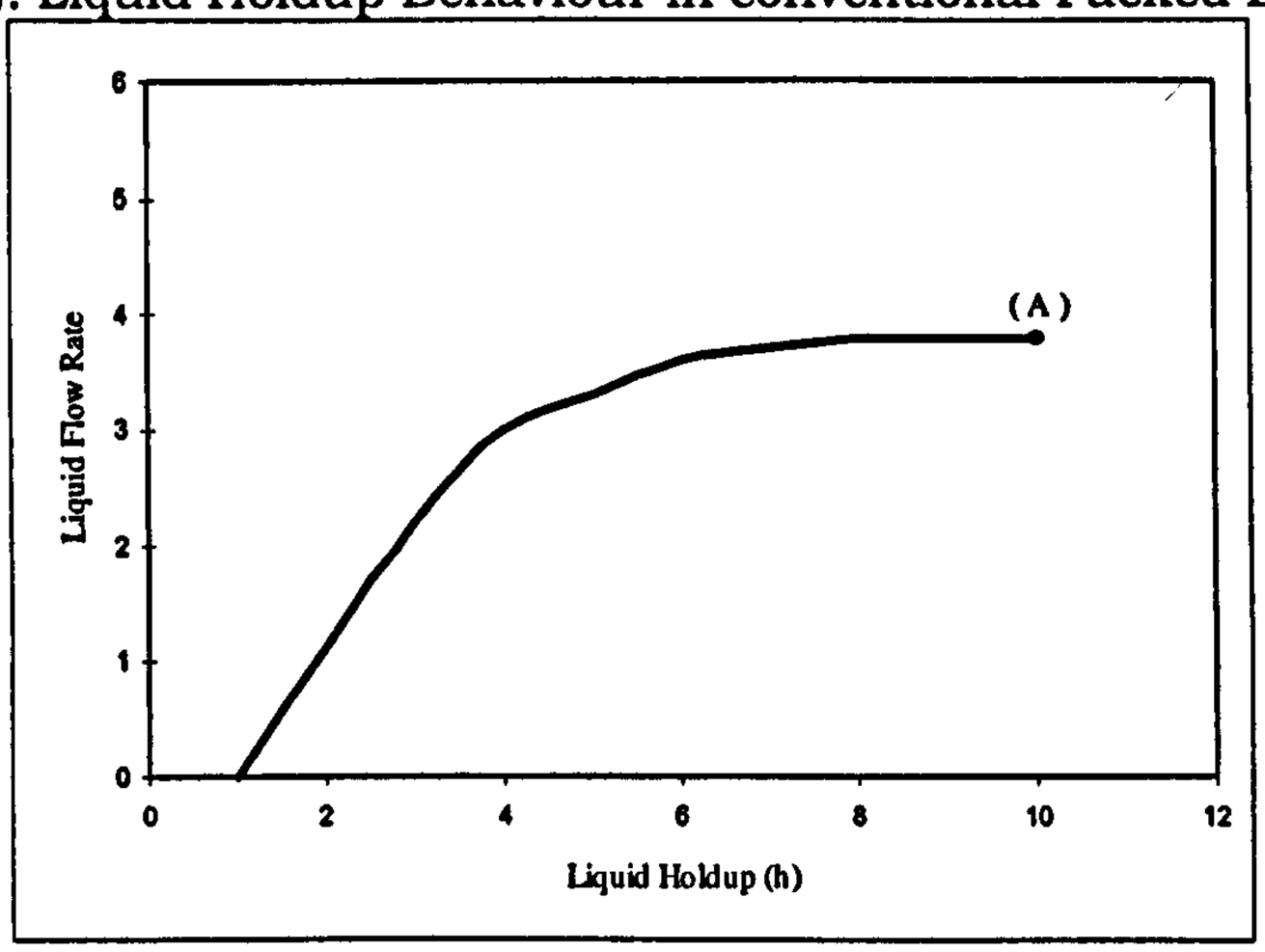

5.3.1-Sherwood Correlation.

As can be seen from Sherwood flooding correlation, figure 1.1 for a given system, the physical properties and the superficial mass flow rates for liquid and gas will fix the value in the abscissa in the Sherwood plot. If ' g ' is replaced by ($\omega^2 r_i$), where ω and r_i are the rotational speed and inside radius of the bed, respectively, then the fixed value of the ordinate $\left(U_g^2 a_p / \omega^2 r_i \varepsilon^3\right)$ allows to use either higher flooding velocity (U_g), and hence lower gas flow area, or high density packing material (a_p). The combination of using higher gas velocity and density packing can explain the major reduction in HTUs achieved by using rotating packed beds in mass transfer systems with liquid film limitation.

5.3.2-Wallis Correlation.

Wallis [W4] discussed the flooding criterion in vertical tubes and proposed a correlation, equation 5.1 for flooding which could also be applied to packed beds:

$$J_g^{*1/2} + m J_L^{*1/2} = C \qquad (5.1)$$

where,

$$J_g^* = U_g \left(\frac{\rho_g}{\rho_L - \rho_g} \right)^{0.5}$$

$$J_L^* = U_L \left(\frac{\rho_L}{\rho_L - \rho_g} \right)^{0.5}$$

U_g and U_L are the gas and liquid superficial velocities, respectively. m and *C* are the slope and the intercept of equation 5.1. The equation was tested for the range of the experimental data and packings used by Sherwood *et al* [S8]. The values of m and *C* in equation 5.1 are found to be unity and 0.775, respectively.

Lockett [L3] used the Wallis approach to describe the flooding in RPBs. He used structured packing material, a_p= 1770 m^{-1}, for countercurrent flow of air and water. The flooding point was determined by varying the rotational speed while holding water and air flow at constant rates. The pressure drop of the bed was determined as the difference between the measured pressure drop values with and without the packing in the rotor. As the rotational speed decreases the pressure drop across the bed increases to a maximum value after which starts to fall. At this condition, the bed was considered to be flooded. Lockett [L4] found that when the Wallis approach is used to study the flooding behaviour in RPBs, for sets of different rotational speeds, all sets should exhibit similar trends (i.e. the values of the slope m in equation 5.1 for each set of experimental data should be the same). It was claimed that in this manner any departure can be readily discovered.

Munjal *et al* [M1,M8] have studied the flooding in rotating packed beds, using air/water system, and packing of 1.09 and 3mm glass spherical beads. The ratio of centrifugal acceleration, based on inside radius of the bed r_i, to gravitational acceleration was varied between 35 to 135. The determination of flooding point was carried out similar to the way used in packed beds when the value of the slope between the log pressure drop and the log gas flow rate becomes equal to or greater than 2. They concluded that the Sherwood flooding correlation, for dumped rings, underpredicts the flooding point by 40-70% and the loading point by 40%. This will result in a rather conservative design.

Keyvani and Gardner [K1] have studied the pressure drop characteristics in rotating packed beds. In their model the pressure drop is not confined to the bed but also include the pressure drop between the rotating bed and the casing. The model predicted the experimental data fairly well. They have noticed an unusual behaviour in their pressure drop data. It was found that the pressure drop would be lower when the bed is irrigated than when it was dry (gas flow only). It was mentioned in this work

that, the liquid films lubricate the surface of the packing thereby minimising the drag exerted on the gas by the wetted packing.

Singh [S6] studied the hydraulic performance in RPBs using metal foam packing material. Based on the criterion in which the flooding point was determined when the pressure drop increases at a rate of 500 Pa for every 100 rpm decrease in rotational speed, it was found that the Sherwood correlation overpredict the flooding velocity. A semitheoritical model for the pressure drop was given for the pressure drop depending on the sum of the rotational pressure drop ($\Delta P_{rot} \alpha \omega^2$) and the pressure drop due to the inertial of the gas ($\Delta P_{inertia} \alpha U_g^2$). The model was found to predict the experimental data within an accuracy of ±30%.

Sirenko and Lukov [S4] studied fluid dynamics in RPBs. They used three structurally different packing materials. They showed that, the irrigation rate has a minimal effect on the gas dynamics within the bed prior the flooding point. They claimed this occurred as a result of less interactions between the thin liquid films, flowing over the packing, and the gas at very high centrifugal acceleration. Also, they showed two unusual findings of the behaviour of the pressure drop for empty beds (without packing). First, the pressure drop can be as high as three times the pressure drop in packed bed, and they attributed this to the role of the packing to organise the gas within the narrow gap sizes of the bed. Secondly, the pressure drop decreases with increase in the irrigation loads for a range of rotational speed. They attributed this to the capability of liquid films to lubricate the edge of the rotor basket. Finally they proposed different correlations for the pressure drop for the three packing material used. These correlations were found to predict the experimental data within an accuracy of ±10%.

Liu et al [L1], studied the pressure drop behaviour in RPBs. They used two different packing material with surface areas of 524 and 1027 m^2/m^3 having porosities of 0.533 and 0.389, respectively. They concluded that the pressure drop was strongly dependent

on the gas flow rate. Furthermore, it has been demonstrated that at low rotational speed, the type of the packing (i.e. geometry) affects the pressure drop behaviour due to the liquid holdup change.

5.4-Experimental Equipment for Flooding Tests.

A second smaller experimental rig was used for the flooding tests. Figure 5.3 shows the flow diagram of the test rig used in the flooding tests. A motor (1.5 kW, max. 3000 rpm, Technodrive, model: 90EL-4G MVFO) was used to drive the rotor. The rotational speed was controlled by a speed controller type (CHEETAH SM). Air and Water were used as working fluids. The air and water enter and leave the motor in a similar way as in the mass transfer test rig. As no chemicals were involved throughout the runs, the air was allowed to leave freely from the eye of the rotor to the laboratory space. The air was supplied from the departmental compressed air facilities and a 30mm diameter orifice was used to measure the different air flow rates (Appendix A: calibration of orifice meter). Water was supplied from a 0.20 m^3 tank. The water flow rate was measured using liquid rotameter (model: 35 XS) and the water leaving the rotor returned to the same tank by using a return pump. A small surge reservoir was used for the water leaving the rotor. The water level in the surge reservoir was controlled by a level controller interconnected with the return pump. The liquid was distributed using a single pipe distributor figure 5.4 similar to that one used in the mass transfer runs. The distributor has twenty holes (10x 1mm and 10x 2.3mm in diameter) and each hole was threaded so that the injection velocity can be controlled at any pre-set liquid flow rate.

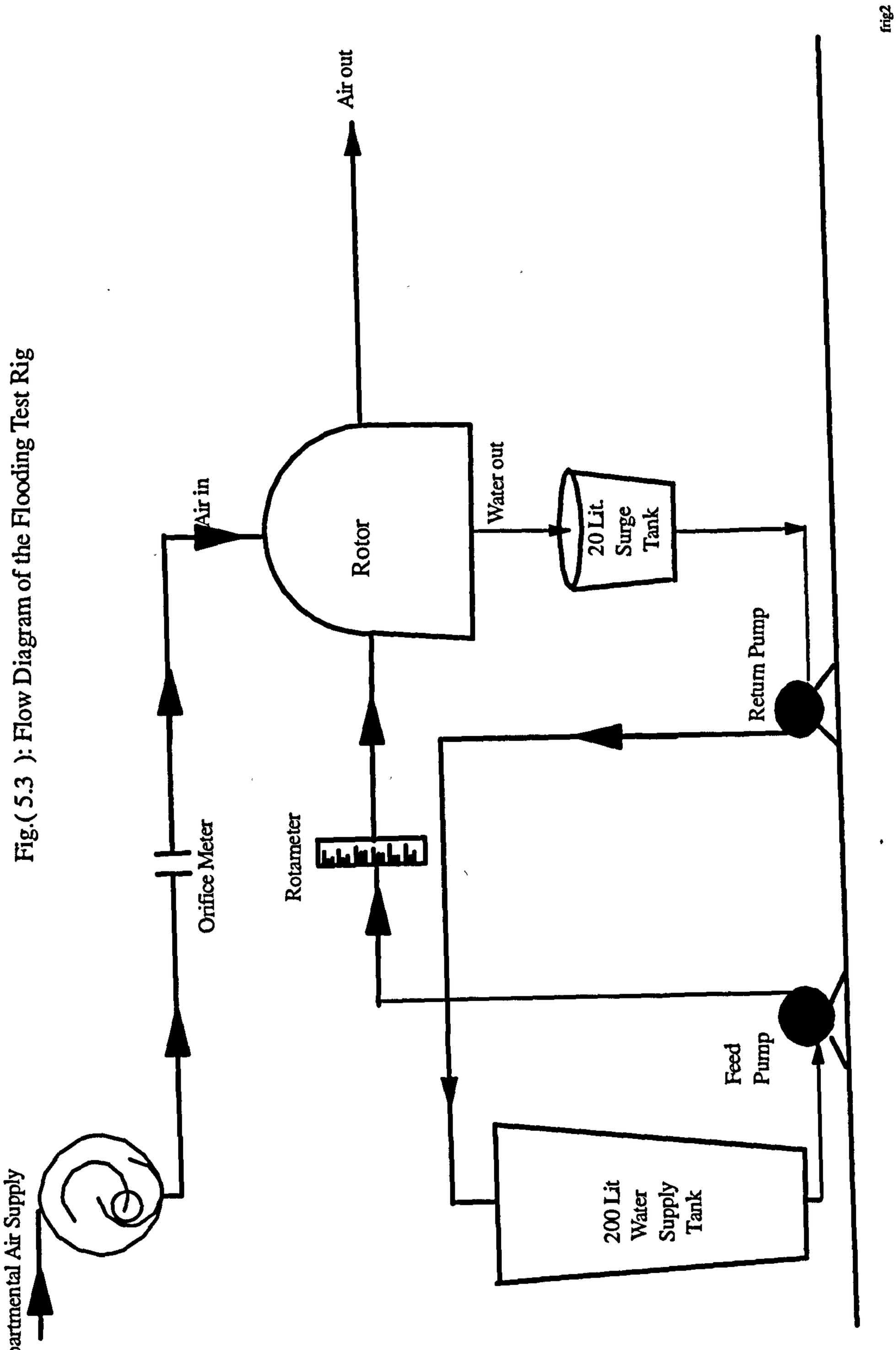

Fig.(5.3): Flow Diagram of the Flooding Test Rig

Fig. (5.4): Single Pipe Distributor

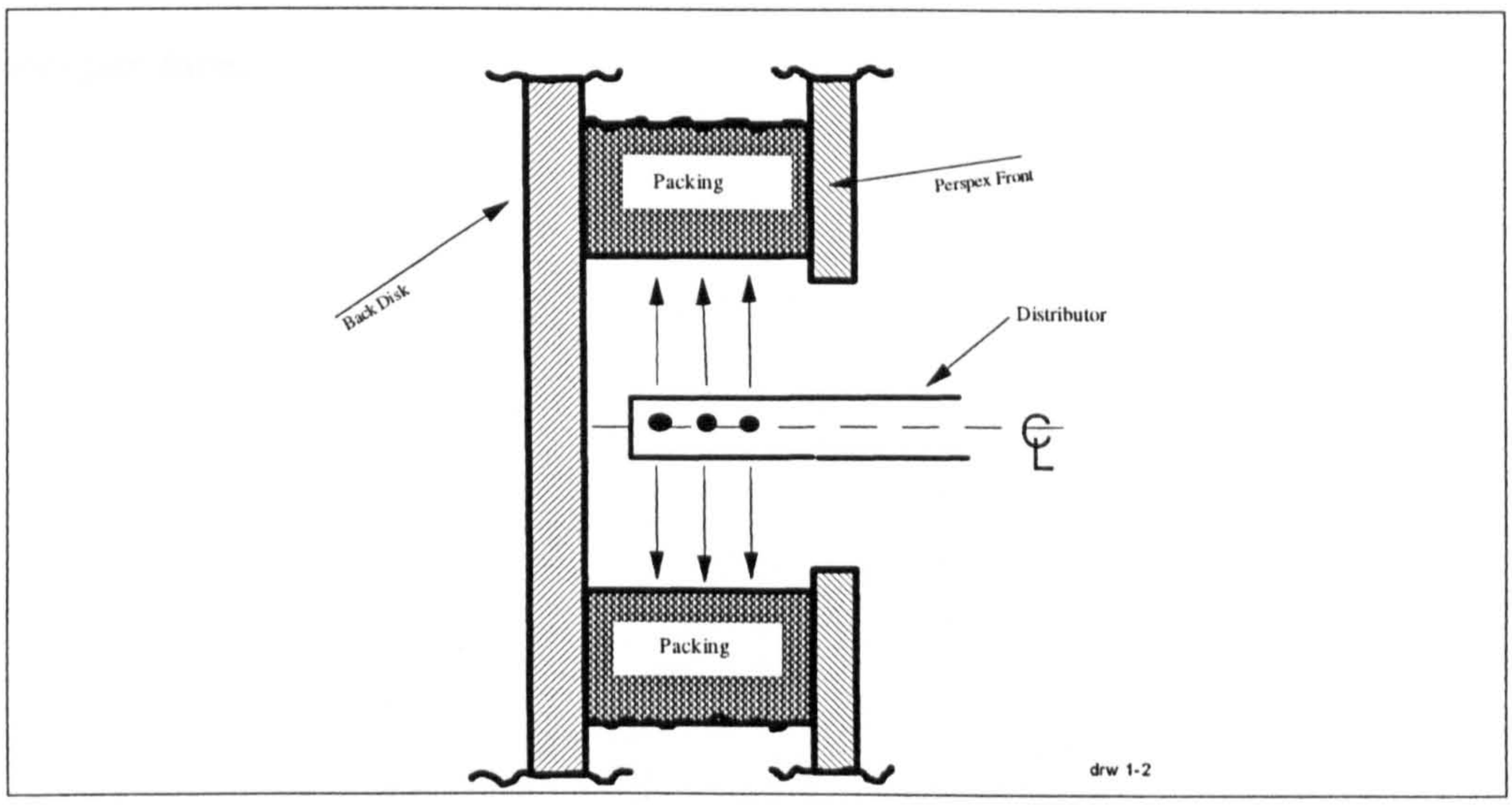

Figure 5.5 shows section through of the rotor used in the flooding runs. It resembles the test rig used for mass transfer runs, but with a smaller dimensions. The packing material used throughout the flooding tests was Declon. It has OD and ID of 210 and 70mm respectively, and an axial depth of 22mm. The rotary union (DEUBLIN UNION, model: 355-021-222) was mounted onto the shaft at the rear end. The union was modified in order to accommodate the slip ring assembly as shown. Two miniature pressure transducers (Druck, model: PDCR 81, operating pressure 3 bar g) were used to measure the pressure at two different radial positions at 35 and 105mm respectively. Additionally, a 10mm OD stainless steel tube was fixed in the back disc of the rotor to house, safely, the wires of the two pressure transducers. As shown in figure 5.5 the stainless steel tube was then laid out coaxially with the rotor. It was extended along the shaft and fixed into the front part of the slip ring assembly.

Figure 5.6 shows the details of the rotor. Twenty five holes of 5mm in diameter were drilled to allow the air to flow through into the bed. Four peripheral fixing rods were fixed in the back disc of the rotor to help to mount the bed on the rotor. A perspex front disc was used to sandwich the bed (packing) with the back disc. Further a number of five equally spaced cut-outs (for the liquid leaving) were machined on the perspex peripheral edge. A stainless steel peripheral lip was used to establish the liquid

seal at the periphery. A gap of about 2mm was maintained between the lip and the front perspex face.

Fig.(5.5): Section Through The Flooding Test Rotor

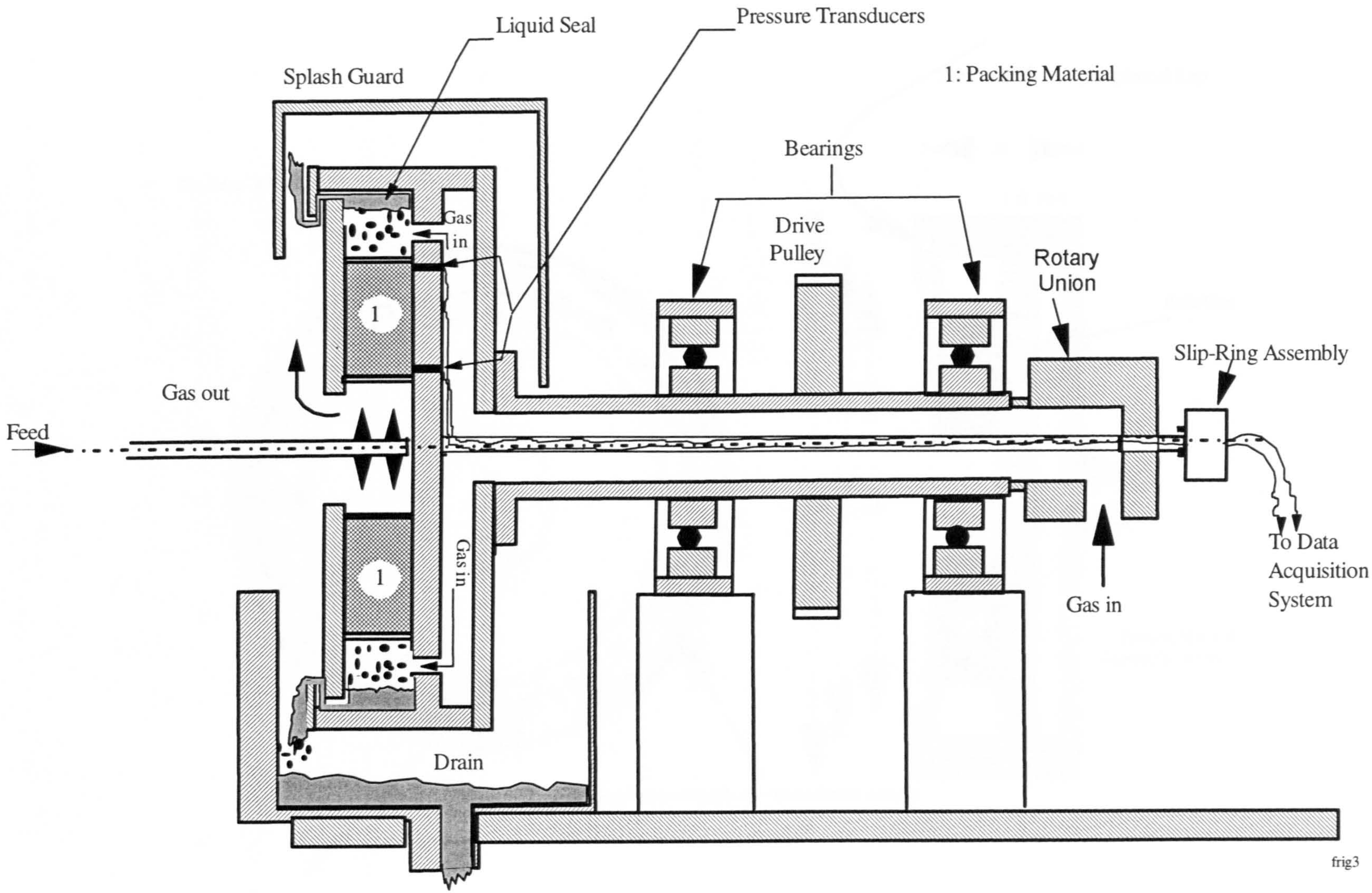

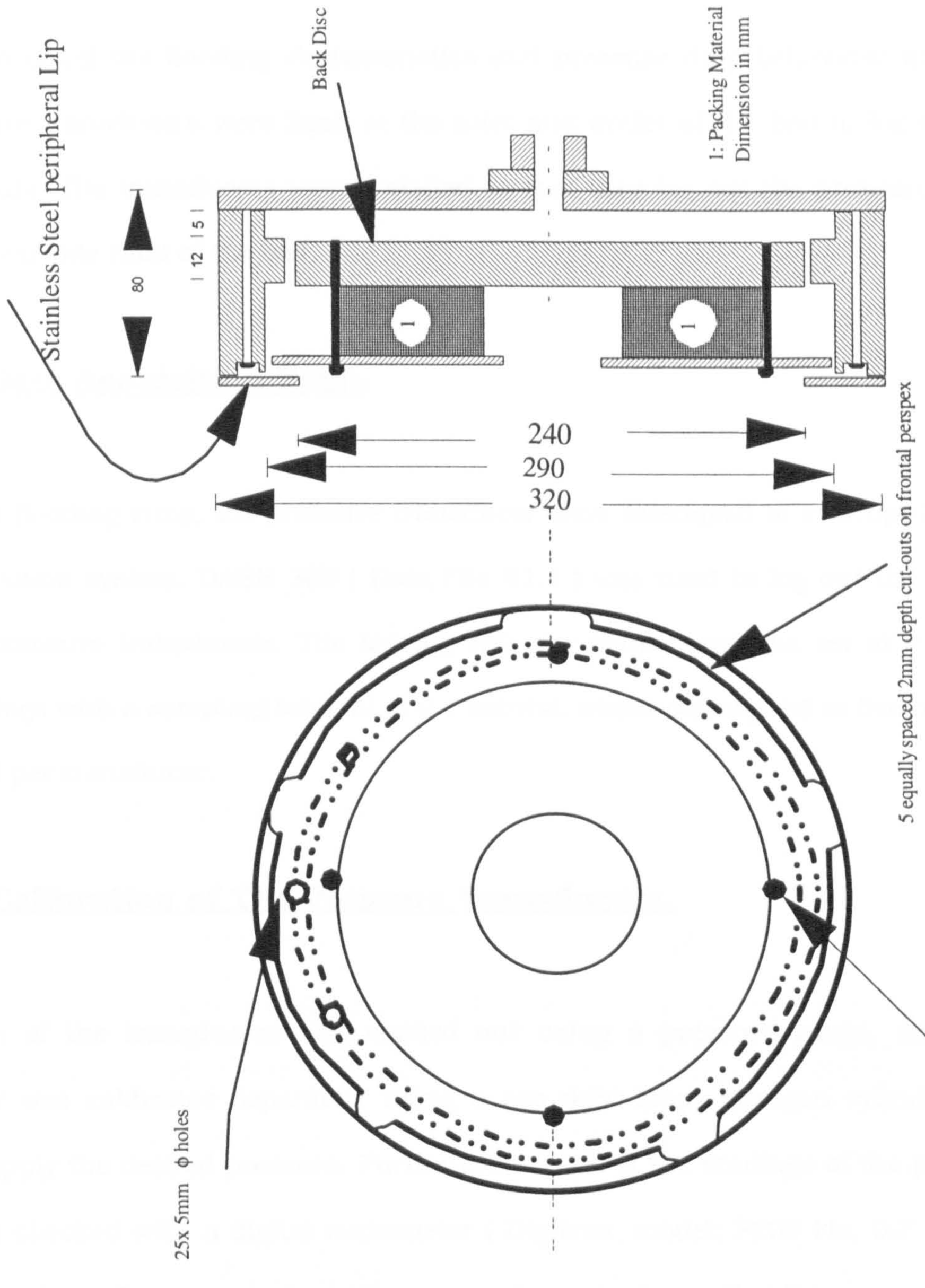

Fig:(5.6): Rotor Details of the Flooding Rig.

5.4.1-Data Acquisition System.

5.4.1.1-Introduction.

To study in detail the flooding characteristics and pressure drop behaviour in RPBs, two pressure transducers were fixed at the inlet and outlet of the bed to log out the pressure data. The transducers were installed so that they log out the pressure at the inside and outside radii of the bed.

5.4.1.2-Data Acquisition Type.

During the flooding runs, the pressure transducer were interfaced to a computer. The data acquisition system, DASH 300 (Data File V1.1) was used to log out the signals from the pressure transducers. The logging rate per transducer was set at a rate of 1000 readings with a sampling interval of 0.1 second, which correspond to five readings per second per transducer.

5.4.1.3-Calibration of The Pressure Transducers.

Calibration of the transducers was carried out using a pressure gauge, and each transducer was calibrated separately using a gas tight loop. Nitrogen cylinder, was used to supply the desired pressure. Furthermore, each of the readings of the pressure gauge was checked with a digital manometer (Digitron, model; P200 Hx, 0.7 Bar g). Further details on the pressure transducers are shown in Appendix (E).

During rotation both transducers exhibited trends as shown typically in figure 5.7. The transducers were fixed into the back disc as shown in figure 5.5 at two different position corresponding to the inside and the outside radii of the bed. As typically the pressure drop for in any packed bed is proportional to the square of the gas velocity (

e.g. Fanning model: $\Delta P \alpha U_g^2$), the sensors' readings can be reasonably expressed by a second order polynomial.

Fig.(5.7): Typical Pressure Transducers Readings at Two Radial Positions.

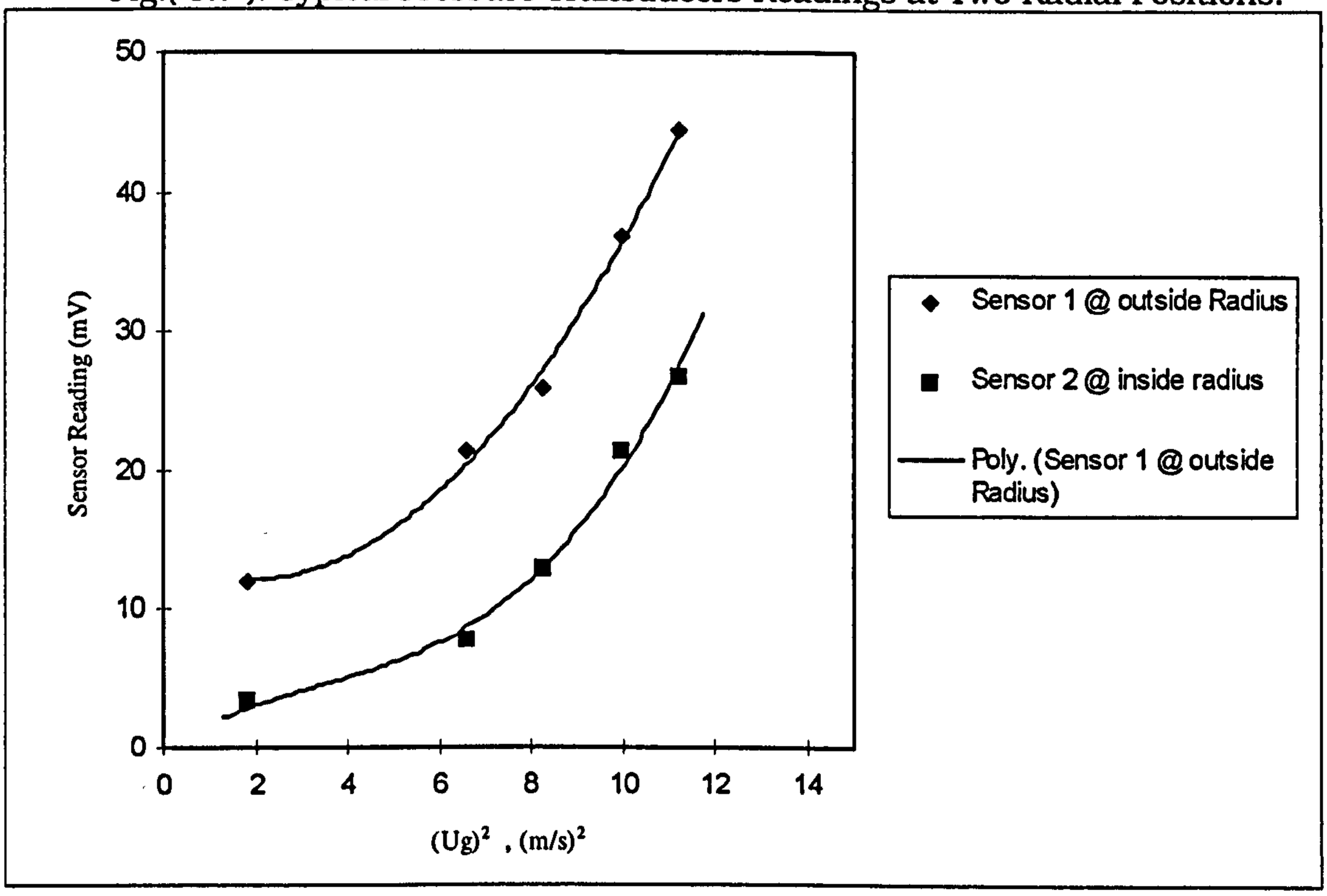

5.5 -Flooding Point Determination.

The flooding data are shown in figures 5.8 through 5.11. Each flooding run was carried out by fixing the rotational speed and the liquid flow rate, then the gas flow rate was gradually increased. The flooding point was determined by visual observation where an excessive splash of water was noticed at the eye of the bed.

A further test on the flooding point determination was carried out whereby the gas and liquid flow rates were fixed and the rotational speed was gradually reduced from a high speed. In this test the amount of water noticed, to accumulate at the eye of the bed, at the flooding point was similar to that obtained in the above procedure. The obtained rotor speeds in these tests were within the experimental error of ±20 rpm of the rotor speeds obtained in the procedure mentioned earlier. Apart from some noise in the

pressure data near flooding, this finding will indicate the fundamental difference in the behaviour of liquid holdup between RPBs and gravity packed beds as discussed in section 5.3. This conclusion was supported by Burns [B4] where the liquid holdup in the bed was found to, continuously, decrease thus less liquid will be effectively flowing through the bed at the flooding conditions.

It should be pointed out that at flooding the pressure readings across the bed have maintained its monotonic trend and no sudden change in the pressure data were experienced. Some of the data recorded during the flooding experiments are shown in Appendix (E). Figures E1 through E4 show the pressure readings (in milli-Volt) as the gas flow rate increases until the flooding point. Beyond the flooding point very low voltage was recorded as a result of turning the gas off.

5.5.1- Flooding at Arbitrary Liquid Injection Velocity.

Figure 5.8 shows the flooding points for Declon determined according to the procedure mentioned above. The data were compared with the Sherwood flooding line. It can be seen that, if the Sherwood line for random packing, was used to determine the hydraulic capacity of a rotating bed, it would yield a conservative design. In this set of runs the injection velocity was not fixed, but it was kept high enough so that the jets could easily impinge on the packing and were not affected by the free vortex at the eye of the rotor.

5.5.2- Flooding Data at Constant Injection Velocity.

In order to maintain constant injection velocity, the number of holes must be changed for every liquid flow rate. The liquid was distributed using the single pipe distributor, as shown in figure 5.4. The distributor has a total of 20 holes; 10 holes each has 2.3mm in diameter and the other 10 each has 1.0mm in diameter. For each liquid flow

rate, the number of holes, to be used, were selected on the condition that the irrigation density (i.e. the same number of jets per each zone at the inner area of packing) was maintained. The injection velocity was maintained at about 12 (m/s). This was chosen to ensure that the jets, before and at the flooding condition, reach the bed with minimum entrainment and the tangential component of the injection velocity of the jets was higher than the tangential velocity of the bed. Figures 5.9 and 5.10 show the rotational speed at flooding condition for different gas flow rates at various liquid flow rates. At constant rotational speed, if the liquid flow rate is increased then a lesser gas flow rate would be needed to flood the bed as expected. This can be explained on the basis that at fixed rotational speed, as the liquid flow rate increases the apparent residence time of the liquid will drop, hence the liquid holdup in the bed becomes greater and subsequently the bed would be closer to the flooding condition in comparison with low holdup values at lower liquid flow rate.

Figure 5.11 shows the data in figures 5.9 and 5.10 plotted in the Sherwood plot. It can be seen, the flooding velocity will be higher than the predicted values by Sherwood line.

Figure 5.11 is different from figure 5.8. In the latter, the liquid injection velocity was arbitrary and in the former the liquid injection velocity was constant. For constant liquid flow rate if the gas flow rate is increased the rotational speed must be increased to avoid flooding. However, for liquid flow rates 10.5 to 21.9 (L/min) the trend of the flooding velocity did not follow the Sherwood line by having higher Y-values when both the rotational speed and gas flow rate were increased. This would tend to imply that, the effect of the gas velocity will apparently have more profound effect at lower liquid flow rates on the Y-values than the increase in the rotational speed (g's).

Fig.(5.8): Flooding Data Obtained at Different Injection Velocity.

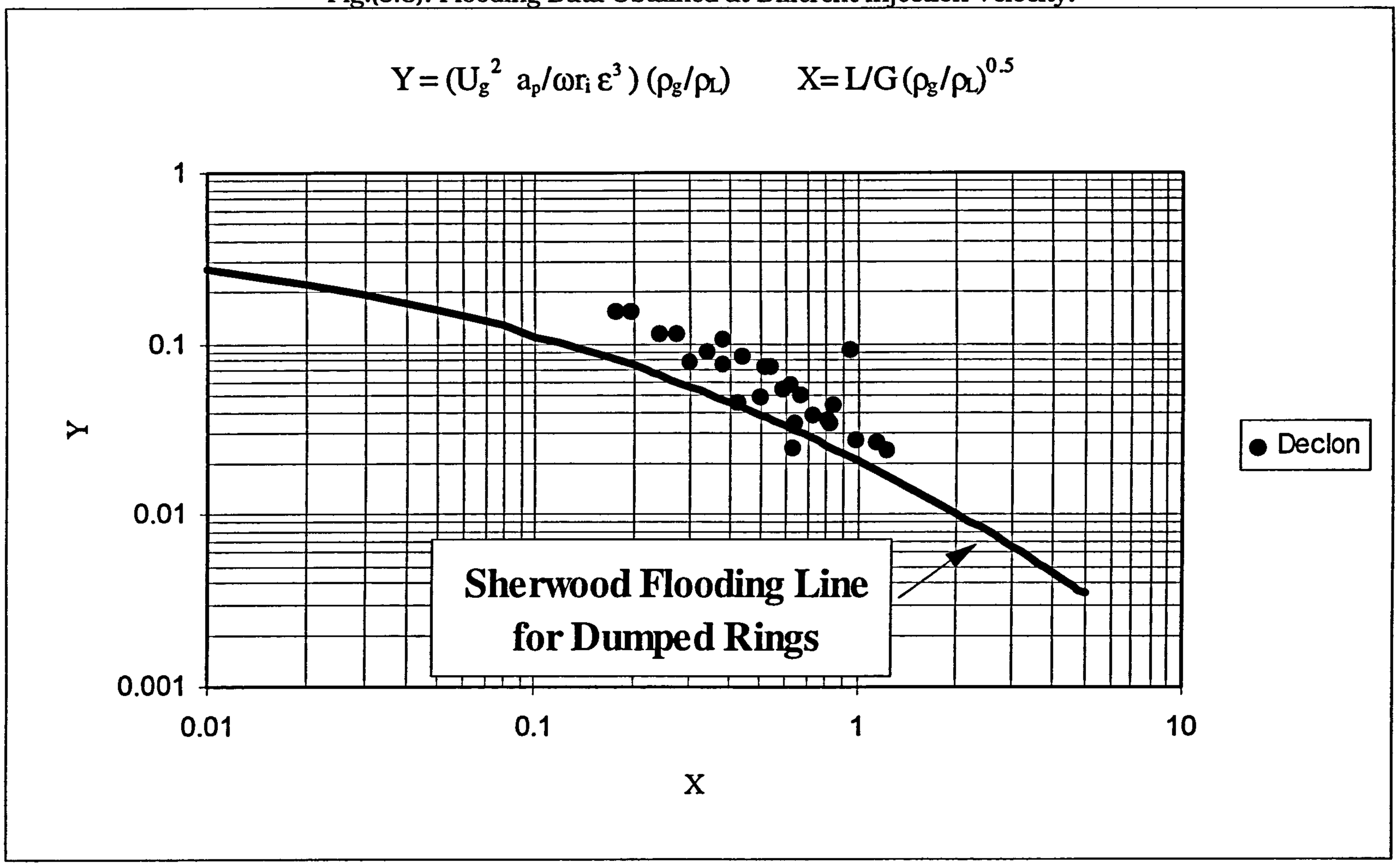

Fig.(5.9): Experimental Flooding Point Data: rpm Vs. G for Various L

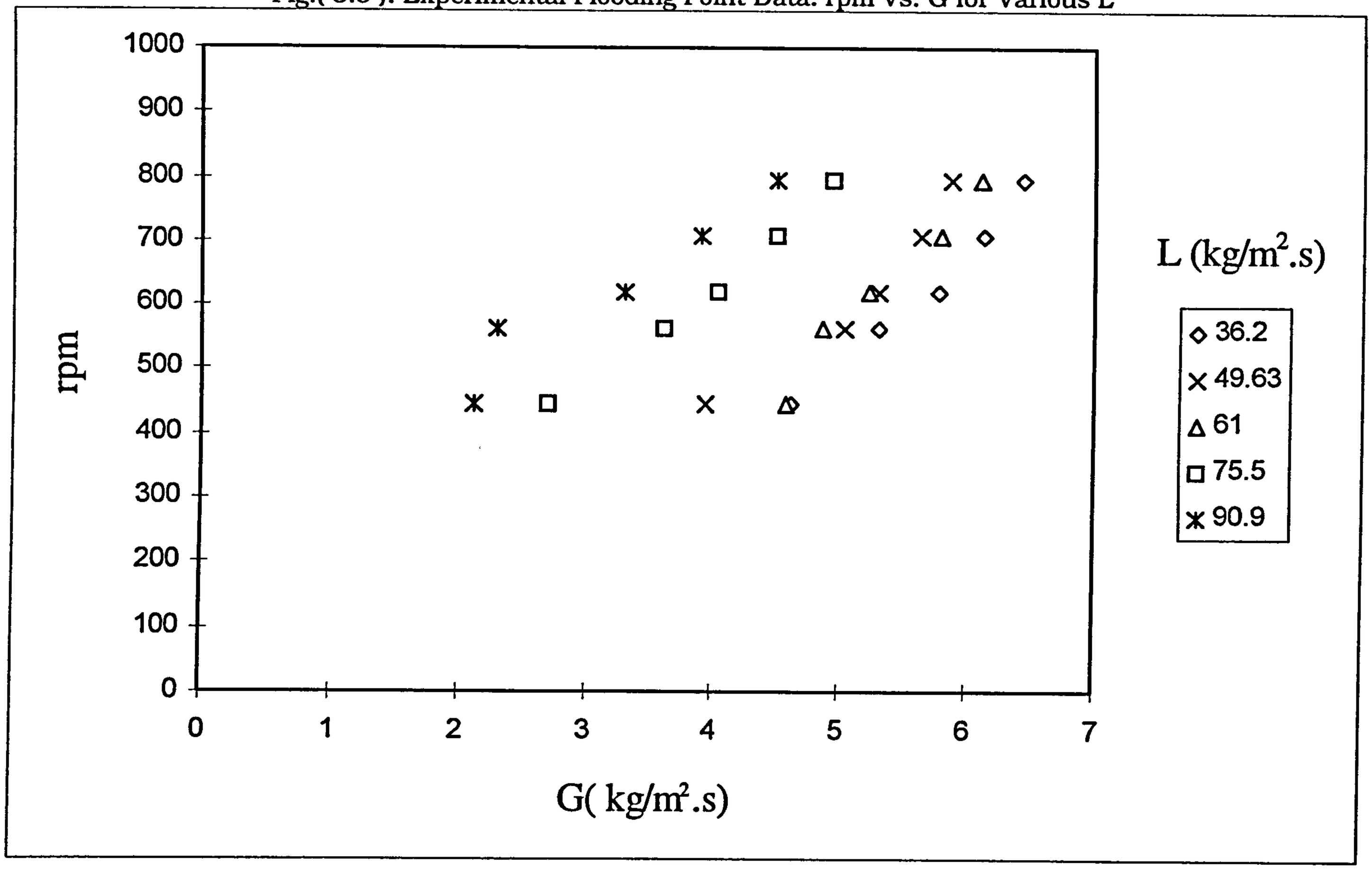

Fig.(5.10): Experimental Flooding Point Data: L/G Vs rpm for Various L.

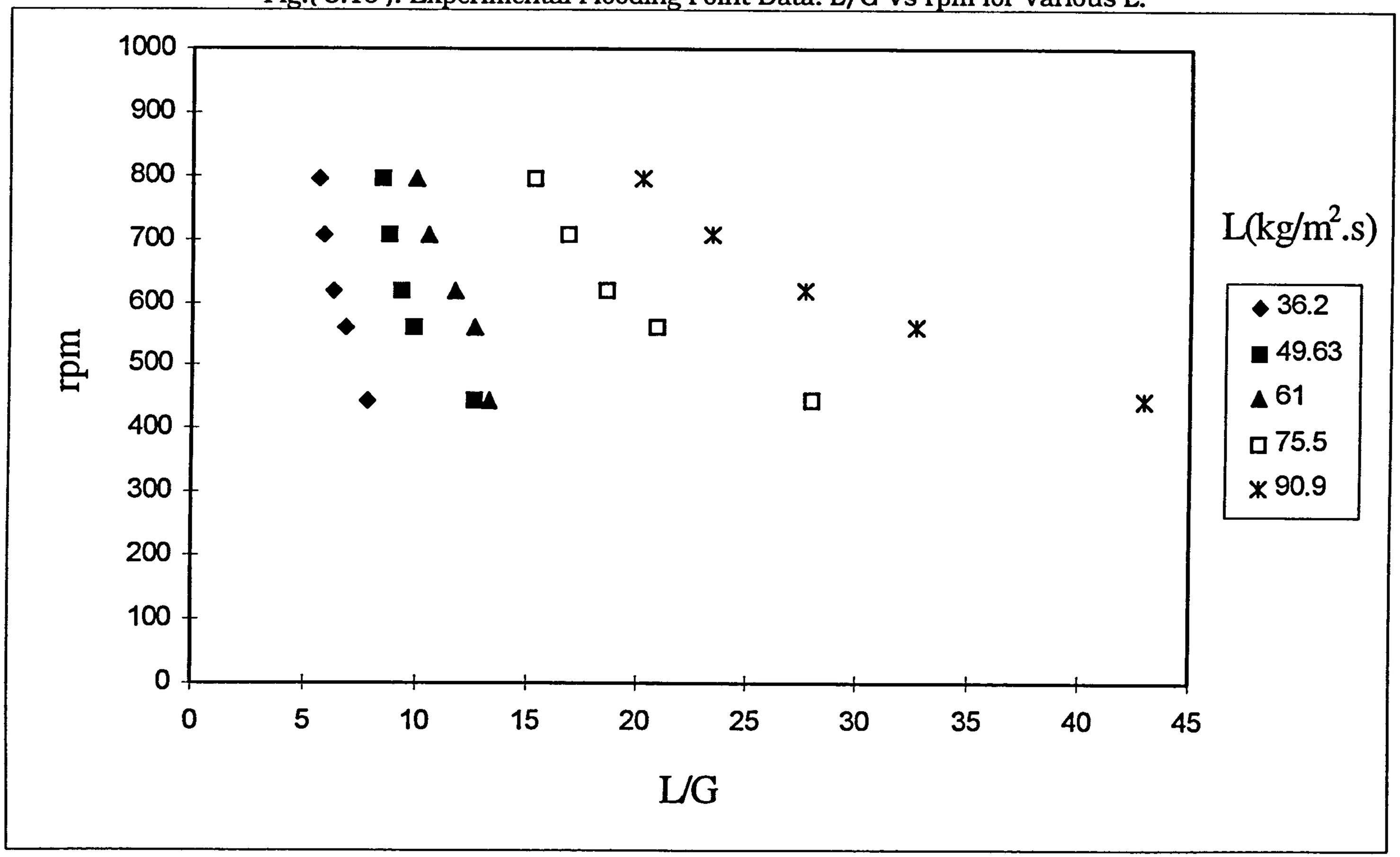

Fig(5.11): Presentation of the Experimental Data on the Sherwood Plot for Various Liquid Flow Rate.

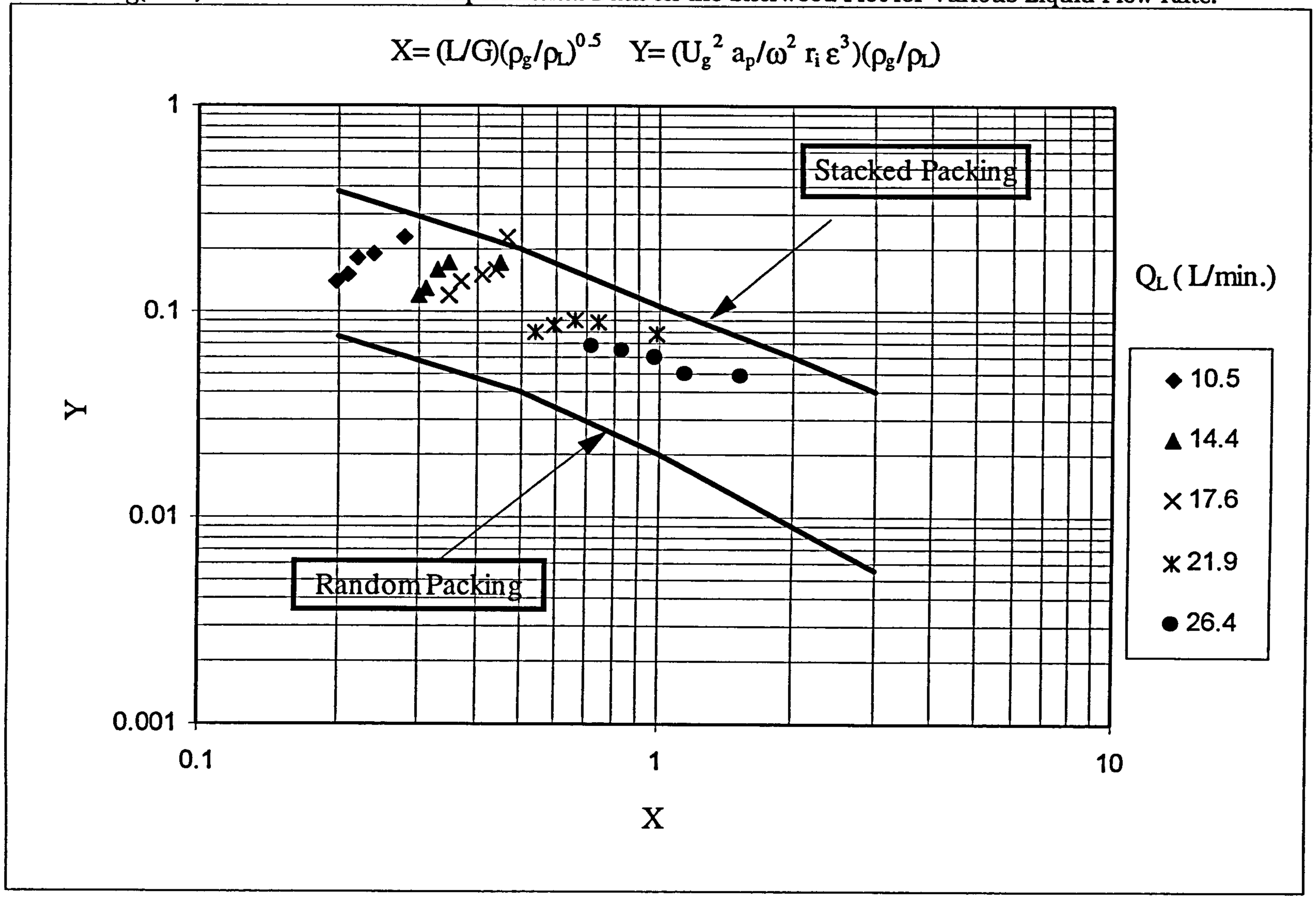

As mentioned earlier in section 5.5, in RPBs the flooding will first take place at the eye of the rotor, consequently at the flooding conditions, the customary indication of flooding as a sudden and abrupt instability through the bed yielding higher pressure drop will not occur. Instead the phenomenon will involve a monotonic increase in the pressure drop up to and beyond the flooding point as the gas flow rate increased. This findings was supported, experimentally as shown in figures 5.12 and 5.13.

Fig.(5.12): Pressure Drop Vs Q_g@ 620 rpm.

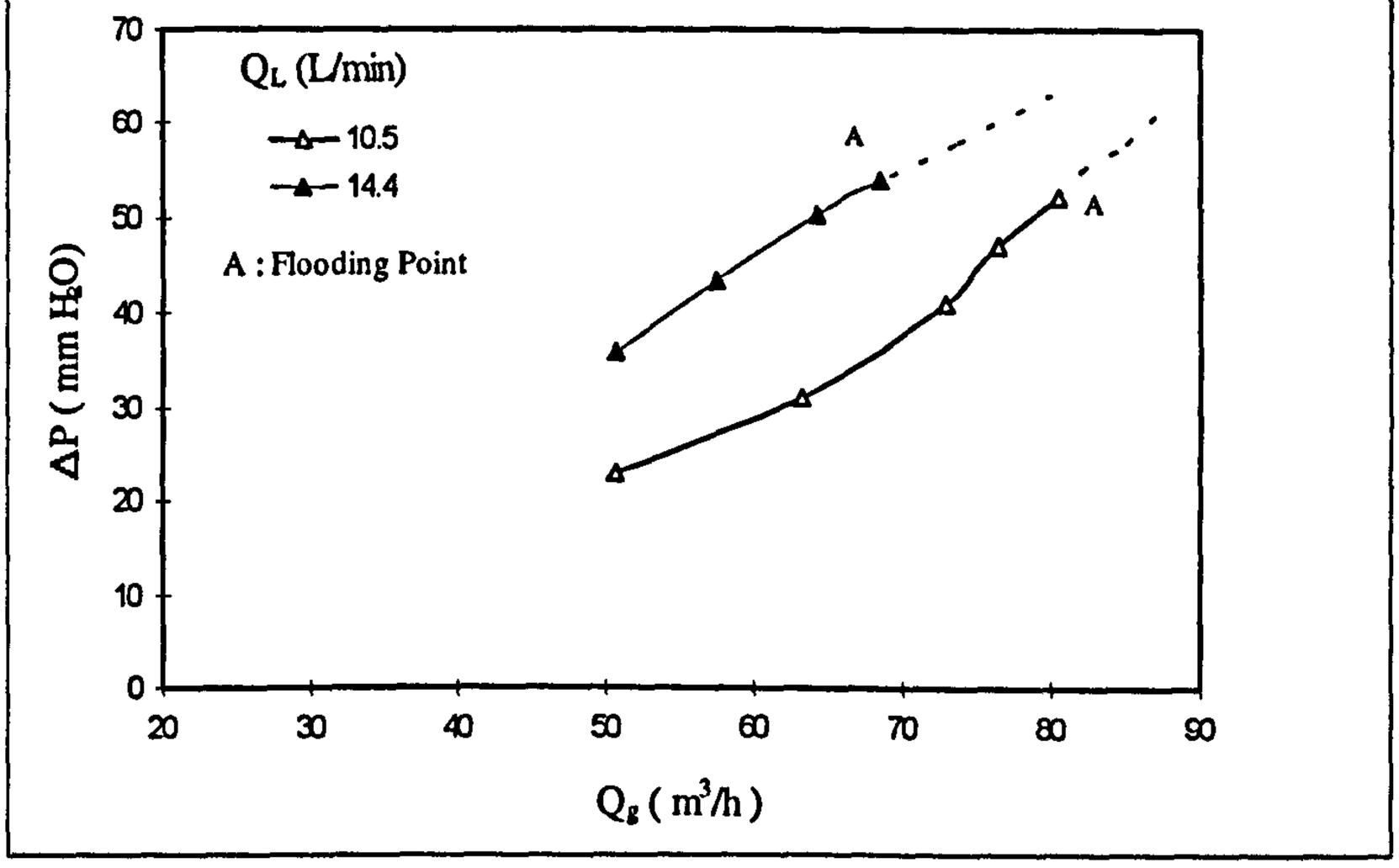

Fig.(5.13): Pressure Drop Vs Gas Flow Rate @ 444 rpm.

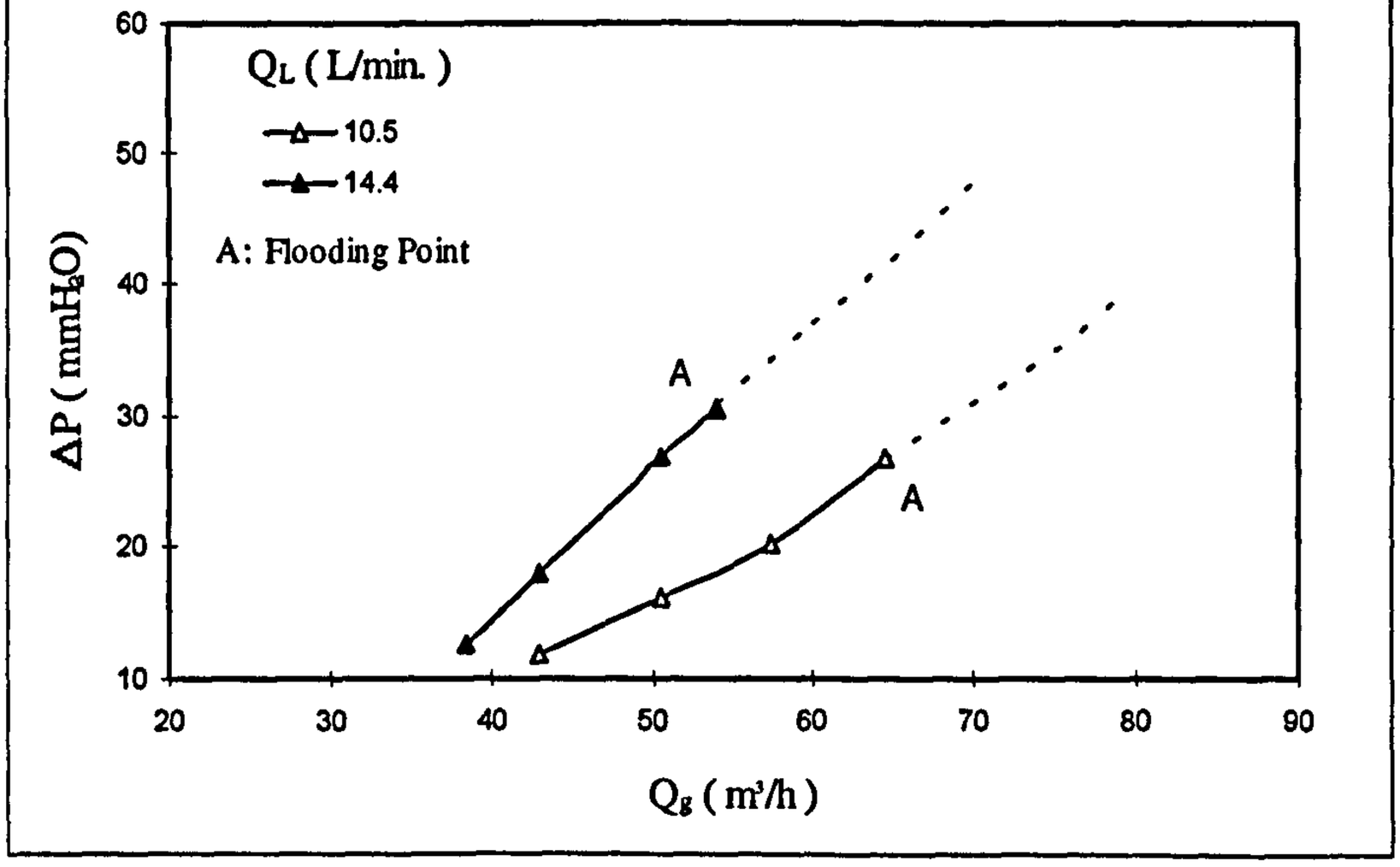

5.6-Mathematical Modelling.

5.6.1- Modelling of the Pressure Drop.

The overall momentum balance for a countercurrent flow between the gas and liquid through the bed is :

$$\left\{\begin{matrix}rate\ of\\ momentum\ in\end{matrix}\right\}-\left\{\begin{matrix}rate\ of\\ momentum\ out\end{matrix}\right\}+\left\{\begin{matrix}sum\ of\ forces\\ acting\ on\ system\end{matrix}\right\}=0$$

For stationary cylindrical co-ordinates the Navier Stokes equation of motion for the gas in rotating packed bed can be written as follows:

$$r-component \qquad \rho_g\left(V_r\frac{dV_r}{dr}-\frac{V_\theta^2}{r}\right)=-\frac{dp}{dr}-\psi_r \qquad (5.4)$$

$$\theta-component \qquad \rho_g\left(V_r\frac{dV_\theta}{dr}+\frac{V_r\,V_\theta}{r}\right)=-\psi_\theta \qquad (5.5)$$

In equation 5.4 the momentum change in the radial direction equal to the pressure drop, centrifugal force and the drag force exerted on unit volume of the gas. The momentum change in the tangential direction, equation 5.5 is equal to the coriolis force and the drag exerted on a unit volume of gas. The drag forces ψ_r *and* ψ_θ in the radial and tangential component in equations 5.4 and 5.5 can be expressed as follows:

$$\psi_r=\alpha\frac{1}{R_h}\frac{\rho_g V_r^2}{2} \qquad (5.6)$$

$$\psi_\theta=\alpha\frac{1}{R_h}\frac{\rho_g}{2}(V_\theta-r\omega)^2 \qquad (5.7)$$

The values of the tangential velocity V_θ can be calculated using equations 5.5 and 5.7. However, as the gas would synchronise with the bed as a result of drag forces imposed on it by the packing, V_θ and indeed the liquid tangential velocity can be assumed equal to the bed's tangential velocity ($r\omega$). The pressure drop across the bed equation 5.8 can be calculated by solving equation 5.4 and using the V_θ values obtained from equations 5.5 and 5.7 as follows:

$$\Delta P = \int_{r_i}^{r_o} \alpha \frac{\rho_g}{2R_h}\left(\frac{Q_g}{2\pi r \Delta x}\right)^2 dr - \frac{\rho_g Q_g^2}{4\pi^2 \Delta x^2}\int_{r_i}^{r_o}\frac{1}{\varepsilon^2 r^3}dr + \int_{r_i}^{r_o}\rho_g \frac{V_\theta}{r}dr \qquad (5.8)$$

and hence,

Changing the integral limits in equation 5.8, the pressure drop ($-\Delta P$) can be expressed as:

$$-\Delta P = \underbrace{\alpha \frac{\rho_g}{2R_h}\left(\frac{Q_g}{2\pi \Delta x \varepsilon}\right)^2\left(\frac{1}{r_i} - \frac{1}{r_o}\right)}_{Frictional} + \underbrace{\frac{\rho_g Q_g^2}{8\pi^2 \Delta x^2 \varepsilon^2}\left(\frac{1}{r_i^2 - r_o^2}\right)}_{Inertial} + \underbrace{\int_{r_i}^{r_o}\rho_g \frac{V_\theta^2}{r}dr}_{Centrifugal} \qquad (5.9)$$

In rotating packed beds the hold up is very small beyond the inner jet impact zone, Burns[B4], and thus the effective porosity can be approximately equal to the dry bed porosity. R_h and α are the hydraulic radius which equal to ε/a_p and the drag coefficient, respectively.

5.6.1.1- Determination of Drag Coefficient.

This section details the experiments carried out to determine the drag coefficient to calculate the pressure drop using equation 5.9. For gas liquid countercurrent flow the drag coefficient (or the resistance factor) will depend on the liquid flow rate, gas flow rate and rotational speed. The drag coefficient for dry and wet conditions was

determined using equation 5.10 which has been derived by balancing the shear forces at the interface between the gas and the liquid to determine the pressure drop in packed beds Billet [B5].

$$\frac{\Delta P}{\Delta r} = \frac{1}{2}\alpha F_V^2 \frac{a_t}{\varepsilon'^3} \qquad (5.10)$$

where,

$\frac{\Delta P}{\Delta r}$ is the pressure gradient

α Drag Coefficient

F_V Gas Capacity Factor (= $< V_{avg.} > \sqrt{\rho_g}$)

ε' Effective porosity

a_t Packing Specific Surface Area

The effective porosity (ε') is equal to the difference between the bed porosity (ε) and the liquid holdup. As the liquid holdup is RPBs can be safely assumed very low, and hence the effective porosity was assumed to be equal the bed porosity. Furthermore the average radial gas velocity $< V_{avg.} >$ is calculated from the following equation instead the simple arithmetic average, as it varies with the radial position:

$$\langle V_{avg} \rangle = \frac{1}{r_{out} - r_{in}} \int_{r_{in}}^{r_{out}} \frac{Q_g}{2\pi r \Delta x} dr$$

The above equation gave radial velocity values similar to those estimated by equation the following equation:

$$V_r = \frac{Q_g}{2\pi r \varepsilon \Delta x}$$

5.6.1.2-Drag Coefficient Determination(Dry Bed)

The drag coefficient was determined in terms of the pressure drop and gas flow rate for various rotational speeds. The results shown in table 5.1 represent the pressure drop across the bed. Further the data were plotted as shown in figure 5.14 as $\Delta P \alpha (Q_g)^2$. For the whole range or rotational speeds, the value of the drag coefficient did not change significantly as the rotational speed is increased. The average value of the drag coefficient $< \alpha >$ was 0.125 calculated using equation 5.10.

Fig.(5.14): Pressure Drop Vs $(Q_g)^2$ @ Various Rotational Speed for a Dry Bed.

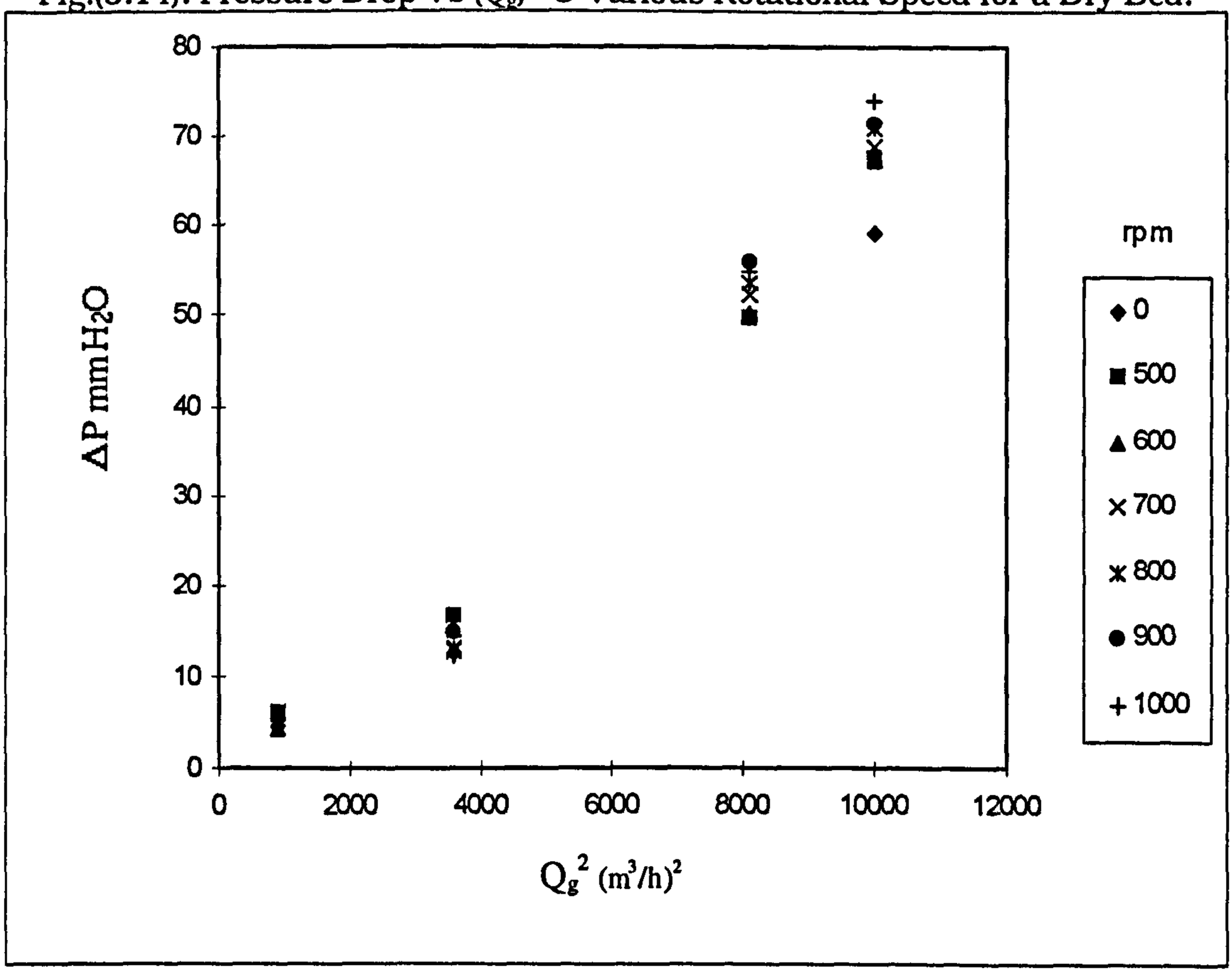

Table(5.1): Pressure Drop Across The Bed (in mm H_2O) for Drag Coefficient (α) Determination.

$Q_g(m^3/h)$ / rpm	30	60	90	100
0	4.5	12.5	49.78	59.34
500	5.82	16.65	49.95	67.77
600	4.22	14.97	50.34	67.44
700	5.97	12.84	52.41	69.12
800	6.11	13.15	53.79	71.1
900	6.11	14.72	56.39	71.6
1000	5.39	12.25	54.97	74.1

5.6.1.3-Drag Coefficient Determination(Wet Bed)

The drag coefficient for wet bed was determined by using equation 5.10. The experimental data for wet condition given in table 5.2 were used to determine the drag coefficient values. The drag coefficients in wet condition were higher than those estimated at dry condition as a result of higher pressure drop values when the bed was irrigated.

5.6.1.4- Validation of the Pressure Drop Model.

For the irrigated bed, the drag coefficient will depend on liquid flow rate, gas flow rate and the rotational speed. The pressure drop behaviour across the bed (packed section) is shown in figure 5.15. The pressure drop will increase as the gas converges towards the centre 'eye space' of the rotor. Table 5.2 shows the values of the drag coefficients and the comparison between the experimental against calculated value of the pressure drop calculated from the model equation 5.9.

Comparisons between the experimental data and the model was shown in figure 5.16. It can be seen that the equation 5.9 has overpredicted the experimental data. The pressure drop model can predict the experimental data within a +20% accuracy, however the model gave consistent results with the experimental values.

Fig.(5. 15): Calculated Pressure Profile at Qg = 63.2 m^3/h, rpm = 620, α =1.73.

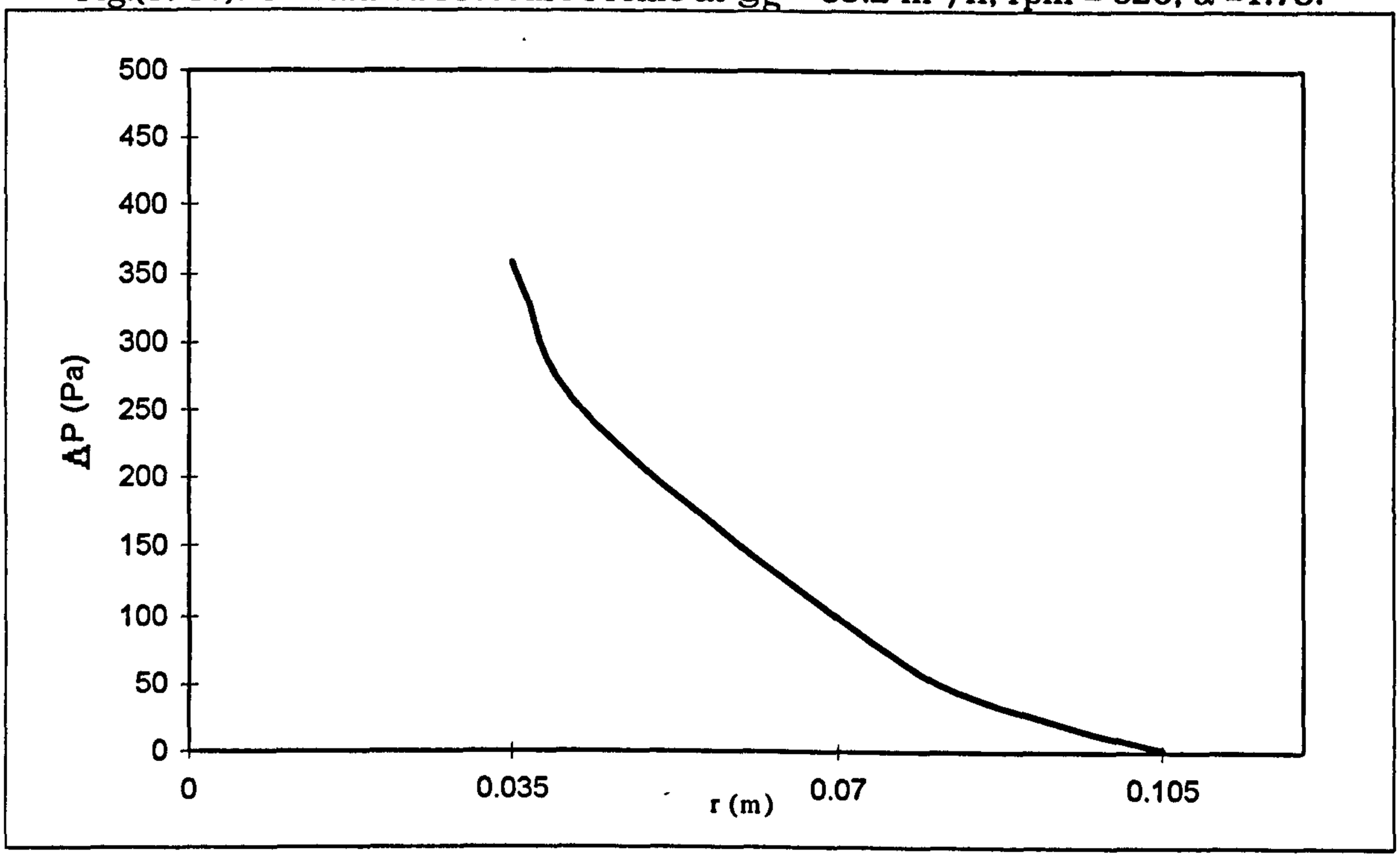

Fig.(5.16): Comparison Between the Experimental and Calculated Pressure Drop.

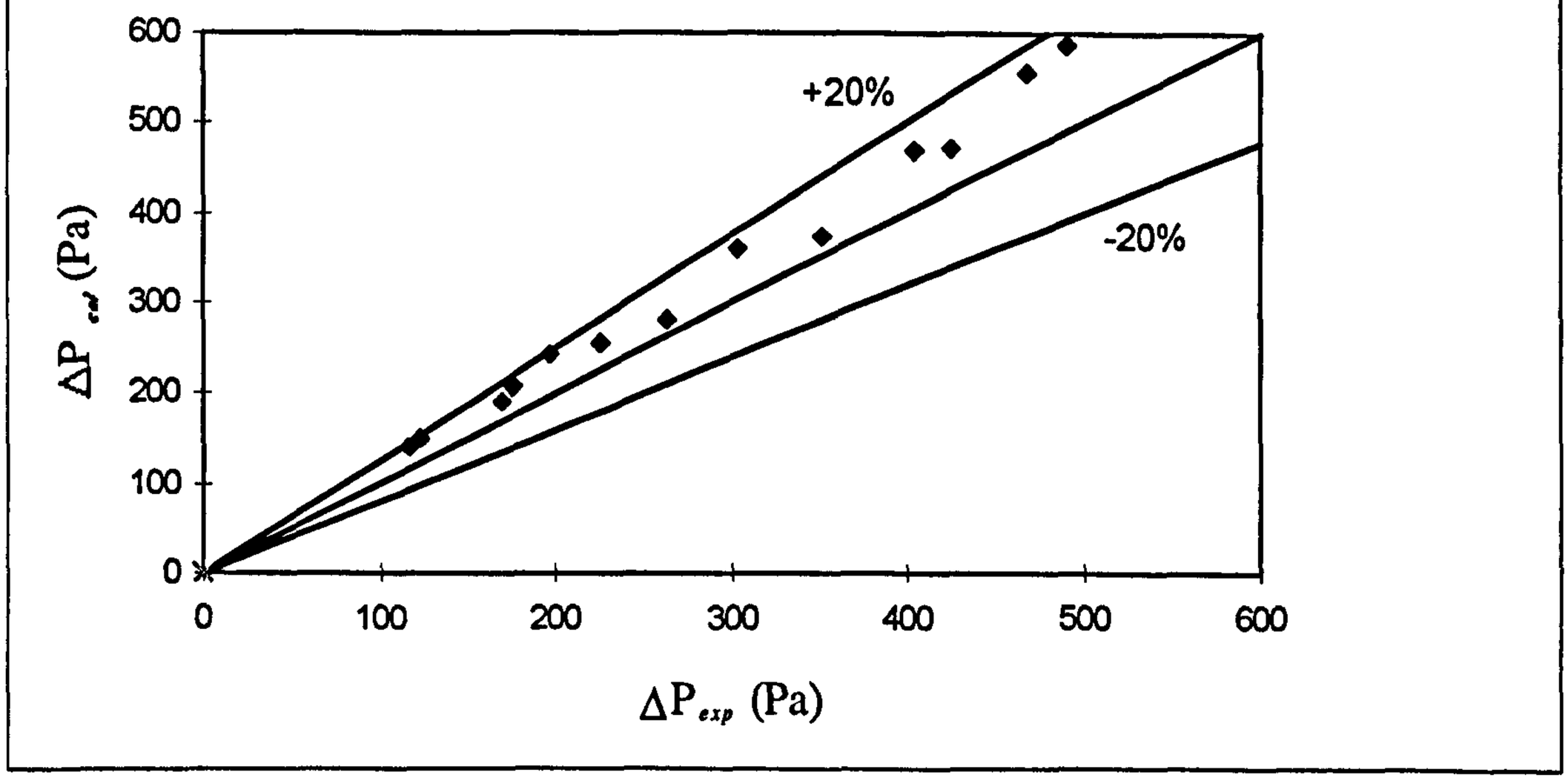

Table (5.2): Comparison Between the Calculated and Experimental Pressure Drop.

rpm	Q_L (L/min.)	Q_g (m^3/h)	Δp *(exp.)* (Pa)	α eq.(5.9)	Δp^a *(cal.)* (Pa)	$<\alpha>$	Δp^b *(cal.)* (Pa)
444	10.5	43	116	1.44	142		142
		50.6	169	1.50	199	1.44	190
		57.4	197	1.37	252		241
		64.3^F	260	1.44	298		299
	14.2	39.98	123	1.77	150		180
		43.02	176	2.18	208	2.16	206
		50.61	264	2.35	304		280
		54.82^F	309	2.35	353		326
620	10.5	50.6	225	2.00	269		256
		63.2	304	1.73	360		384
		72.85	404	1.73	469	1.86	501
		77.03	469	1.80	541		556
		80.5^F	569	2.00	651		605
	14.2	50.61	352	3.14	414		374
		57.4	452	2.94	493	2.81	473
		64.3	491	2.71	566		587
		69.2^F	516	2.46	594		675

Note:(a): Δp calculated based on eq. (5.9), (b): Δp calculated based on $<\alpha>$, (F) Δp: Flooding Condition

Chapter 6

Conclusions and Recommendations.

6.1 Conclusions.

6.1.1 Mass Transfer:

(1) The centrifugal acceleration has direct influence in producing high volumetric mass transfer coefficients in RPBs.

(2) The use of high packing density has little effect on the mass transfer performance in RPBs. Expamet and Declon packings, which have approximately 2/3 and 1/3 the surface area of Knitmesh packing, respectively, gave similar separation performance.

(3) RPBs have a flexible turn down ratios. Therefore this would tend to imply that RPBs would meet processing requirements (i.e. constant L/G for higher or lower throughputs) without changing the desired mass transfer separation targets.

6.1.2 Liquid Distribution.

With the liquid limited system investigated in this thesis, it has been shown that the mass transfer performance of RPBs are not very sensitive to the following:

(1) The initial liquid distribution. Distributing the liquid with a single arm (e.g. using the 4-armed distributor) gave a similar performance to that of the same distributor with four arms, at least for the low liquid flow rates which could be achieved.

(2) The angled liquid distribution, either when distributing the liquid countercurrently or when cocurrently with respect to the bed.

6.1.3 Flooding Behaviour.

(1) The Sherwood correlation underpredicts the flooding velocity in RPBs, giving overdesigned beds. Experimental results are mid way between Sherwood's stacked and dump packing arrangements.

(2) At the flooding point the liquid holdup decreases. During the flooding experiments, a significant amount of liquid was accumulated at the eye space as a result of the drag on the liquid by the gas and the bed inability to accelerate the liquid.

(3) Pressure drop data were reasonably modelled.

6.2 Recommendations.

6.2.1 Mass Transfer.

(1) Mass transfer should be investigated as a function of bed radius to establish the location of high performance zones. The bed can be divided into equivalent zones having the same inner diameter and different outer diameters: then liquid and gas samples can be collected across the radial depth of the bed. In this way, it will be easier to investigate the efficiency of RPBs. Results should be, then, compared with the overall results of the performance of all the zones tested collectively to help to develop more effective designs.

(2) Because of the high shearing zone that extends from the inner surface of the packing to a few millimetres deep into the bed, whereby the liquid is synchronised with the bed, it would be beneficial to investigate the effect of the flow pattern and film flow behaviour at this zone on the separation performance.

(3) Testing different lower surface area packings with a mesh-like skeleton shapes similar to the tested Expamet which gave very good mass transfer performance.

6.2.2 Liquid Distribution.

(1) The importance of the effect of liquid distribution shown during this work should be further investigated. The Four armed distributor has given better mass transfer results than the single central pipe distributor. Therefore, improved designs of multi-arms distributors should be tested. It has been shown that distributors with high injection velocity can function very well with respect to mass transfer despite the way that liquid is distributed (i.e. the fewer the arms the higher the kinetic energy).

(2) As shown, in chapter 4, that higher injection velocities produce good performance, and hence such distributors should be assessed by testing them on different packing densities and radial depths in order to justify the pumping cost incurred.

(3) The effect of axial distribution on mass transfer behaviour should be investigated to ascertain whether or not the resultant type of flow, such as wall flow, will have a detrimental effect on the overall performance of RPBs..

6.2.3 Flooding Behaviour in RPBs.

Because the original work of Sherwood et al [S8] did not mention to the effect of 'g' on their results, it would be worthwhile to conduct:

(1) A theoretical study to investigate the interaction between the gas, liquid and packing at higher rotational speeds (i.e. g's). The model should help to predict the flooding point in RPBs more accurately.

(2) A study to obtain a relationship between the liquid flow rate and liquid holdup at the flooding point. The liquid which is rejected by the bed should be quantified. The sought relationship can be a very important tool to understand the flooding mechanism in RPBs.

Appendix (A)

1-Liquid Flow Rate Measurement Charts.

Because water was the working liquid used for all the experimental work and the temperature range was relatively close to the temperature that was used in the manufacture's calibration, no further calibration of the liquid rotameters was performed and the calibration charts supplied by the manufacturer shown in figures A.1 and A.2 were used to measure the water flow rate.

2-Gas Flow Rate Measurement.

For the mass transfer rig a Nixon type rotameter, with a cpacity of 180 m^3/h, was used for air flow measurements. However, in the flooding rig an orifice with 30mm diameter was used for air flow rate. The orifice was calibrated using the above rotameter and the calibration data are given in table (A.1) as follows:

Table(A.1): Calibration Data of the Orifice.

Q_g (m^3/h)	ΔH, manometer (cm Hg)
30	0.8
40	1.5
60	3.7
70	5.71
90	11.4
100	14.6
110	19
120	25.1

Fig.(A.2): Calibration Chart for 35X Water Rotameter..

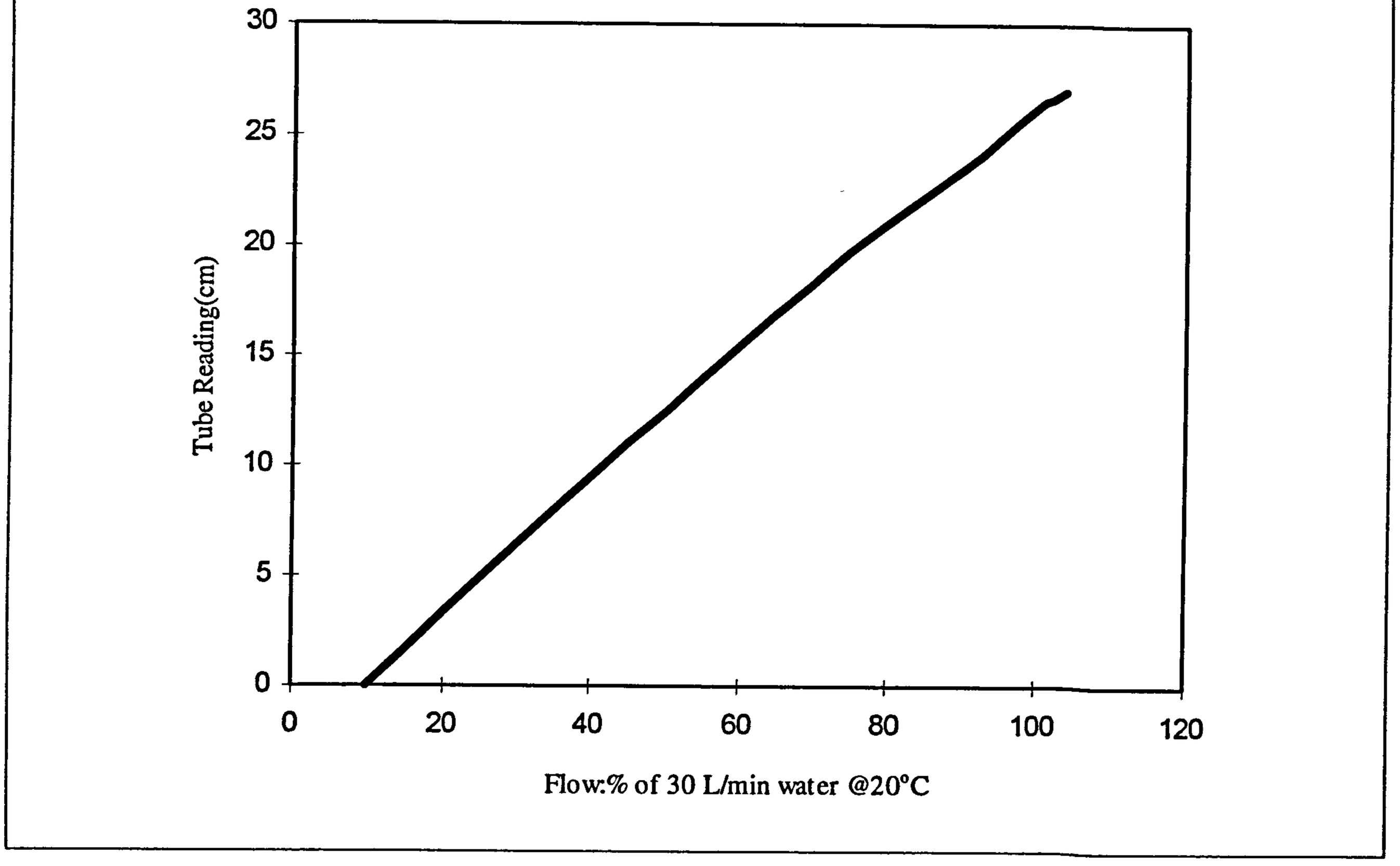

3-Filament Thickness Determination for Declon.

A Travelling microscope (J.SWIFT&SON 29571) was used to determine the average thickness of the filaments of the packing material. The microscope was calibrated to 500μm. Twenty five different measurements table A.2 were carried out. An average value of 229.5 μm was estimated for the filament thickness, which with a bed porosity of 0.95 would correspond to a specific surface area per unit volume of the packing roughly about 870 m^2/m^3.

Table(A.2): Film Thickness for Declon Packing Material.

232	250	206	234	238
184	239	199	258	239
149	244	242	204	190
247	286	206	314	216
254	217	273	212	204

4-Calibration of the Rotational Speed.

To calibrate the rotational speed with the output voltage of the motor, the front perspex of the bed was marked out by a white colour spot, and then the bed was allowed to speed up. A stroboscope was used to gauge the rotational speed. The number of flashes of the stroboscope was varied so that the mark on the perspex appeared to be stationary. At this condition, the speed of the bed must correspond to the number of flashes per minute. The data in table A.3 shows the relation between the controller readings and rotational speed. The angular velocity can be found as follows:

$$\omega = \frac{2\pi \text{ rpm}}{60}$$

where, ω is in radian/s.

Table (A.3): Calibration of the rotational speed of the bed.

rpm	1450	1421	1383	1330	1298	1235
Controller Reading	1454	1430	1388	1338	1306	1241
rpm	1172	1148	1077	1026	988	928
Controller Reading	1179	1154	1085	1031	994	934
rpm	868	838	779	719	690	570
Controller Reading	874	844	784	723	696	575
rpm	541	425	396	335	-	-
Controller Reading	548	431	401	341	-	-

In the flooding rig the bed was driven by a variable speed motor (1.5 kW) connected to a small generator 'Tachometer', which was connected to a digital voltmeter (Thandar TS 351 digital multimeter) to log out the voltage. The correlation between the speed and the voltage can be expressed as follows:

$$\text{rpm} = 3.144 + 29.2366(\text{V})$$

where, V is the output voltage (in Volts)

Appendix (B)

1-Surface Area Estimation for Expamet Packing.

The Expamet packing material was made of aluminium sheets figure (B.3). Each sheet has dimensions as in table (B.4). In order to calculate the surface area of each sheet of expamet based on the dimension given for every single strand, the estimation of the surface area is carried out follows:

Fig.(A.3)

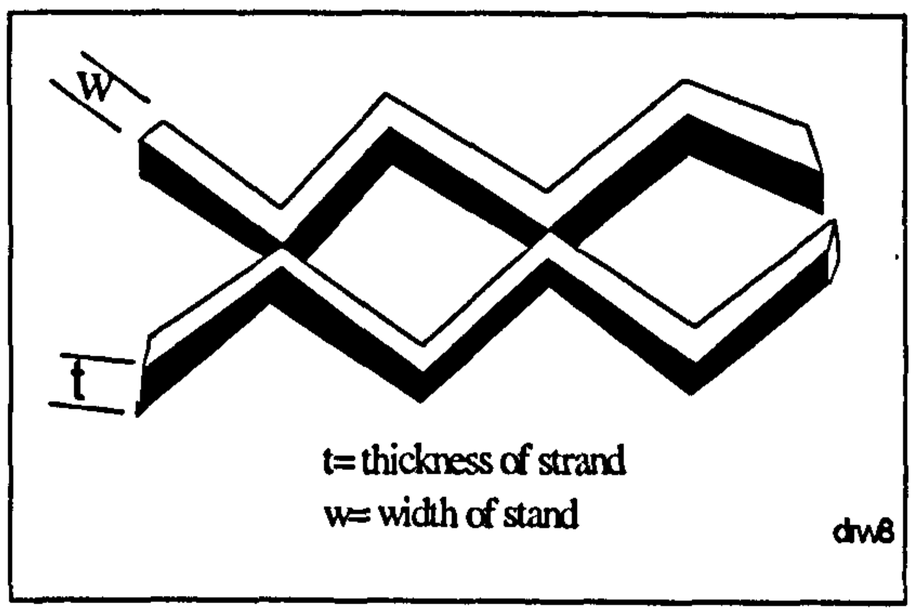

Table(B.4): Properties for Expamet Packings

Mesh Ref. No.	Mesh Size Pitch to Centre (mm)		Size of a Strand (mm)		Approximate Weight (Kg/m^2)
702A	LW	SW	width	thick	0.638
	4.75	2.38	0.559	0.5	

From figure (B.4) the following relation between LW and SW can be found as:

$$\tan\theta = \frac{SW}{LW} \quad \text{or } \theta = \tan^{-1}\left(\frac{SW}{LW}\right)$$

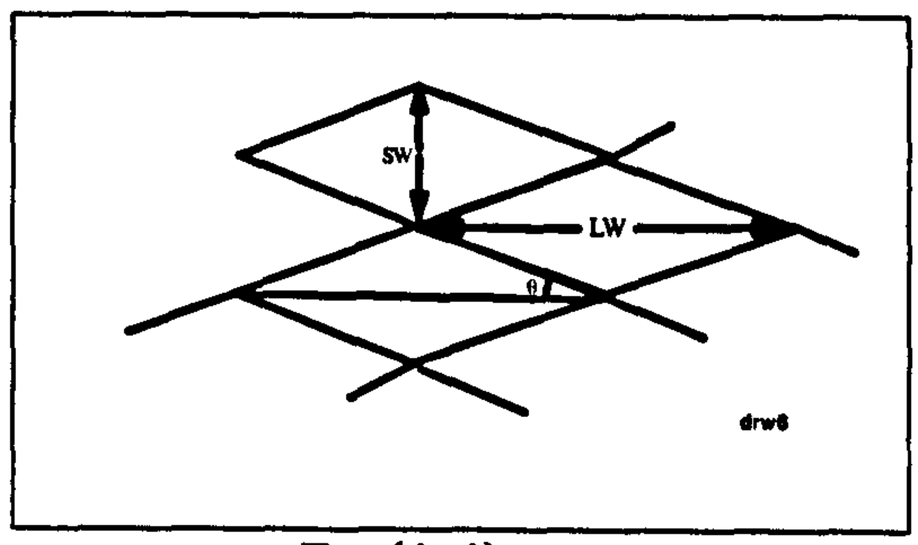

Fig:(A.4)

since the length of each strand figure (B.5) can be calculated as: D = n . LW

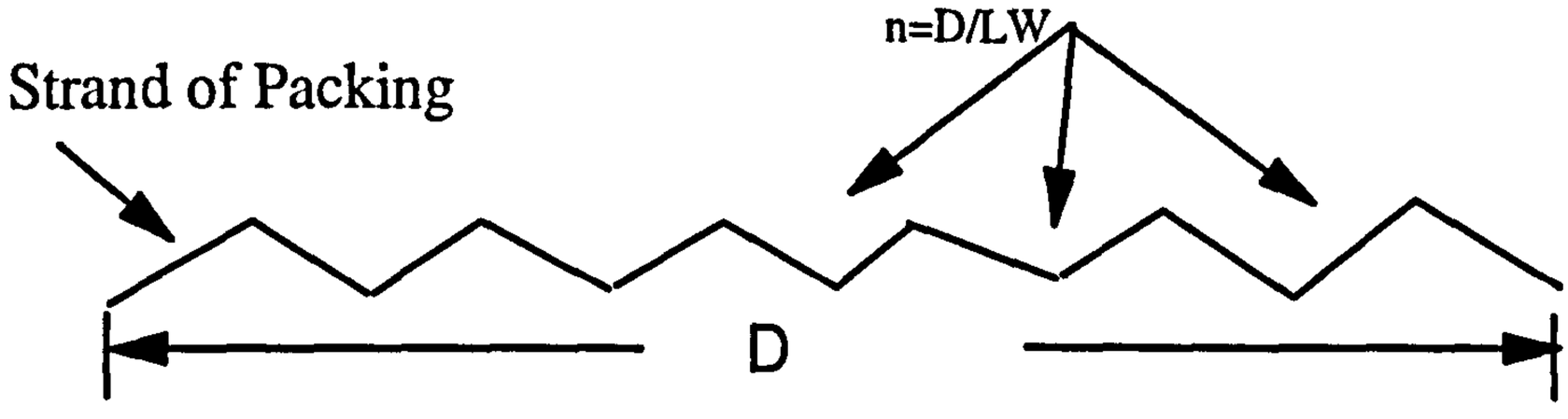

Fig.(B.5)

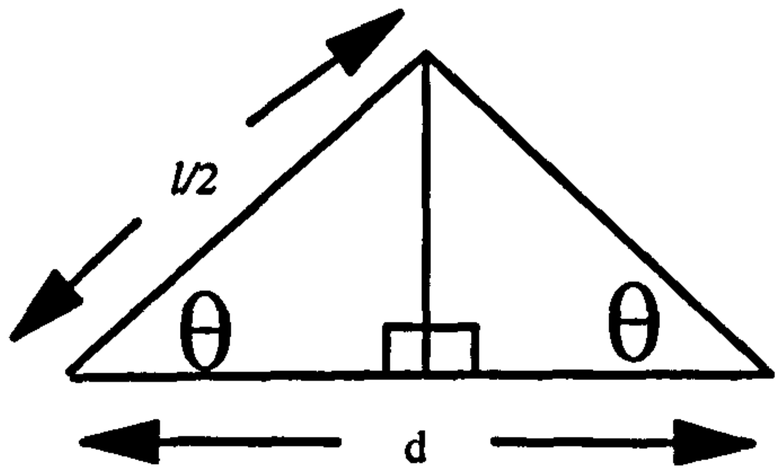

Fig.(B.6)

From figure (B.6) the length (l) of each strand is equal to:

$$l = \frac{d}{\cos\theta}$$

Therefore the surface area of each strand having a length D in figure(B.7), would be equal to:

$$A_{strand} = 2\,(W + t)\;\; l\;\; n \;\; = 2\,(W+t)\,\frac{D}{\cos\theta}$$

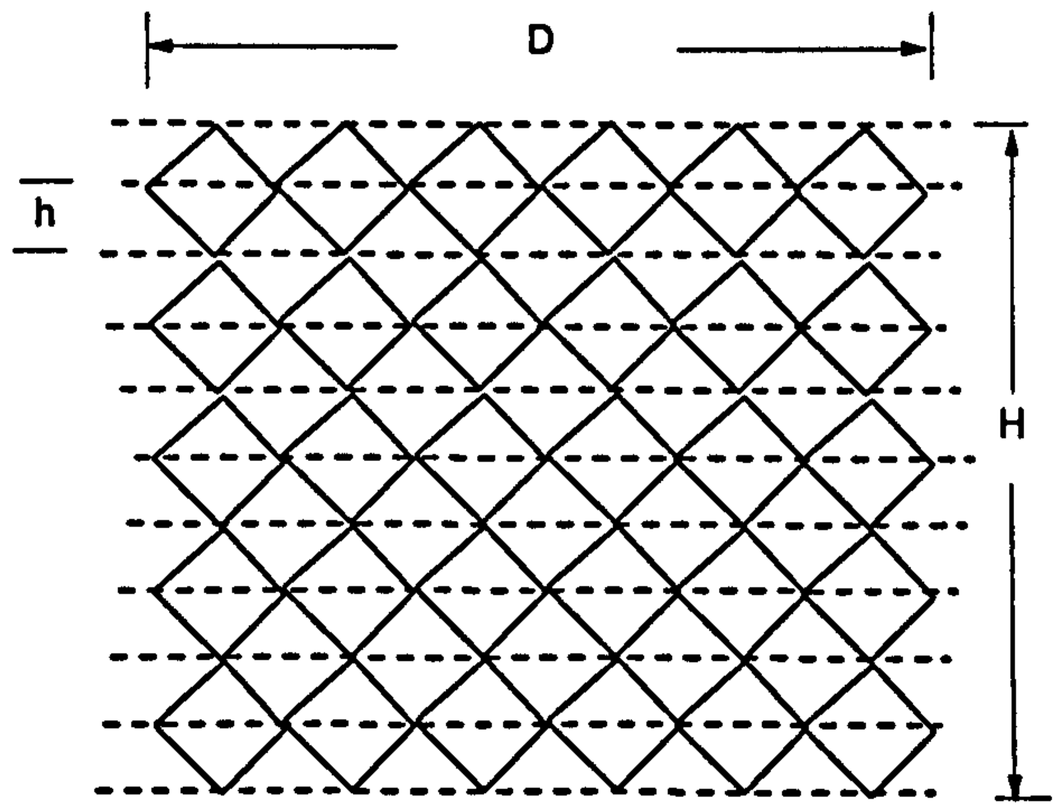

Fig.(B.7)

Further the number of strands in a sheet having dimension H by D is equal to:

$$n' = Number\ of\ Strands = \frac{H}{h} = \frac{2H}{LW.\tan\theta}$$

where, h is equal to $\frac{LW}{2}\tan\theta$ from Figure(B.8):

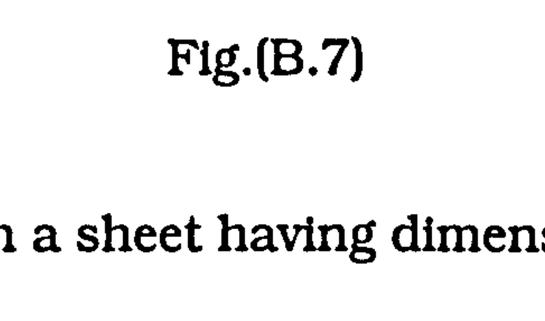

Fig.(B.8)

Finally every sheet of the Expamet consists of filament with length D and number of strands n', the surface area figure (B.7) of any single sheet would equal to:

$$A_S = \frac{2H}{LW\tan\theta}\ \frac{2(w+t)D}{\cos\theta}$$

$$A_S = \frac{4(w+t)}{LW\sin\theta}\ DH \qquad (B.1)$$

2-Sample Calculation of the Surface Aea of Expamet.

Given the Dimension of the Expamet 702A as Follows:

width (w)= 0.559mm

thickness(t)= 0.5mm

number of sheets (N)= 30

LW = d = 4.250mm

$$\therefore \quad \theta = \tan^{-1}\left(\frac{SW}{LW}\right) = 26.6$$

For a bed with 158mm, 402mm ID and OD respectively and an axial depth of 60mm the volume~ 64.4 10^{-4} m^3 and Area(DH) ~ 1366m^2, substituting the above value into eq.(B.1), the surface area per unit volume(packed section) would be equal to:

$$a = 2.226 \times DH \times 33 = 1428\ m^2/m^3.$$

3- Determination of Expamet Aluminium Mesh Density.

The density of Expamet 702A was determined by weighing 10 sheets cut so that each would have 50x50 mm, their weight was 15.74g, then the sheets were placed in a known volume beaker 125ml, to which water was added and the amount of water was 117.5ml. The density, (ρ_{al} =2060 Kg/m^3), was calculated as the qoutient of the weight of the sheets and the volume displaced by the sheets which is 7.5ml. The reported values[P] of ρ_{al} were 2550-2800 Kg/m^3)

4- Determination of Expamet Porosity.

The data supplied by the manufacturer for the approximate weight per unit area, AW, (0.638 Kg/m^2) was used to calculate the density and subsequently the porosity of the

bed. Since the axial depth of the bed Δx is 60mm and 33 sheets of expamet(cut as 158,410mm I.D. and O.D. respectively) were used to form up the skeleton of the bed, therefore the density of the bed is:

$$AW \times \frac{(No.\ \text{of Sheets})}{\Delta x} = 350.9\ \text{Kg}/\text{m}^3$$

The mean density of the porous body (the bed) ρ, can be estimated as:

$$\rho = \rho_{al}(1-\varepsilon)+\varepsilon\rho_{air}$$

where, ρ_{al} is the aluminium density equal to 2069 Kg/m^3. By neglecting the desnity of air, the bed porosity would be:

$$\varepsilon = 1-\left(\frac{\rho}{\rho_{al}}\right) = 1-\left(\frac{350.9}{2069}\right) = 0.83$$

5- Pore Length Determination.

To calculate the pore length of each packing material, the packing material was assumed to be made up many grids attached to each other. Each grid would have a similar shape to the grid shown in Figure B.9, and the grid was made up of four elements each having a length equal to 3d. The thickness of the film, which has a cylindrical shape was equal to f.

B.9: Grid Details.

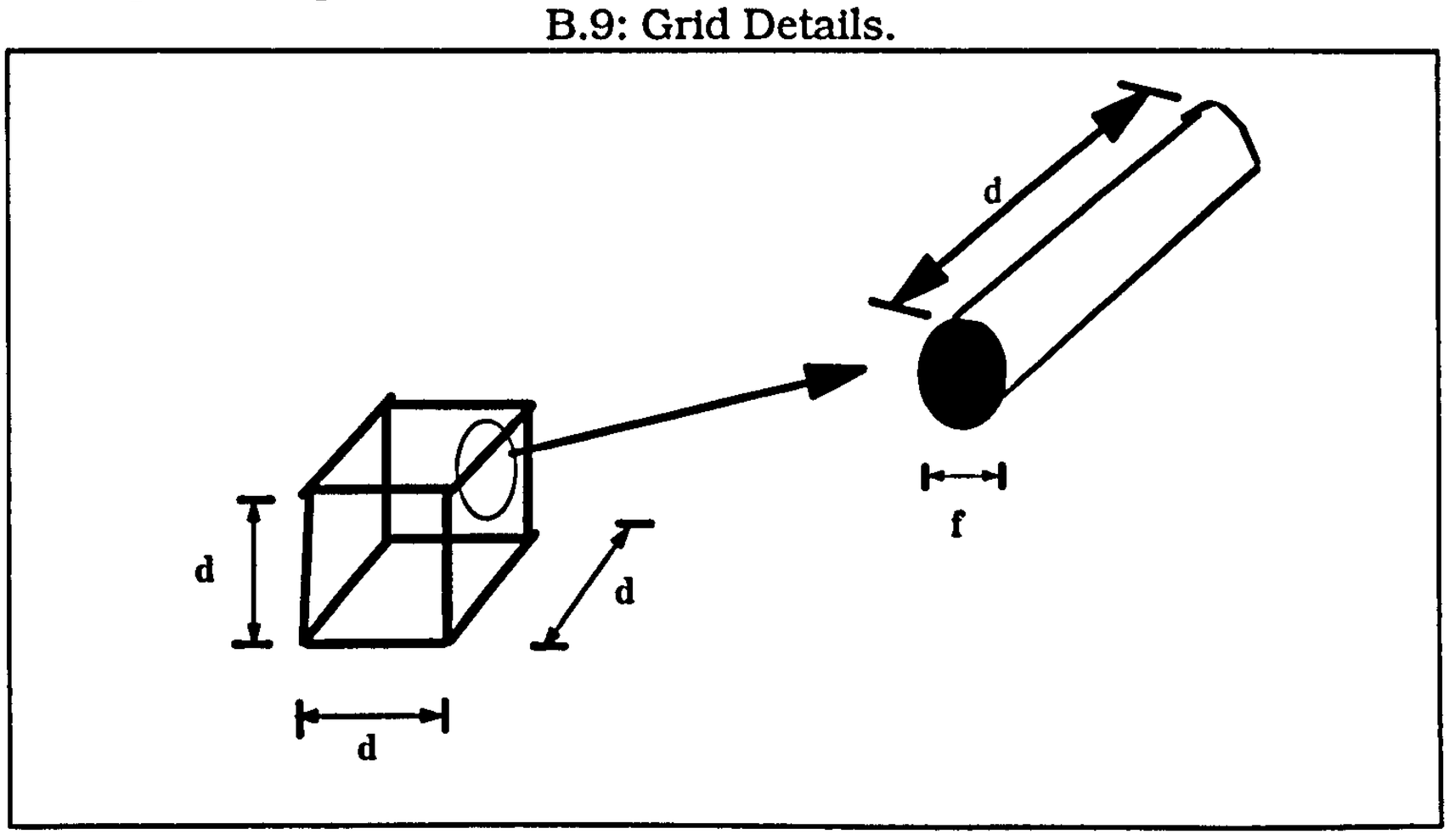

As the length of each element was equal to 3d, the filament volume can be calculated as follows :

$$\text{Filament Volument } F = \frac{\pi}{4} f^2 3d$$

and the volume of the grid is equal to d^3 , the spatial volume would be equal to:

$$1-\varepsilon = \frac{\frac{\pi}{4} f^2\ 3d}{d^3}$$

$$\therefore \qquad d = \sqrt{\frac{3\pi}{4(1-\varepsilon)}}\, f$$

Appendix (C)

1- Determination of the Required Time for Gas Sampling .

Figure (C.1) depicts how the gas samples were sampled to check the material balance around the bed. To sample the gas (leaving the the rotor), a Teflon tube 10mm in diameter and 2m long was connected to the gas sampling vessel, in figure (C.2), at one end, while the other end was fixed at the center of the rotor 'eye'. The other end of the vessel was connected to a vacuum to extract the sample. Two Teflon rotoflo (V1 & V2) valves are used to control the amount gas to be sampled .

A material balance of the solute accumulated in the vessel fig.(C.2) can be written as follows:

$$V\,dc = Q\,c'\,dt - Q\,c\,dt \qquad (C.1)$$

$$V\,dc = Q\,(c' - c)\,dt \qquad (C.2)$$

B.C. @ t = 0 c = 0

@ t = t c = 99.99% c'

Integrate eq.(C.2)

$$\int_{c'}^{99.99\%c'} \frac{dc}{c'-c} = \frac{Q}{V}\int_0^t dt$$

let c'-c= v $\Rightarrow$ dv = -dc

$$-\int \frac{dv}{v} = \ln v + B$$

$$-\int_{0}^{99.99\%c'} \frac{dc}{c'-c} = -\left[\ln(c'-c)+B\right]_{0}^{99.99\%c'}$$

after substituting the values of the inetgration the final form of the solution would be:

$$t = -\frac{V}{Q}\ln(0.01)$$

Figure (C.1): Gas sampling

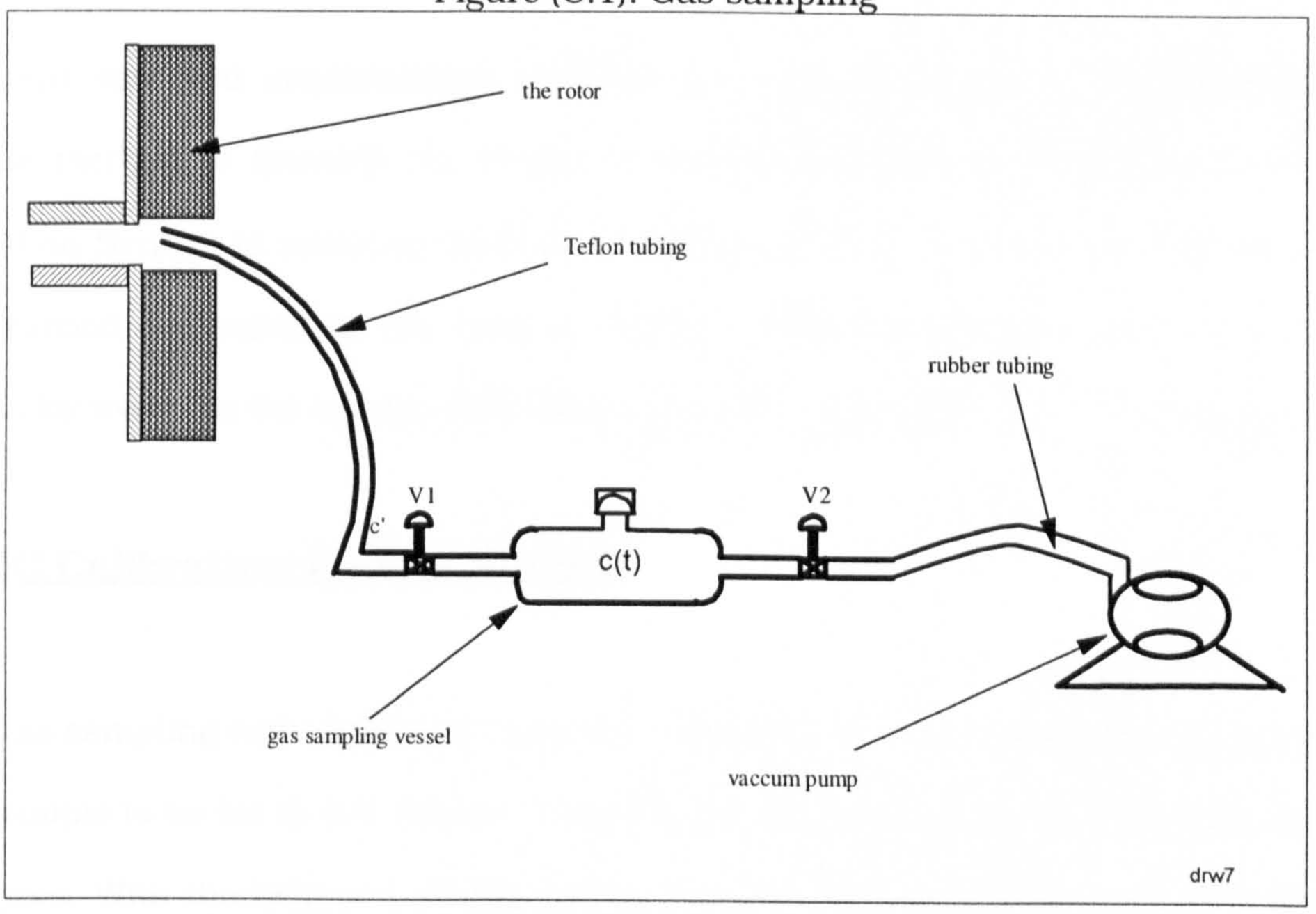

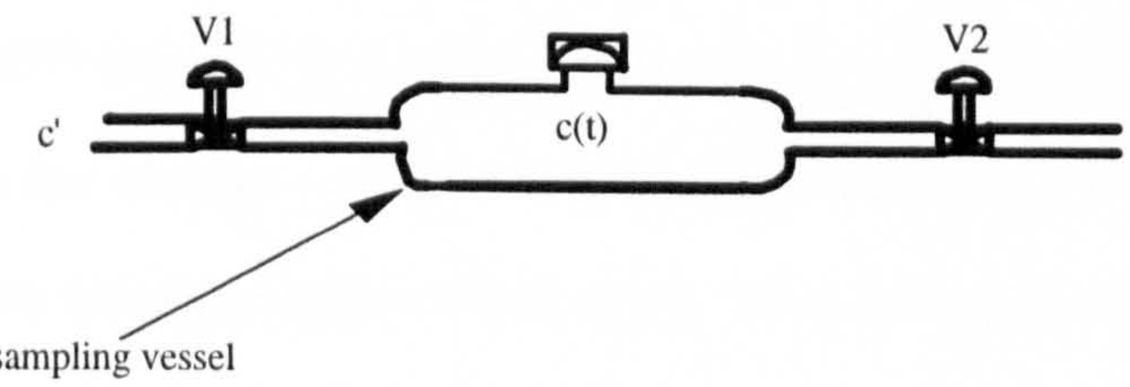

Fig.(C.2): Gas Sampling Vessel (Volume=1078 cm^3)

Note: the more %c' required the longer time would be needed (i.e. if 99.999%c' is required then the time (t) would be ~ 50% longer than that needed for 99.99%c')

2-Gas Chromatography Calibration and Analysis.

Perkin Elmer AutoSystem Gas Chromatography (GC) has been used to analyse the liquid and gas samples. The GC is integrated with a PC-based integrator (Personal Integrator model 1020) for chromatographic data acquisition and results. A 2 meter and 1/8" stainless steel column was used and packed with Porapak™ QS 80/100.

3- GC Calibration for Liquid Samples.

Different standard concentration samples has been prepared in the laboratory. A simple method to quantify the weight of the solute to be added was to use a 5μL Hamilton Syringe to measure the desired amount of EDC. A further gravimetric check was carried out, minimise the error in adding certain amounts of (solute) EDC to the water, by weighing the syringe filled before and after draining the solute into water.

4- GC Calibration for Gas Sample.

The gas sampling valve (solenoid valve) was employed to control the required amount of gas sample to be fed to the column, a 2ml stainless steel loop was used throughout the analyses. With the help of a syringe pump, the gas samples in the gas tight syringe is pumped to the CG, the tubing connecting the syringe and inlet port to the gas sampling valve was a 1/8" Teflon™ tubing. The gas sampling vessel in figure C.2 was used in the calibration of the GC for the gas phase. A known amount of pure (liquid) EDC was injected at a time, leave for some time to evaporate. With the help of some small (4~5) glass beads, the vessel was shaken and gas sample was drawn from the middle port by a gas tight syringe (20ml), and then injected into the GC as mentioned earlier. Two methods were programmed on the GC to analyse both the liquid and gas samples summarised as follows:

5-GC Method of Analysis.

A-Liquid samples:

Carrier Gas	: Nitrogen 35 cc/min.
Column	: Porapak^{TM} QS 80/100
Detector	: FID
Oven Temperature	: 240 ^{o}C for 5.5min.
Injection Temperature	: 280 ^{o}C
Detector Temperature	: 300 ^{o}C
Initial Attenuation	: 64
Events	: after 1.5 min. attenuation 4
Sample Size	: 2 µL
Range	: 1

B-Gas Samples:

Carrier Gas	: Nitrogen 45 cc/min.
Column	: Porapak^{TM} QS 80/100
Detector	: FID
Oven Temperature	: 175 ^{o}C
Injection Temperature	: Off
Detector Temperature	: 300 ^{o}C
Initial Attenuation	: 64
Events	: after 0.1 min. Gas sampling Valve(GSV) On, then @ 0.3 min (GSV) Off. @ 2.5 min. attenuation becomes 1.
Sample Size	: 2 mL (loop size)

Appendix (D)

Table(D.1): Predictions for Knitmesh,4 arms Distributor, hole size Φ 1mm.

T=21.2°C, Q_L (L/min.)=6.5

Gas flow rate (m^3/h)	rpm	HTU (cm)	Penetration model		Onda correlation		Davidson model		Vivian correlation		a_e , Onda correlation (1/m)
			k_L (m/s) x10^5	HTU (cm)	k_L (m/s) x 10^5	HTU (cm)	k_L (m/s) x10^5	HTU (cm)	k_La (1/s) x10^3	HTU (cm)	
30	500	6.30	98.3	0.33	4.4	7.3	172	0.19	19	9.9	585
60		4.97									
90		4.65									
30	1000	4.91	122.1	0.25	6.4	4.7	213	0.14	32.2	5.8	620
60		3.08									
90		3.78									
30	1200	3.95	129.1	0.23	7.2	4.2	225	0.13	37.01	5.1	630
60		3.77									
90		3.48									

T =24 4°C , Q_L(L/min.)=12.5

30	500	7.20	114.7	0.433	5.2	9.7	200.	0.25	36.2	10.0	729
60		6.05									
90		5.67									
30	1000	5.78	141.9	0.33	7.5	6.3	247.5	0.189	61.3	5.9	771
60		5.77									
90		4.44									
30	1200	5.64	150.2	0.31	8.3	5.5	261.7	0.177	70.4	5.14	782
60		4.74									
90		3.15									

Note: Calculated HTU based on the average liquid flow rate calculated at the radii of the bed.

Table(D.2): Predictions for Declon , 4 arms Distributor, hole size Φ 1mm.

T=24.4°C, Q_L (L/min.)=6.5

Gas flow rate (m^3/h)	rpm	HTU (cm)	Penetration model		Onda correlation		Davidson model		Vivian correlation		ae , Onda correlation (1/m)
			k_L (m/s) x10^5	HTU (cm)	k_L (m/s) x 10^5	HTU (cm)	k_L (m/s) x10^5	HTU (cm)	k_La (1/s) x10^3	HTU (cm)	
30	500	5.97	100.9	0.63	4.7	13.7	176.	0.36	20.2	9.34	294
60		5.72									
90		5.70									
30	1000	4.68	124.9	0.48	6.9	8.8	218	0.28	34.1	5.5	310
60		4.53									
90		4.32									
30	1200	4.35	132.0	0.45	7.6	7.8	230.2	0.26	39.2	4.80	315
60		4.42									
90		4.20									

T =21 °C , Q_L (L/min.)=12.5

30	500	6.55	116.5	0.86	5.5	18.4	203.2	0.49	37.4	9.6	361
60		6.16									
90		6.00									
30	1000	4.91	144.3	0.66	8.1	11.76	251.7	0.378	63.3	5.7	380
60		4.93									
90		4.94									
30	1200	5.17	152.7	0.62	8.9	10.5	266.3	0.36	72.7	4.98	385
60		4.85									
90		4.93									

Note: Calculated HTU based on the average liquid flow rate calculated at the radii of the bed.

Table(D.3): Predictions for Expamet, 4 arms Distributor, hole size Φ 1mm.

T=21.2 °C , Q_L (L/min.)= 6.5

Gas flow rate (m^3/h)	rpm	HTU (cm)	Penetration model		Onda correlation		Davidson model		Vivian correlation		ae , Onda correlation (1/m)
			k_L (m/s) x10^5	HTU (cm)	k_L (m/s) x 10^5	HTU (cm)	k_L (m/s) x10^5	HTU (cm)	k_La (1/s) x10^3	HTU (cm)	
30	500	6.28	60.4	0.74	6.7	6.65	10.4	0.43	22.1	8.8	420
60		5.91									
90		5.58									
30	1000	4.60	75	0.56	9.9	4.3	130.2	0.32	36.4	5.2	445
60		3.72									
90		3.59									
30	1200	3.57	79	0.53	11	3.8	137.7	0.30	41.9	4.5	452
60		3.33									
90		-									

T =22.4 °C Q_L (L/min.)=12.5

30	500	6.62	70	1.0	7.8	8.9	122.3	0.56	39.4	9.2	520
60		5.60									
90		5.37									
30	1000	4.57	86.7	0.76	11.6	5.7	151.3	0.43	66.7	5.4	550
60		4.16									
90		3.89									
30	1200	3.97	91.7	0.71	12.8	5.06	160.2	0.41	76.6	4.7	557
60		3.58									
90		-									

Note: Calculated HTU based on the average liquid flow rate calculated at the radii of the bed.

Table(D.4): Predictions for Knitmesh, 4 arms Distributor, hole size Φ 2.3mm.

T=18.7 °C , Q_L (L/min.)=6.5

Gas flow rate (m^3/h)	rpm	HTU (cm)	Penetration model		Onda correlation		Davidson model		Vivian correlation		ae , Onda correlation (1/m)
			k_L (m/s) $x10^5$	HTU (cm)	k_L (m/s) $x10^5$	HTU (cm)	k_L (m/s) $x10^5$	HTU (cm)	k_La (1/s) $x10^3$	HTU (cm)	
30	500	6.14	98.3	0.33	4.4	7.32	172	0.19	19	9.89	585
60		4.12									
90		3.71									
30	1000	4.58	122.1	0.25	6.48	4.7	213	0.14	32.2	5.8	620
60		3.67									
90		3.34									
30	1200	3.80	129.1	0.23	7.2	4.2	225	0.13	37.01	5.1	630
60		3.49									
90		3.39									

T =22.4 °C Q_L (L/min.)=12.5

30	500	6.58	114.5	0.433	5.2	9.7	200	0.25	36.2	10.0	729
60		5.76									
90		5.05									
30	1000	4.50	141.9	0.33	7.5	6.3	246.9	0.19	61.3	5.9	771
60		3.59									
90		3.25									
30	1200	3.95	150.2	0.31	8.3	5.6	261.1	0.18	70.4	5.14	782
60		3.86									
90		3.53									

Note: Calculated HTU based on the average liquid flow rate calculated at the radii of the bed.

Table(D.5): Predictions for Declon, 4 arms Distributor, hole size Φ 2.3mm.

T=18.7 °C , Q_L (L/min.)=6.5

Gas flow rate (m^3/h)	rpm	HTU (cm)	Penetration model		Onda correlation		Davidson model		Vivian correlation		ae , Onda correlation (1/m)
			k_L (m/s) $x10^5$	HTU (cm)	k_L (m/s) $x 10^5$	HTU (cm)	k_L (m/s) $x10^5$	HTU (cm)	k_La (1/s) $x10^3$	HTU (cm)	
30	500	5.76	100.9	0.63	4.6	13.7	176	0.36	20.2	9.34	294
60		6.01									
90		5.84									
30	1000	5.87	124.9	0.48	6.9	8.8	218	0.28	34.1	5.5	310
60		5.26									
90		5.34									
30	1200	5.71	132	0.45	7.6	7.8	230.0	0.26	39.2	4.8	315
60		5.21									
90		5.16									

T =21.7 °C Q_L (L/min.)=12.5

30	500	6.44	116.5	0.86	5.5	18.3	203.9	0.49	37.4	9.6	361
60		5.75									
90		5.88									
30	1000	5.15	144.3	0.66	8.1	11.7	254.2	0.138	63.3	5.7	380
60		4.89									
90		4.96									
30	1200	4.97	152.7	0.62	8.9	10.44	267.1	0.35	72.7	4.98	385
60		4.90									
90		4.83									

Note: Calculated HTU based on the average liquid flow rate calculated at the radii of the bed.

Table(D.6): Predictions for Expamet 4 arms Distributor, hole size Φ 2.3mm.

T=24 °C , Q_L (L/min.)=6.5

Gas flow rate (m^3/h)	rpm	HTU (cm)	Penetration model		Onda correlation		Davidson model		Vivian correlation		a_e, Onda Correlation (1/m)
			k_L (m/s) $x10^5$	HTU (cm)	k_L (m/s) $x10^5$	HTU (cm)	k_L (m/s) $x10^5$	HTU (cm)	k_La (1/s) $x10^3$	HTU (cm)	
30	500	5.85	60.4	0.74	6.7	6.65	105.4	0.43	22.1	8.8	420
60		4.90									
90		5.11									
30	1000	3.96	75	0.56	9.9	4.3	130.2	0.32	36.4	5.2	445
60		3.92									
90		3.53									
30	1200	3.77	79	0.53	11	3.8	137.7	0.30	41.9	4.5	452
60		3.45									
90		3.44									

Note: Calculated HTU based on the average liquid flow rate calculated at the radii of the bed.

Appendix (E)

1- Flooding Data

Table (E.1): Experimental Flooding Data as shown in Figure 5. .

rpm	L (L/min.)	Qg (m^3/s)	Flooding Velocity Ug (m/s)	X	Y
444	10.5	64.3	3.69	0.28	0.23
561		74.1	4.25	0.24	0.19
619		80.5	4.62	0.22	0.18
707		85.5	4.91	0.21	0.15
796		89.8	5.15	0.198	0.14
444	14.4	54.8	3.15	0.45	0.17
561		70.2	4.03	0.35	0.171
619		74.1	4.25	0.33	0.16
707		78.6	4.51	0.31	0.13
796		82.07	4.71	0.298	0.12
444	21.9	37.7	2.16	0.99	0.078
561		50.6	2.9	0.74	0.088
619		56.2	3.22	0.66	0.09
707		62.7	3.60	0.59	0.086
796		68.8	3.95	0.54	0.080
444	26.4	29.5	1.69	1.52	0.048
561		38.9	2.23	1.15	0.05
619		45.8	2.63	0.98	0.06
707		54.2	3.11	0.83	0.064
796		62.7	3.60	0.714	0.067

Fig. (E.1): Transducer Voltage for Q_L 10.5 L/min. and 444 rpm

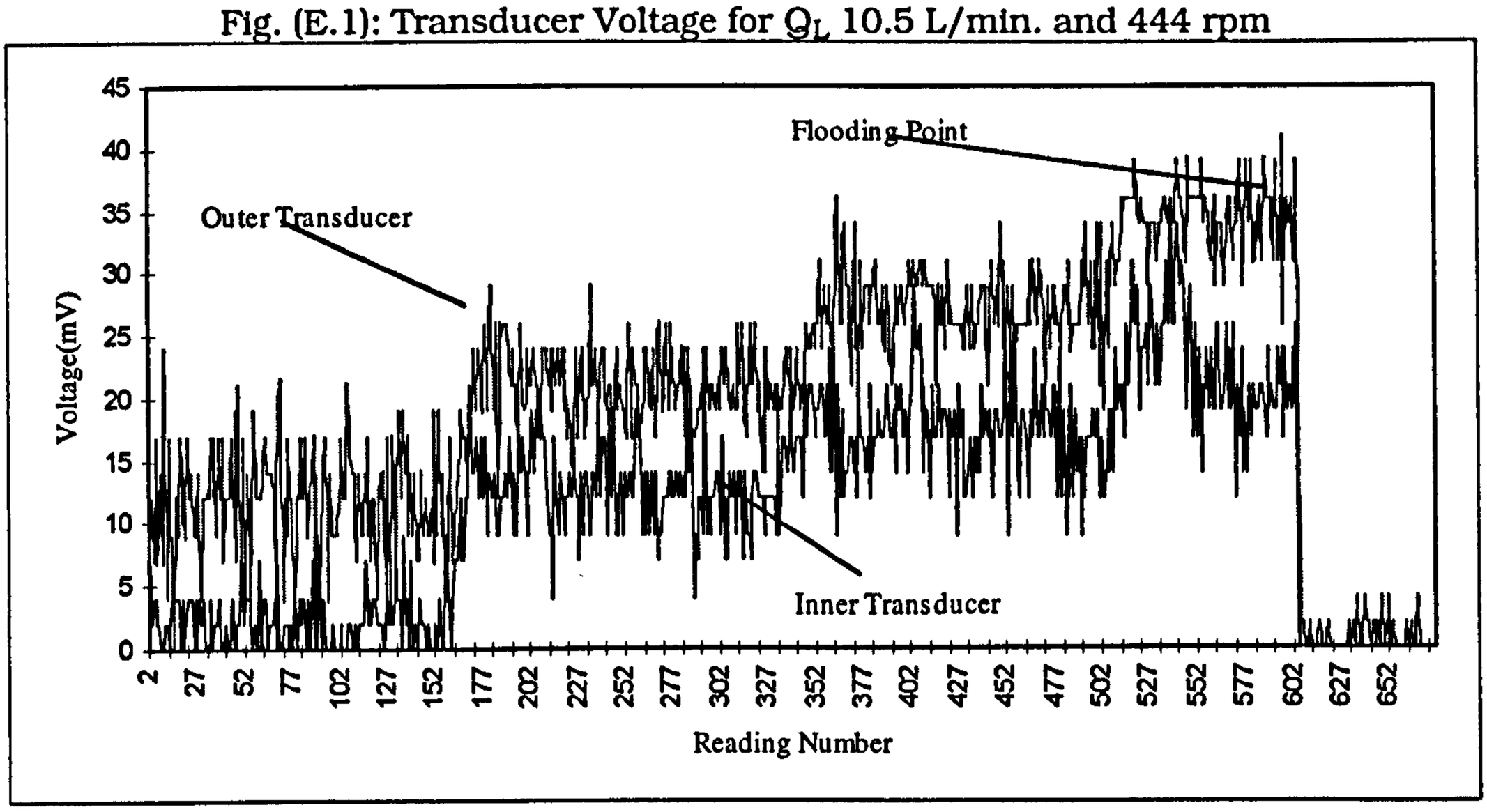

Fig. (E.2): Transducer Voltage for Q_L 10.5 L/min. and 560 rpm

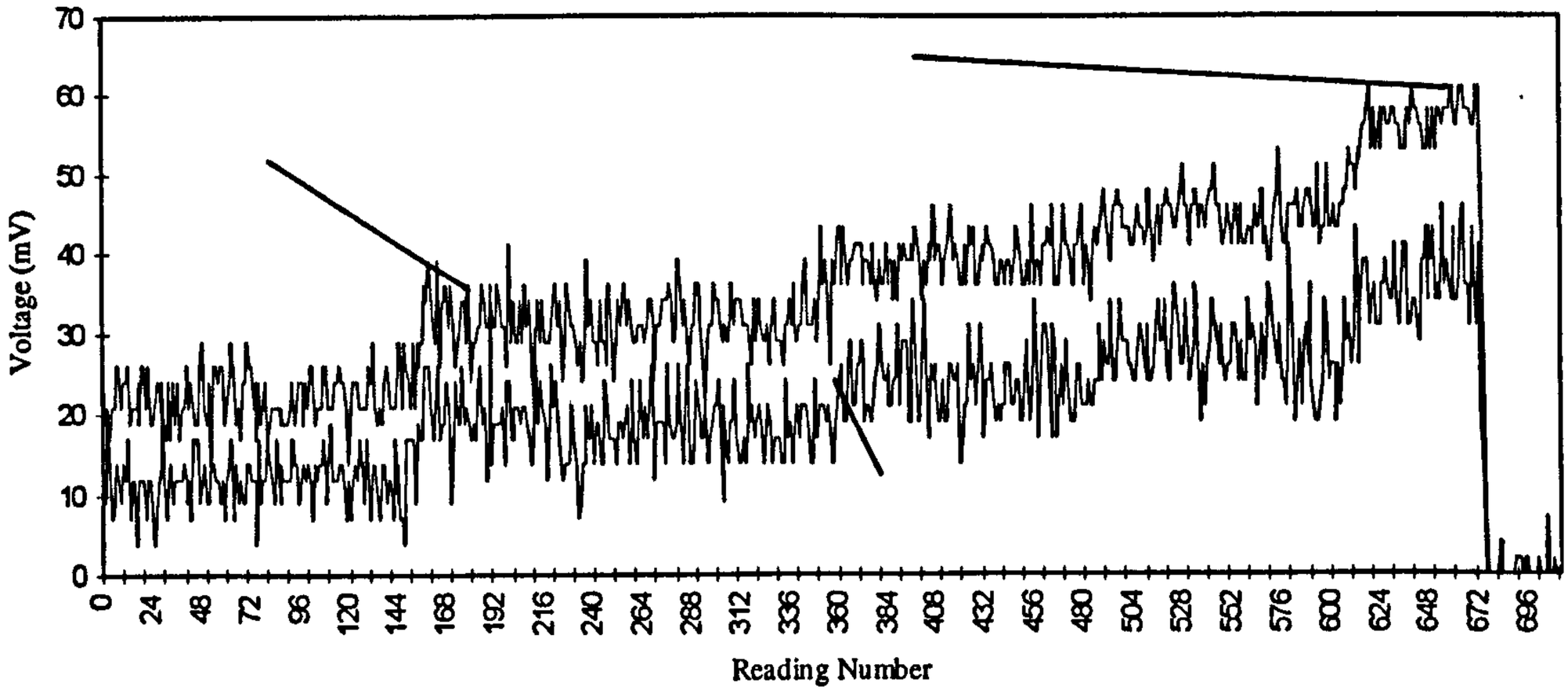

Fig. (E.1): Transducer Voltage for Q_L 10.5 L/min. and 444 rpm

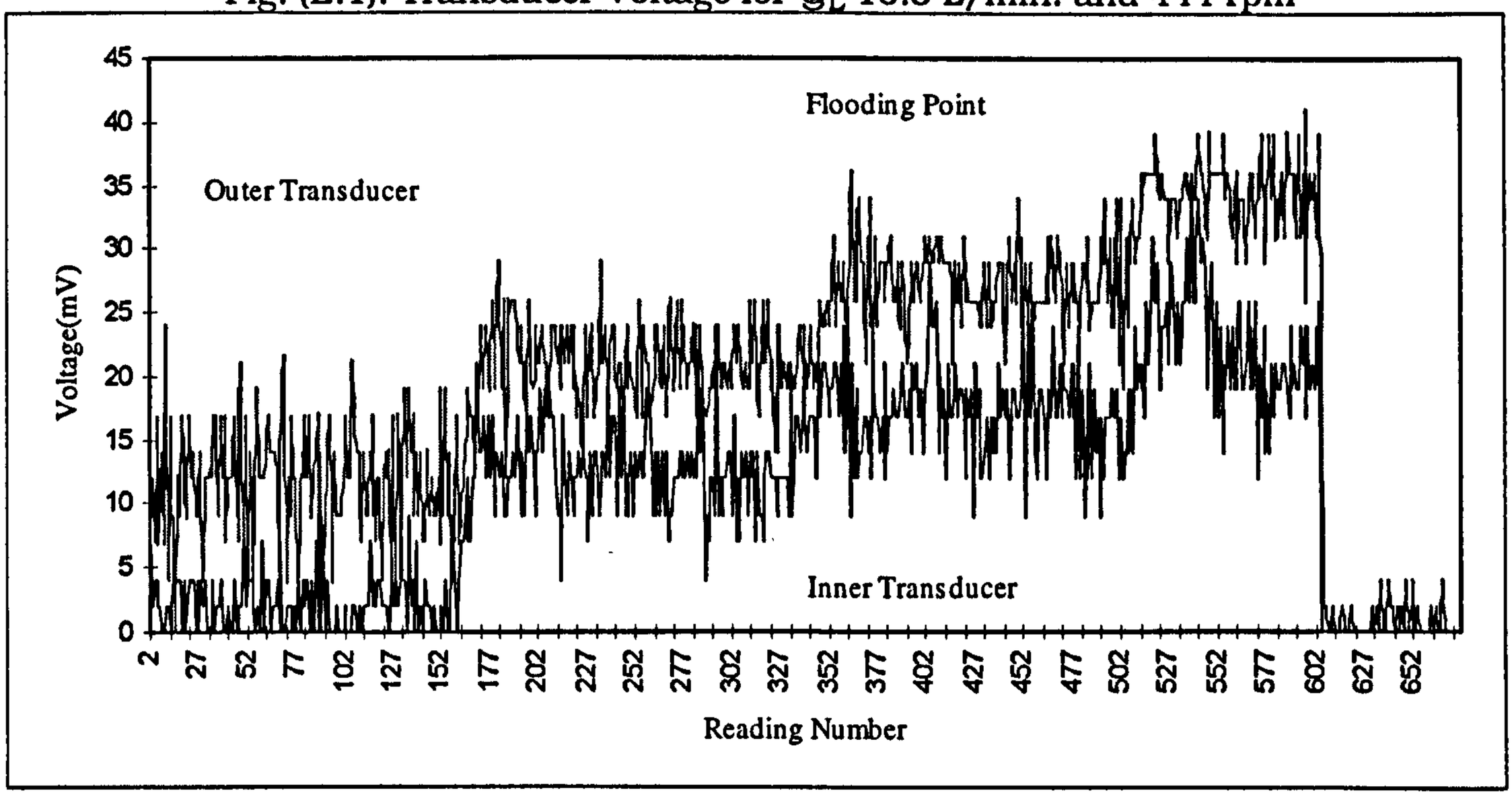

Fig. (E.2): Transducer Voltage for Q_L 10.5 L/min. and 560 rpm

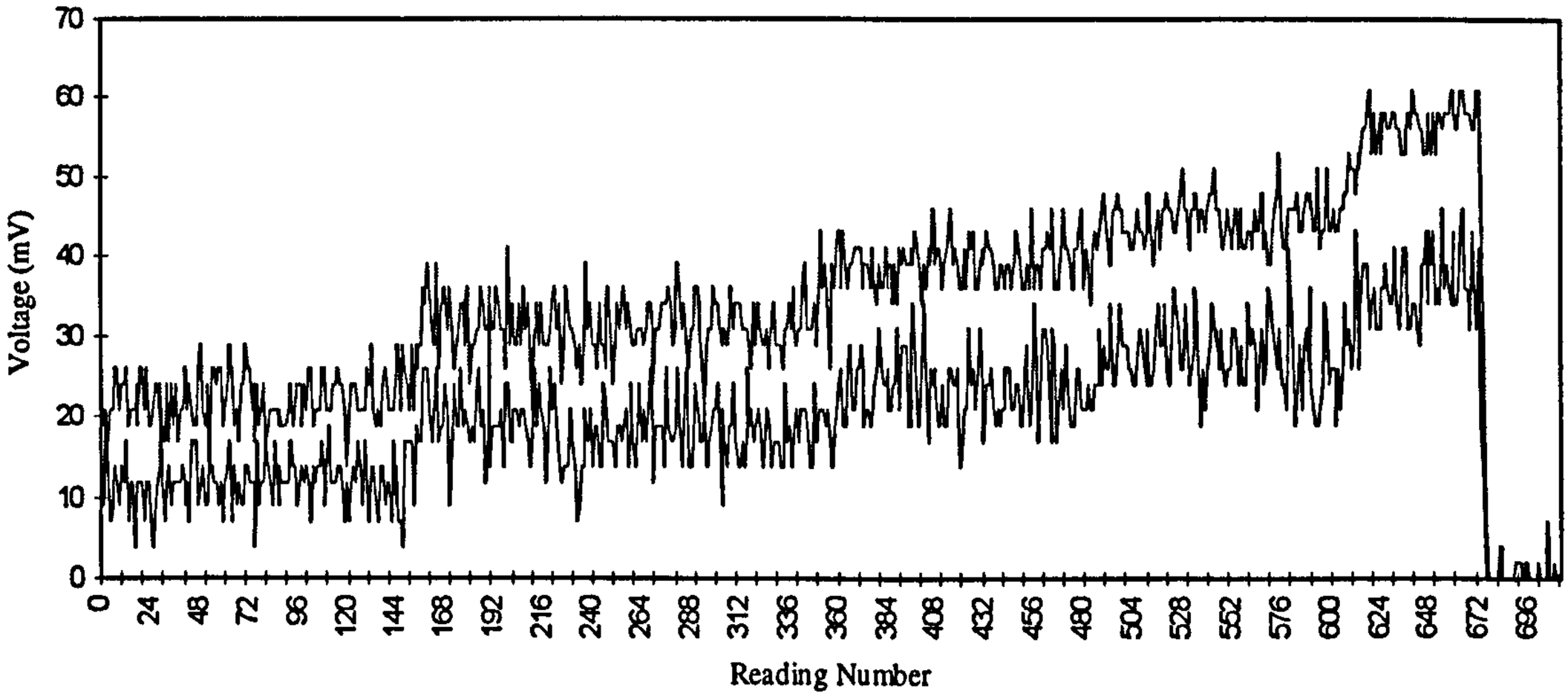

Fig. (E.3): Transducer Voltage for Q_L 10.5 L/min. and 620 rpm

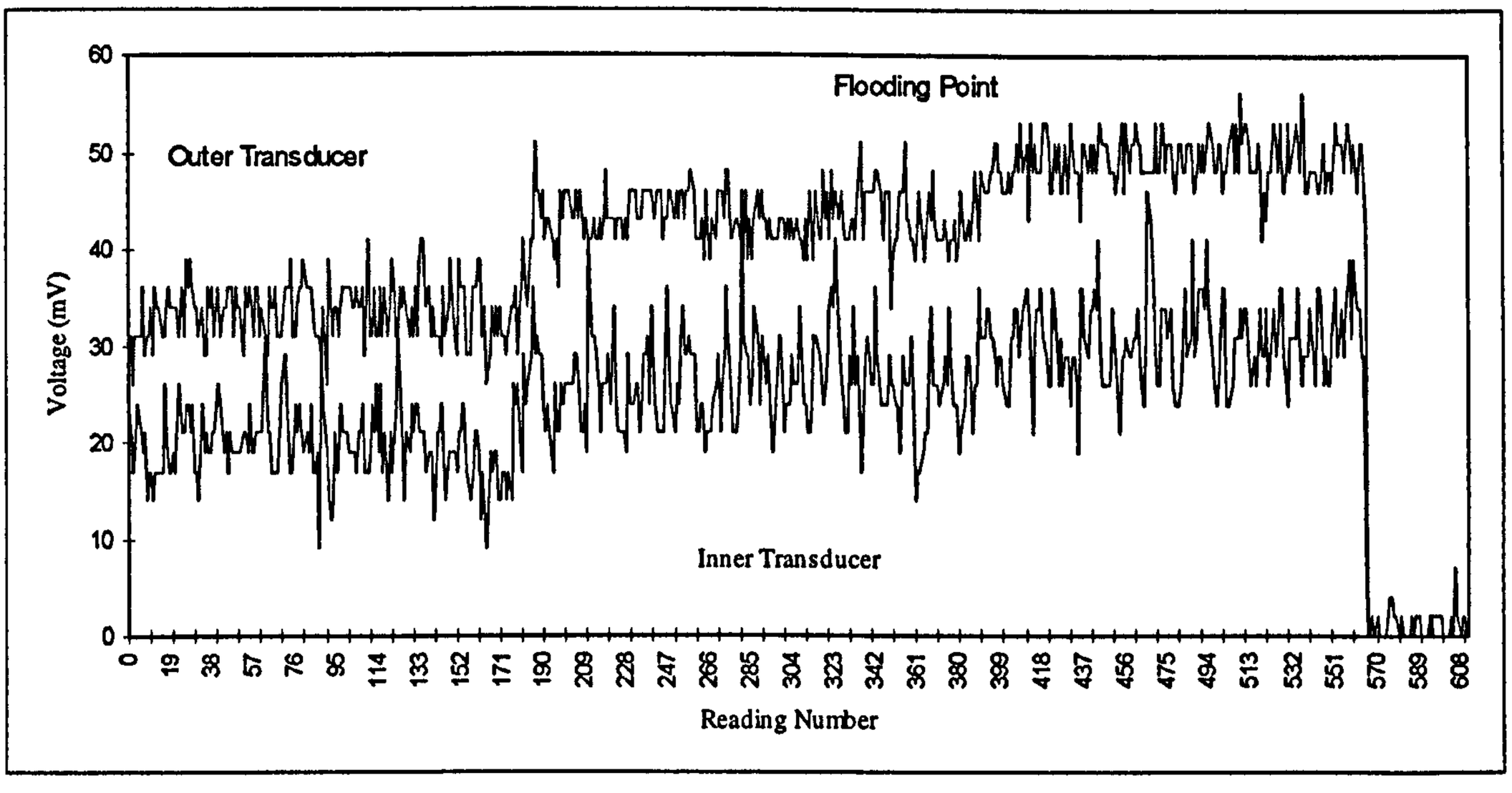

Fig. (E.4): Transducer Voltage for Q_L 10.5 L/min. and 707 rpm

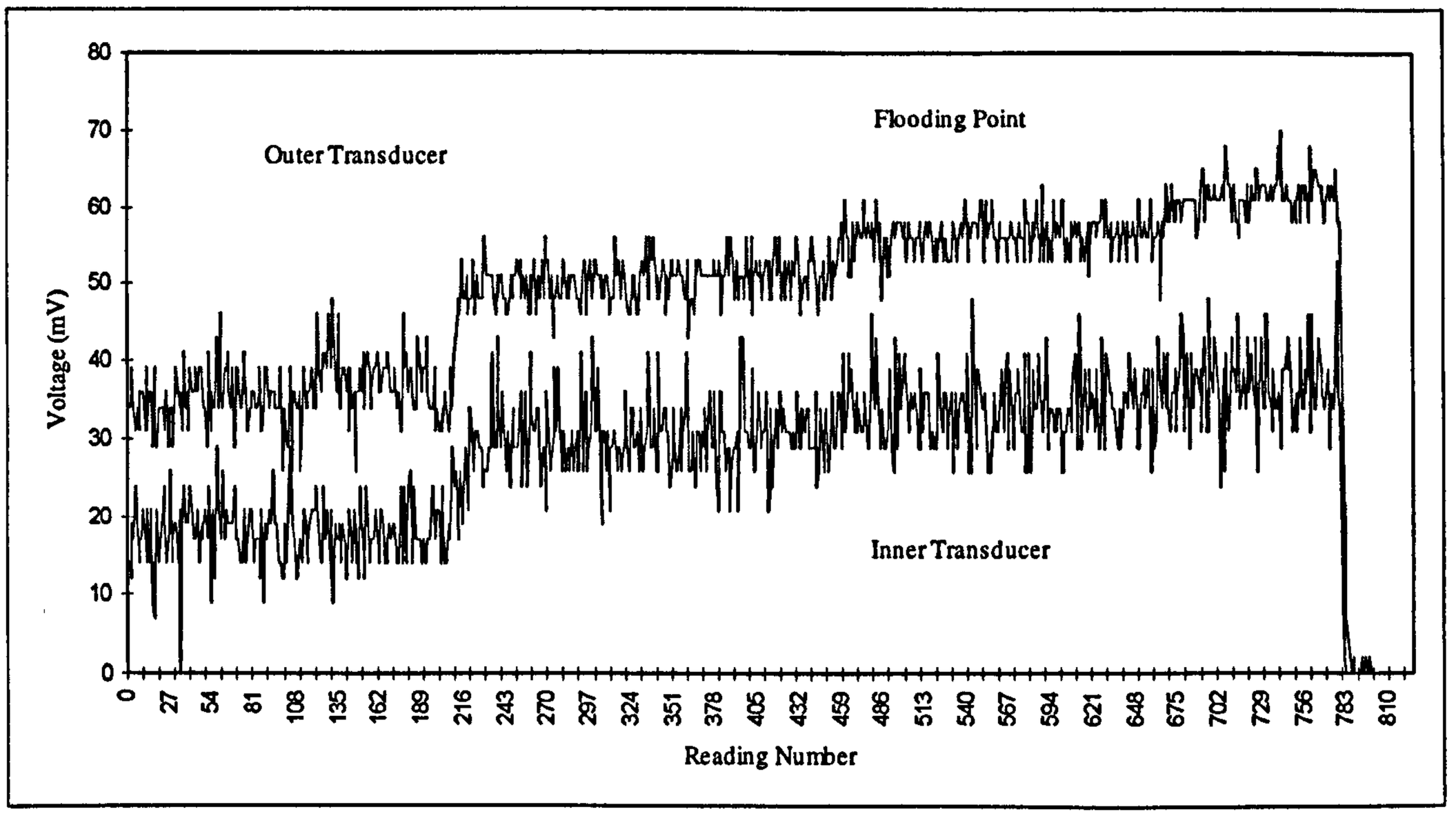

Druck

CALIBRATION CERTIFICATE

Calibration date:	13.11.95 SO: M08014
Transducer type:	PDCR 81
Serial Number:	7490
Range:	3 bar g
Supply:	5 Volts
Sensitivity:	5.548mV/V/bar
Non-linearity & hysteresis:	+/-0.2% BSL
Temperature operating range:	-20 to +120°C
Temperature compensated range:	
Temperature error band:	
Thermal zero shift:	0.05%/FSO/°C
Thermal sensitivity shift:	0.02%/°C

Electrical connection

Supply positive:	RED
Supply negative:	BLUE
Output positive:	YELLOW
Output negative:	GREEN
Screen:	

Notes:

5 mtrs cable
refer to note 6 overleaf

Druck Limited Fir Tree Lane, Groby, Leicester LE6 0FH, England.
Telephone: (0116) 231 4314. Facsimile: (0116) 287 5022

Druck

APPLICATION NOTES

1(a). Where the supply voltage engraved on the transducer body states " . . . V d.c." it is VERY IMPORTANT to use the STATED SUPPLY VOLTAGE AND POLARITY since the transducer uses an active compensation circuit.

1(b). Where the supply voltage engraved on the transducer body states " . . . VOLTS" then the compensation circuit is passive and any supply voltage up to a maximum of 12 VOLTS may be used. Transducer sensitivity and current consumption will be proportional to supply voltage.

2. Current consumption will not be greater than 15mA for 1 (a) with stated supply voltage and 5mA for 1 (b) with 10 Volts supply.

3*. Zero offset (normally less than 3mV) can be nulled using a 250 Kohm potentiometer across the output terminals with the wiper connected via 250 Kohm to the negative supply.

4. For best temperature stability, transducer must have a load impedance of greater than 50 Kohm.

5*. A calibration resistor may be used. For positive output, connect Rcal between negative output terminal and negative supply. For negative output, connect Rcal between positive output terminal and negative supply. Note that calibration output can be temperature-sensitive. In case of difficulty refer to supplier.

6. If a power supply earth is used, it is preferable to earth the positive side.

7. Following conventional practice, the cable screen is not connected to the transducer body. (On some PDCR 22 devices the flying green lead is connected to cable screen and may be connected to the solder post on the back of the transducer).

* **NOTE:** For transducers with amplified outputs, Notes 3 and 5 do not apply.

Appendix (F)

Listing of the Computer Programme used to estimate the tangential velocity V_θ at any radial positions. A fourth order Runge Kutta method is used to solve the differential equation.

```
C     MAIN PROGRAMME
C     FORTRAN PROGRAM TO SOLVE THE FIRST ORDER DIFFERENTIAL EQUATION
C     Y'(X)=F(X,Y)
C     WITH INITIAL CONDITION OF
C     Y(BEGIN)=YBEGIN
C     TO THE POINT  XEND, USING THE FOURTH ORDER RUNGE-KUTTA METHOD.
C     A FUNCTION SUBPROGRAM CALLED 'F' MUST BE SUPPLIED
C
C
      INTEGER I,N,NSTEPS
      REAL  DERIV,H,K1,K2,K3,K4,XBEGIN,XN,XEND,YBEGIN,YN,G,
     *RPM,EPS,AP,DX,DF
      COMMON /BLK1/G,RPM,EPS,AP,DX,DF
      OPEN(1,FILE='VEL.IN')
      OPEN(2,FILE='VEL.OUT')
    1 READ(1,*)XBEGIN,XEND,NSTEPS
      READ(1,*)RPM,G,DX,EPS,AP,DF
      WRITE(*,*)XBEGIN,XEND,NSTEPS,RPM,G,DX,EPS,AP,DF
      YBEGIN=(3.14/30.)*RPM*XBEGIN
      WRITE(*,*) YBEGIN
      WRITE(2,602)
  602 FORMAT(4X,'N',12X,'H',19X,'Xn',20X,'Yn',15X,'Derivative',/)
      IF (NSTEPS.LT.1) STOP
C     STOP
      H=(XEND-XBEGIN)/NSTEPS
      WRITE(*,*) H
      XN=XBEGIN
      YN=YBEGIN
C     CALL URW(G,RPM,DF,DX,EPS,AP,W,X,CDF)
      WRITE(*,*)XN,YN
      DERIV=F(XN,YN)
      N=0
```

```
      WRITE(*,601)N,H,XN,YN,DERIV
 601  FORMAT(2X,I3,4E21.9)
      DO 10 N=1,NSTEPS
C
      K1=H*F(XN,YN)
      K2=H*F(XN+H/2.,YN+K1/2.)
      K3=H*F(XN+H/2.,YN+K2/2.)
      K4=H*F(XN+H,YN+K3)
      WRITE(*,*)K1,K2,K3,K4
      YN=YN+1./6.*(K1+2.*K2+2.*K3+K4)
      XN=XBEGIN+N*H
      DERIV=F(XN,YN)
      WRITE(*,*)K1,K2,K3,K4
  10  WRITE(2,601)N,H,XN,YN,DERIV
C     GO TO 1
      STOP
      END

C     SUBPROGRAM 'F' OR THE DERIVATIVE
      REAL FUNCTION F(X,Y)
      REAL X,Y,G,RPM,DF,DX,EPS,AP,CDF,W,URF
      COMMON /BLK1/ G,RPM,EPS,AP,DX,DF
      GS=G
      W=RPM*3.14/30.
      RH=EPS/AP
      UR=GS/(2.*3.14*X*DX*EPS)
      CD=DF/(2.*RH*UR)
      F=-1.*Y/X+CD*(Y-X*W)
      RETURN
      END
```

Nomenclature

English Alphabet

		Units
a_p	specific surface area of the packing	(m^2/m^3)
a_e	effective interfacial area	(m^2/m^3)
a_w	wetted surface area	(m^2/m^3)
c_1	outlet concentration of inlet stream	(mol/m^3)
c_2	solute concentration of outlet stream	(mol/m^3)
c_{e1}	equilibrium solute concentration of outlet stream	(mol/m^3)
c_1	ammonia concentration in the inlet liquid	(mol/m^3)
c_2	ammonia concentration in the outlet liquid	(mol/m^3)
C	intercept of eq.(5.1)	$(m/s)^{0.5}$
g	acceleration of gravity	(m^2/s)
H	axial bed depth	(m)
HTU	height of transfer unit	(cm)
k_L	liquid film mass-transfer coefficient	(m/s)
k_G	gas film mass-transfer coefficient	(m/s)
L	superficial liquid mass flow rate	(kg/m^2 s)
M_{wt}	molecular weight of ammonia	(kg/mol)
m	slope of eq.(5.1)	$(s/m)^{0.5}$
P_t	total pressure of the system	(Pa)
r	radius	(m)
Vr	gas radial velocity	(m/s)
V_θ	gas tangential velocity	(m/s)
V	volume of the packing	(m^3)
$<V_{avg}>$	average gas radial velocity	(m^3)
y_{e1}	mole fraction of ammonia in the gas in equilibrium with an ammonia/water solution of concentration c_1	
y_{e2}	mole fraction of ammonia in the gas in equilibrium with an ammonia/water solution of concentration c_2	
y_2	mole fraction of ammonia in the outlet gas stream	

Subscript:

i	inlet
L	liquid
G	gas

o	outlet
r	radial direction
z	axial direction
θ	tangential direction

Greek Letter:

α	drag coefficient	
ε	porosity	
ε'	effective porosity	
δ	liquid film thickness	(m)
μ	viscosity	(Pa.s)
ρ	density	(kg/m^3)
σ	surface tension	(m N / m)
σ_c	critical surface energy of Packing Martial	(m N / m)
Ψ_r	drag force in the radial direction	(N/m^3)
Ψ_θ	drag force in the tangential direction	(N/m^3)
ω	rotational speed	(rad/s)

Dimensionless Groups:

Fr	Froud Number	(L^2 ap/ ρ^2 g)	
Gr	Grashof Number	(d_p^3 ρ^2 g/μ^2)	
Re	Reynolds Number	(L/apμ)	
Re	Reynolds Number	(2 π L/apμ)	
Sc	Schmidt Number	(μ/ρD)	
Sh	Sherwood Number	(K_L dp/D)	
We	Weber Number	(L^2 / ρ ap σ)	(in equation 1.5.2)
We	Weber Number	(dp L^2 /$\rho\sigma$)	(in equation 1.5.3)

Bibliography

[A1] Albright M.A., Hydrocarbon Processing, , pp173-177, sep.(1984).

[A2] AL-Shaban et. al., Energy Effeciency in Process Technology, Edited by P.A.Pilavachi, Elsevier Applied Sciences, (1992).

[B1] Bremer G.G. and F.J. Zuiderweg, Chem. Eng. Sci., Vol. 33, pp1637-43, (1978).

[B2] Bucklin R.W., K.W.Won, 37th Annual Oklahoma University, Laurance Reid Gas Conditioning Conference, pp D1- D16, (1987).

[B3] Bucklin R.W., P.A. Buckingham and K.W.Won, 38th Annual Oklahoma University, Laurance Reid Gas Conditioning Conference, pp 227- 237, (1988).

[B4] Burns J., Ph.D. Thesis, University of Newcastle, U.K., (1996).

[B5] Billet R., Packed Towers, VCH Publishers, Inc., New York, NY (USA) , (1995).

[C1] Cross, W.T. and Ramshaw, C., Chem. Eng. Res. Des., 64, 293 (1986).

[C2] Caruana C.M., Chem. Engr. Progr, April (1996).

[C3] Crank J., The mathematics of Diffusion, Oxford Clarendon Press (1975).

[D1] Davidson J.F.,Transaction of the Institute of Chemical Engineering, 37, 131, (1959).

[F1] Fowler R., The Chemical Engineer,35-37,Jan (1989).

[F2] Fredenslud A., J.Gmehling and Rasmussen, VLE using UNIFAC, A Group Contribution Method, Elsevier, Amsterdam (1977).

[G1] Gamson, B.W., Thodos, O. and Hougen, D.A., Trans. of AIChE, 39, 1 (1943).

[G2] Gosset et al., ESL-TR-85-18, Engineering and Services Laboratory, Air Force Engineering and service Centre, Tyndall AFB, Florida, (1985).

[H1] Hoek P.J., Wesseling, J.A. and F.J. Zuiderweg, Chem Eng Res Des, Vol. 64, pp 431-449, Nov. (1986).

[H2] Hartley D.E. and Murgatroyd W., Int. J. of Heat and Mass Transfer, 7,1003, (1967)

[H3] Higbie R., Trans Amer. Inst. Chem. Eng., 31, pp365-388 (1935).

[H4] Hutton B.E.T., Leung L. S.,Brooks, P. C.and Niclin,D.J., Chem Eng Sci., 29, pp 493-500 (1974).

[H5] Hewitt G.F. and N.S. Hall-Taylor, Annular Two Phase Flow, Pergamon Press (1970).

[K1] Keyvani M. and Gardner N.C. ,77th Annual AIChE Meeting , paper 64b, Chicago Nov. (1985).

[K2] Kumar M.P. and Rao D.P. Ind Eng Chem Res,29, pp920-924 (1990).

[L1] Liu, H.S. et al, Ind. Eng. Chem. Res., 35, 3590-3596, (1996).

[L2] Leighton D.T. and J.M. Calo, J Chem Eng Data, 26, pp382-385 (1981).

[L3] Leva M., Chem.Engng Progr.Symp.Ser. 50,10,51 (1954).

[L4] Lockett M.J.,Trans IChemE, Vol. 73, Part A, pp379-384, May(1996).

[M1] Munjal S., D.Sc. Thesis, Washington University, Missouri (1986).

[M2] Mallinson R.H. and C. Ramshaw, European Patent No. 0053881, November (1991).

[M3] Munjal S., Dudukovic P. and Ramachandran P., Chem Eng Sci, 44,pp2257-68,(1989).

[M4] Munjal S., Dudukovic P. and Ramachandran P., Chem Eng Sci, 49,pp2245-56, (1989).

[M5] Mohr R.J., Report of GPA meeting,Dallas,(1985).

[M6] Martin C.C. and M. Martelli, AIChE, paper 53a, Spring National Meeting, March 29-April 2, New Orleans, (1992).

[M7] Munz C. and R.V. Robert, JAWWA, pp62-69,May (1987).

[M8] Munjal S., Dudukovic P. and Ramachandran P.,77th Annual AIChE, paper 63b, Chicago Nov. (1985).

[O1] Onda K.,Takeuchi, H. and Koyama K., Chem.Eng Japan, 31, 127, (1967).

[O2] Onda, K, Takeuchi, H. and Okumoto, Y., J. of Chem. Eng. Japan, 1 (1), 56 (1968).

[P1] Perry D., D.E. Nutter and Hale A., Chem Eng Prog, pp30-45 Jan (1990).

[P2] Ponter A.B. et al, Int. J. of Heat and Mass Transfer, 10, 349 (1967).

[P3] Puranik S.S. and Vogelphol A., Chem Eng Sci , 29, pp502-507, (1974).

[P4] Podbielniak W.J., US Patent, 3,233,880 (1966).

[P5] Pilo C.W., European Patent No. 1366312, Sep. (1974).

[P6] Pilo C.W. and S.W Dahlbeck, US Patent No. 2,941,872, June (1960).

[P7] Perry R.H. and D Green, "Chemical Engineering Handbook", 7th edition, McGraw Hill.(1997)

[R1] Ramshaw, C., The Chemical Engineer, pp13-14, 389 (1983).

[R2] Ramshaw, C., The Chemical Engineer, 415 (1985).

[R3] Ramshaw, C., The Chemical Engineer, June (1987).

[R4] Ramshaw C., Heat Recovery Systems & CHP, vol. 13, No. 6, pp 493-513, (1993).

[R5] Ramshaw C. and R.H.Mallinson, United States Patent 4,283,255 August (1981).

[S1] Stanek S.V., "Fixes Bed Operations: Fundamental and Applications", Ellis Horwood, Ch.4, (1994).

[S2] Shulman H.L., Ullrich C.F., Proulx A.Z, and Zimmerman J.O., AIChEJ, 1, 2, pp 253, (1955).

[S3] Short H., Chemical Engineering,Feb. 21,(1983).

[S4] Sirenko V.I. and N.N.Kulov, [Translated from Russian], Teoreticheskie Osnovy Khimicheskoi Tekhnologii, Vol. 26, No. 2, pp 173-186, March-April (1992).

[S5] Schendel R.L. 36th Annual Oklahoma University, Laurance Reid Gas Conditioning Conference, pp M1- M17, (1986).

[S6] Singh S.P., Ph.D Thesis, The University of Tennessee, USA (1989).

[S7] Silvey F.C. and Keller G.J. Chem Eng Prog, vol. 62, no.1, pp 68-74 Jan. (1966).

[S8] Sherwood T.K., Shipley G.H. and F.A.L. Holloway, Ind. and Eng Chem, vol.30, no. 7, pp 765-769, July (1938).

[S9] Szekely J. and Mendrykowski J., Chem. Eng. Sci., vol 27, pp 959-963 (1972).

[S10] Shearer C.J. and J.F.Davidson, J. of Fluid Mechanic, Vol.22, part 2, pp 321-335, (1965).

[T1] Tung H.H. and Mah R.S.H., Chem Eng Commun, vol.39, pp147-153, (1985).

[V1] Vivian J.E., Brian P.L.T. and Krukonis V.J., AIChE J, 11, 1088 (1965).

[W1] Wegeng R.K., Call C.J. and K. Dorset, Spring Metting AIChE, New Orleans, LA,

[W2] Whitman, W.G. Chem and Met. Eng. 29,147 (1923).

[W3] Wem J.W., United States Patent No. 4,382,900 May (1983).

[W4] Wem J.W., United States Patent No. 4,382,045 May (1983).
Feb. 25-29 (1996).

[W5] Wallis G.B.," One Dimensional Two Phase Flow", Ch.11, McGraw Hill, New York (1969).

[X1] Xumei Z. et al, Proceedings of the Asian-Pasific Chemical Reaction Engineering Forum, 26-28 June, Beijing- China (1996).

[Z1] Zuiderweg F.J. and P.J. Hoek, I ChemE Symposium Series No.104.

[Z2] Zuiderweg F.J., J.G. Kunesh and D.W.King, Trans I ChemE, Vol.71, Part A, Jan. (1993).

[Z3] Zheng C. et al, Proceedings of the Asian-Pasific Chemical Reaction Engineering Forum, 26-28 June, Beijing- China (1996).

[Z4] Zheng C. et al, 5th World Chemical Engineering Congress, San Diego, USA, July (1996).